ISSN 2095-8137 CN 53-1229/Q
Volume 38 Issue 4
18 July 2017

ZR

Zoological Research

Navigating the complexities of human epilepsy through the use of laboratory rodents

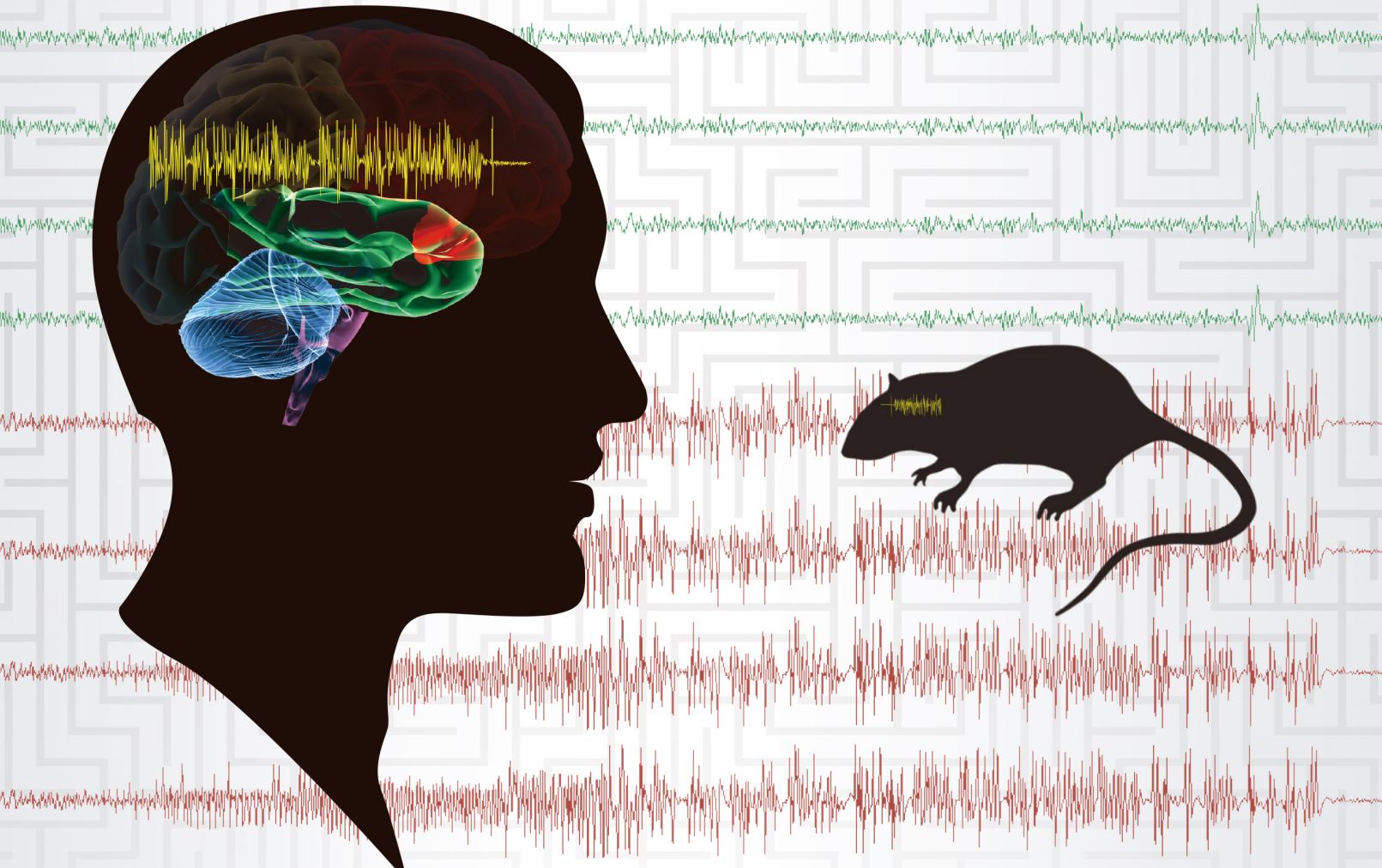

CODEN: DOYADI
www.zoores.ac.cn
Science Press

ZOOLOGICAL RESEARCH

Volume 38, Issue 4 18 July 2017

CONTENTS

Cover design: Bin Gu

Models and detection of spontaneous recurrent seizures in laboratory rodents

Bin Gu[1,*], Katherine A. Dalton[2]

[1] *Department of Cell Biology and Physiology*, *University of North Carolina*, *Chapel Hill*, *NC* 27599, *USA*

[2] *Psychology & Neuroscience Program*, *University of North Carolina*, *Chapel Hill*, *NC* 27599, *USA*

ABSTRACT

Epilepsy, characterized by spontaneous recurrent seizures (SRS), is a serious and common neurological disorder afflicting an estimated 1% of the population worldwide. Animal experiments, especially those utilizing small laboratory rodents, remain essential to understanding the fundamental mechanisms underlying epilepsy and to prevent, diagnose, and treat this disease. While much attention has been focused on epileptogenesis in animal models of epilepsy, there is little discussion on SRS, the hallmark of epilepsy. This is in part due to the technical difficulties of rigorous SRS detection. In this review, we comprehensively summarize both genetic and acquired models of SRS and discuss the methodology used to monitor and detect SRS in mice and rats.

Keywords: Spontaneous recurrent seizures; Animal model; Epilepsy

INTRODUCTION

Epilepsy, a chronic neurological disorder that is characterized by spontaneous recurrent seizures (SRS), is the fourth most common neurological disorder (Hirtz et al., 2007). Epilepsy was first described over 2 500 years ago, yet there is still relatively little known about the underlying cause and currently no disease-modifying therapies exist. Current treatment options include antiepileptic drugs (AEDs), ketogenic diet, neurosurgical resection, and electrical stimulation of the central nervous system (CNS), which work for some but not all afflicted individuals (Laxer et al., 2014). Thus, there is an urgent unmet clinical need to discover treatments for the entire epileptic population. Most currently available AEDs were first identified using simple acute seizure models (i.e., pentylenetetrazol induced seizure and maximal electroshock seizure models) (Löscher, 2011). These acute models fail to mirror the spontaneous nature of seizures seen in epilepsy. This issue is hypothesized to contribute to the large percentage of epileptic patients (~30%) for whom AEDs fail to prevent or control SRS. Therefore, studying epilepsy using laboratory animals exhibiting SRS will provide an important tool to explore the underlying mechanism of epilepsy and develop novel therapeutic approaches.

Epilepsy has been studied in a wide range of species of laboratory animals from simple organisms (e.g., *Drosophila melanogaster*, *Caenorhabditis elegans* and *Danio rerio*) to non-human primates. Along this spectrum, *Rattus norvegicus* (rat) and *Mus musculus* (mouse) are the two most commonly used laboratory animals given their small size, docility, rapid breeding, and availability of advanced genetic tools. Importantly, rat and mouse models provide good construct, face, and predictive validities of epilepsy and demand relatively low cost and maintenance for chronic study of SRS. In this review, we discuss the methodology of SRS recording, and summarize both genetic and acquired models of SRS in rat and mouse, with particular emphasis on modeling and detection of SRS. Mechanism and treatment of epileptogenesis are addressed in other reviews (Goldberg & Coulter, 2013; Löscher et al., 2013; McNamara et al., 2006; Pitkänen & Lukasiuk, 2011; Varvel et al., 2015).

MONITORING AND DETECTION OF SRS IN RODENTS

Chronic recording and detection of SRS in rodents is fundamental for preclinical research of epilepsy. Rigorous monitoring of SRS requires continuous time-locked video-EEG 24/7 in freely moving rodents. To capture biopotentials of the brain, most studies utilize single or multiple unipolar or bipolar recording electrodes which are intracranially placed. Skull or intracerebral electrode arrays are also used to cover broader brain regions. EEGs are acquired via either tethered or telemetry (wireless) recording systems in free-roaming, conscious rodents

Received: 05 April 2017; Accepted: 20 June 2017

Foundation items: This study was supported by the American Epilepsy Society Fellowship (2016)

*Corresponding author, E-mail: bin_gu@med.unc.edu

DOI: 10.24272/j.issn.2095-8137.2017.042

(Figure 1A). If a telemeter is used, it is either directly mounted on the head or tunneled and secured subcutaneously on the back or abdomen of rodents, providing the advantage of eliminating a wired interface between the animal and instrumentation. This minimizes the electrical noise and movement artifacts inherent in a tethered system. An inductive charging technique enables the telemeter to work 24/7 without the interruption of recharging the batteries.

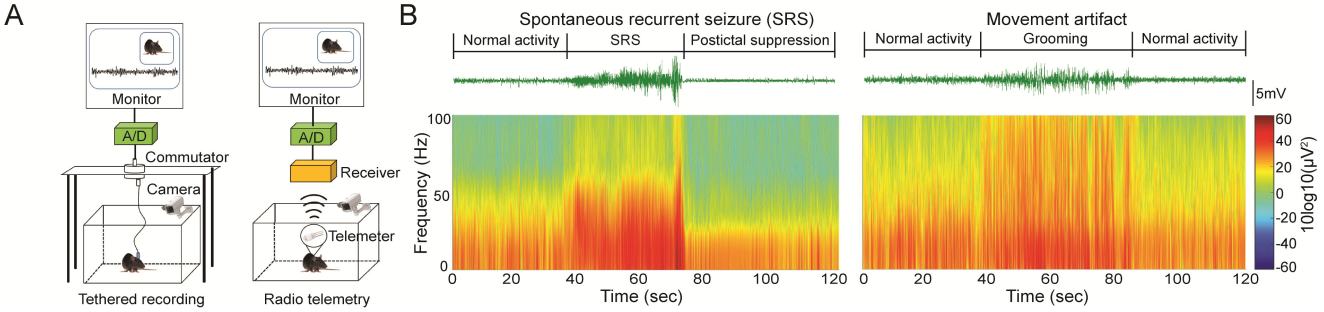

Figure 1 Schematic of video-EEG recording and EEG analyses

A: Schematic of video-EEG recording of mouse using tethered (Left panel) or radio telemetry (right panel) system; B: Representative EEG trace (top panel) and spectrogram (bottom panel) of SRS and movement artifact.

Given the rare, unpredictable nature and extremely diverse morphologies of SRS, identification of SRS is a technically challenging task. In most basic research settings, off-line visual inspection of EEG is performed by investigators to identify possible discrete epileptiform episodes, which are further confirmed by reviewing the time-locked video for behavioral correlates. Typical electrographic SRS features rhythmic neuronal firing characterized by increase of frequency and amplitude (especially in the gamma band) with clear initiation, propagation and termination (Figure 1B, left panel). In rodents, discrete epileptic discharges typically last seconds and are frequently followed by postictal suppression, which lasts minutes until normal electrographic activities resume. Electrographic SRS coincide with behavior phenotypes including rigid posture, facial automatisms, myoclonus, jumping and wild running, loss of postural control, tonic hindlimb extension, and death, which can be further semi-quantified using modified Racine's scale (Ben-Ari, 1985; Racine, 1972). Spontaneous absence seizures characterized by spike-wave discharges (SWD) and behavioral arrest are also frequently observed in some models.

To achieve successful SRS monitoring and detection, the following factors also need to be considered: (1) depending on models, SRS are relatively rare and tend to cluster. The seizure-free latent or interictal period may last days or even weeks before first or subsequent SRS emerge. Therefore, long-term (weeks to months) recording is required to achieve meaningful interpretation; (2) in most studies, brain areas covered by electrodes are limited. Electrographic seizures may occur out of the recording site, and in the absence of overt behavior change; (3) rodents are commonly singly housed during monitoring to minimize damage of recording device and facilitate video analysis. How social isolation affects SRS needs to be evaluated; (4) to visualize animal behavior during dark cycles, in some studies, the recording area is illuminated, thereby disrupting the normal light/dark cycle of monitored animals. Infrared light and imaging devices are recommended for behavior monitoring during dark cycle if circadian rhythm is considered (Cho, 2012; Hofstra & De Weerd, 2009); (5) SRS automatic detection algorithm is available, but manual validation is strongly recommended.

SRS IN RODENT MODELS OF EPILEPSY

SRS in genetic models of epilepsy

Approximately 40% of epilepsies are idiopathic. Genetics play a significant role in the development, maintenance, and difficulty of treating epilepsy. A growing number of epilepsy-related single gene mutations have been identified. Animals possessing analogous genetic manipulations (engineered or spontaneous) have proven useful in the search for the possible treatment for idiopathic epilepsy (Table 1).

Ion channel genes

Ion channels control the electrical transduction of cells, thereby playing a pivotal role in regulating neuronal excitability. Most epilepsy-related genes encode proteins composing voltage- or ligand-gated ion channels. Below we summarize genetic models of epilepsy that result from mutations in various types of ion channels.

Of the many ion channels, a number of disruptions in genes encoding voltage-gated sodium channels have been described in multiple human epilepsies, including genetic epilepsy with febrile seizures plus (GEFS+) and Dravet syndrome. Disruptions of genes encoding either α (SCN1A, SCN2A and SCN8A) or β (SCN1B) subunits of voltage-gated sodium channels are sufficient to trigger SRS in rodents (Chen et al., 2004, 2007; Dutton et al., 2013; Kearney et al., 2001; Martin et al., 2010; Ogiwara et al., 2007; Papale et al., 2009; Wagnon et al., 2015; Yu et al., 2006). In addition, two modifier loci (*Moe1* and *Moe2*) and multiple candidate modifier genes that influence the *Scn2a*^{Q54} epilepsy phenotype have also been identified and refined (Hawkins & Kearney, 2012).

Table 1 SRS in transgenic models of epilepsy

Gene	Modification	Latency	Frequency and features of SRS	References
Scn1a	*Scn1a*$^{-/-}$	P9	Generalized convulsive SRS. SUDEP at P15	Yu et al., 2006
	Scn1a$^{+/-}$	P21–P27	EEG and/or behavioral SRS lasted 20 s. Sporadic SUDEP from P21*	
	Scn1a$^{Flox/+}$*:: Zp3-Cre*$^{+/-}$	N/A	12 out of 23 mice exhibited behavioral SRS (3 times/day, lasted 35 s). Lifespan of P33	Dutton et al., 2013
	Scn1a$^{Flox/+}$*:: Ppp1r2-Cre*$^{+/-}$	N/A	2 out of 6 mice exhibited behavioral and/or EEG SRS	
	Scn1a$^{R1407X/R1407X}$	P12–P16	Multiple tonic-clonic SRS/day confirmed by EEG (lasted 1–3 min, interval: 1–4 hr). SUDEP by P21	Ogiwara et al., 2007
	Scn1a$^{R1407X/+}$	P18	Sporadic SUDEP in 1–3 mo*	
	Scn1a$^{R1648H/R1648H}$	P16	Behavioral SRS lasted 30–90 s. SUDEP P16–P26	Martin et al., 2010
	Scn1a$^{R1648H/+}$	N/A	2 out of 14 mice exhibited 21 SRS in total during 96 h EEG recording	
Scn2a	*Scn2a*^{Q54}	2 mo*	EEG and behavioral SRS. Frequency and duration of SRS increased with age*	Kearney et al., 2001
Scn8a	*Scn8a*$^{8J/+}$*, Scn8a*$^{med/+}$ *or Scn8a*$^{med\text{-}jo/+}$	N/A	SWD with behavioral arrest*	Papale et al., 2009
	Scn8$^{N1768D/N1768D}$	3 wk	No SRS prior to day of SUDEP 3 wk. SRS lasted <1 min	Wagnon et al., 2015
	Scn8$^{N1768D/+}$	8–16 wk	0–3 SRS/day. SRS lasted <1 min. SUDEP 14 wk	
	Scn8$^{N1768D/-}$	8 wk	As many as 25 SRS/day. SUDEP 9 wk	
Scn1b	*Scn1b*$^{-/-}$ or *Scn1b*$^{del/del}$	P10	EEG and behavioral SRS at random intervals with duration from seconds to minutes. SUDEP 3 wk	Chen et al., 2004; 2007
Kcnq2	*Kcnq2*$^{A306T/A306T}$	P24	Generalized EEG and behavioral SRS. SUDEP P16–P32*	Singh et al., 2008
Kcnq3	*Kcnq3*$^{G311V/G311V}$	2 wk	Generalized EEG and behavioral SRS. SUDEP P0–P73*	Singh et al., 2008
Kcna1	*Kcna1*$^{-/-}$	3 wk	Behavioral SRS lasted 20 s–2 min once or twice/hr throughout adult life. SUDEP 3–5 wk	Smart et al., 1998
Kcna2	*Kcna2*$^{-/-}$	N/A	Tonic-clonic SRS. SUDEP at P17	Brew et al., 2007; Douglas et al., 2007
Kcnmb4	*Kcnmb4*$^{-/-}$	N/A	Generalized EEG seizures without overt behavioral manifestation	Brenner et al., 2005
Cacna1a	Deletion ($\alpha_{1A}^{-/-}$)	N/A	Absence seizures. SUDEP 3–4 wk	Jun et al., 1999
Gria2	*Gria2*$^{+/\Delta ECS}$	P12	Behavioral SRS (once/4 hr). SUDEP by P20	Brusa et al., 1995
Chrna4	*Chrna4*$^{S252F/S252F\ or\ +}$ and *Chrna4*$^{+L264/+L264\ or\ +}$	N/A	SRS with high-amplitude, low-frequency cortical EEG activity, prominent theta and delta waves	Klaassen et al., 2006
Gabrg2	*Gabrg2*$^{+/-}$ or *Gabrg2*$^{+/R43Q}$	P20	Behavioral arrest and associated SWD* (up to 50 times/hr and variable)	Reid et al., 2013; Tan et al., 2007
Tsc1/2	*Tsc1/2*$^{flox/flox}$*::GFAP-Cre*	2–3 wk	Generalized tonic-clonic SRS. Few SRS at 3 wk, frequency increased over time. SUDEP 7–10 wk	Zeng et al., 2011
Fgf13	*Fgf13*$^{+/-}$	P15	Behavioral and EEG SRS. Frequency and duration varied by animal	Puranam et al., 2015
Lgi1	*Lgi1*$^{-/-}$	P10	Clonic SRS (1.6 seizures/hr at P14). SUDEP at P20	Chabrol et al., 2010
BACE1	*BACE1*$^{-/-}$	N/A	<40% rats exhibited generalized SRS and/or absence seizures	Hitt et al., 2010
APP	*APdE9*	N/A	65% exhibited SRS, 10%–15% mortality at any age but peak around 3–4 mo	Minkeviciene et al., 2009
	hAPP$_{FAD}$	N/A	Spontaneous nonconvulsive seizure activity. Occurrence of SUDEP	Palop et al., 2007
Ube3a	*Ube3a*$^{m+/p-}$	P18	SWD accompanied by behavioral immobility or tonic-clonic SRS*	Miura et al., 2002, Jiang et al., 1998a; 2010
Mecp2	*Viaat-Mecp2*$^{-/y}$	5 wk	Spontaneous rhythmic EEG activity including SWD*	Chao et al., 2010
	Mecp2$^{308/y}$	N/A	Spontaneous behavioral myoclonic jerks	D'Cruz et al., 2010

Continued

Gene	Modification	Latency	Frequency and features of SRS	References
Shank3	*Shank3 OE*	N/A	Hyperexcitability discharges accompanied by EEG SRS	Han et al., 2013
CNTNAP2	*CNTNAP2*$^{-/-}$	6 mo	SRS with generalized interictal spike discharges	Peñagarikano et al., 2011
Epm2A	*Epm2A*$^{-/-}$	<9 mo	80% exhibited myoclonic SRS, more frequent during dark cycle	Ganesh et al., 2002
Celf4	*Celf4*$^{Ff/Ff}$ *or Celf4*$^{Ff/+}$	3 mo	Recurrent tonic-clonic seizures or absence seizures*	Yang et al., 2007
Map2k1	*caMEK1*$^{flox/flox}$*::Nestin-Cre*	6–8 wk	Lifetime behavioral arrest and forelimb myoclonus (6.2 SRS/7 hr)	Nateri et al., 2007

*: model or strain dependent phenotype; ECS: editing site complementary sequence; OE: overexpression; SRS: spontaneous recurrent seizures; SUDEP: sudden unexpected death in epilepsy; SWD: spike-wave discharges.

Potassium channels also play an important role in action potentials by helping to return the neuron back to its resting membrane potential. *Kcna1* and *Kcna2* encode a pair of proteins (Kv1.1 and 1.2) which are members of the voltage-dependent potassium channel subfamily A. *Kcna1* or *Kcna2* knockout mice display frequent, severe SRS throughout their lives. In addition, SRS caused death in 50% of *Kcna1* or *Kcna2* knockout mice beginning from three weeks of age (Brew et al., 2007; Douglas et al., 2007; Smart et al., 1998). Mutations of *Kcnq2* and *Kcnq3*, which encode subfamily Q of voltage-gated potassium channels have been found in patients with benign familial neonatal convulsions (BFNC). *Kcnq2* or *Kcnq3* mutant mice exhibit early onset generalized tonic-clonic SRS concurrent with M-current defects (Singh et al., 2008). Mice carrying *Scn2a*^{Q54} transgene together with *Kcnq2* mutations (*Szt1* or V182M) result in an exacerbated epileptic phenotype (Kearney et al., 2006). A gain-of-function mutation of gene *Kcnmb4,* which encodes calcium-activated potassium channel accessory β4 subunit also led to SRS (Brenner et al., 2005).

Calcium channels are important for neuronal excitability and intracellular signaling. Activation of T-type calcium channels evoke burst-firing in the thalamocortical circuitry that gives rise to SWD associated with absence epilepsy (Chen et al., 2014; Cheong & Shin, 2013). α1G T-type calcium currents play a critical role in the genesis of spontaneous absence seizures resulting from hypofunctioning P/Q-type channels ($\alpha 1_A^{-/-}$) (Jun et al., 1999; Song et al., 2004). These attacks have also been shown to reflect absence seizures in *tottering* (*tg*), *leaner* (*tg*^{la}) and *rocker* (*rkr*) mice, which have spontaneously occurring mutant (Fletcher et al., 1996; Jun et al., 1999; Zwingman et al., 2001). In addition to pore-forming α1 subunit, loss of function mutations in ancillary subunits of calcium channels, including naturally occurring mutations in the β subunit gene *Cchb4* in the lethargic (*lh*) mouse, loss of α2δ2 subunit protein in *ducky* mouse (*du* and *du*^{2j}) and dysfunctional calcium channel γ2 subunits in *stargazer* (*stg*) and *waggler* (*wgl*) mice also result in SRS (Burgess et al., 1997; Zamponi et al., 2010).

In addition to voltage-gated ion channels, mutations of ligand-gated ion channel genes also result in SRS in mice. Heterozygous mice carrying an editing-deficient GRIA2 subunit allele express AMPA receptors with increased calcium permeability and develop SRS (Brusa et al., 1995). Fast ionotropic nicotinic acetylcholine receptor (nAChR) subunit genes, α2 (*Chrna2*), α4 (*Chrna4*) and β2 (*Chrnb2*), have been affiliated with autosomal dominant nocturnal frontal lobe epilepsy (ADNFLE) when mutated. Mice with *Chrna4* mutations (*Chrna4*^{S252F} or *Chrna4*$^{+L264}$) exhibited frequent SRS with diverse seizure semiology ranging from behavioral arrest to convulsive jerking (Klaassen et al., 2006). $GABA_A$ γ2-subunites have five known seizure associated mutations. Of these mutations, the R43Q mutation is of particular interest because it is related to childhood absence epilepsy and febrile seizures (Wallace et al., 2001). Both heterozygous *Gabrg2* knock-out and R43Q knock-in mice exhibited spontaneous absence seizures accompanied by SWD (Reid et al., 2013; Tan et al., 2007).

Non-ion channel genes

SRS are also related to interruptions of non-ion channel genes that are involved in diverse neurological disorders including tuberous sclerosis complex (TSC), Alzheimer's disease (AD) and autism. Notably, SRS can arise as a comorbid phenotype and/or secondary consequence of gene modification from germline.

Epilepsy is the most common presenting symptom in TSC. Up to 80%–90% of individuals with TSC will develop epilepsy during their lifetime. Two genes, *TSC1* and *TSC2*, encoding the proteins hamartin and tuberin, respectively, have been identified as causing TSC. Both genes, when conditionally inactivated in mice, have been shown to contribute to epileptic phenotype, among which *Tsc2* led to more severe and frequent seizures (Zeng et al., 2011).

Prevalence of epilepsy in Alzheimer's disease is significantly higher than in age-matched control populations. Manipulation of AD related genes (e.g., *BACE1* and *APP*) can also cause SRS in mice. One study showed that *BACE1* knockout mice were predisposed to both spontaneous and chemically induced seizures (Hitt et al., 2010). Autosomal-dominant mutations in amyloid precursor protein (APP) cause hereditary early-onset familial Alzheimer's disease (FAD). Transgenic mice overexpressing a mutant form of human APP ($hAPP_{FAD}$) have spontaneous nonconvulsive seizure activity in cortical and hippocampal networks (Palop et al., 2007). It was shown that 65% of mice carrying human APP with Swedish double mutation (*APPswe*) cointegrated with human preselinin-1 with exon 9 deletion (*PS1dE9*) exhibited unprovoked seizures (Minkeviciene et al., 2009; Um et al., 2012).

Autism spectrum disorder (ASD) related genes are also extensively studied given the fact that epilepsy is common in

individuals with autistic-like behavior resulting from particular genetic predisposition. A null mutation of maternal *Ube3a* gene (exon 1–2 or exon 15 and 16) results in core pathologies of Angelman syndrome including spontaneous EEG abnormality in mice (Jiang et al., 1998b; Miura et al., 2002). Spontaneous behavioral seizures were witnessed in mice with 1.6Mb large deletion (*Ube3a* to *Babrb3*) and loss of *Ube3a* selectively from the GABAergic neurons (Jiang et al., 2010; Judson et al., 2016). Global or conditional manipulation of *Mecp2* gene in Rett syndrome model mice is also sufficient to elicit SRS, including spontaneous epileptiform discharges (Chao et al., 2010; D'Cruz et al., 2010; Shahbazian et al., 2002; Zhang et al., 2014). Mutations in the gene encoding SHANK3 and large duplications of the region spanning SHANK3 both cause ASD. Overexpression of SHANK3 in mice leads to SRS and maniac-like behavior (Han et al., 2013). The *Cntnap2* gene which encodes a transmembrane protein that is essential in interactions between neurons and glia is strongly associated with ASD. Deletion of *Cntnap2* leads to autistic-like behavior as well as SRS (Peñagarikano et al., 2011).

Along these lines, disruption of non-ion channel genes involved in many other disorders with epileptic manifestation also results in SRS in mice. Disruption of fibroblast growth factors 13 (FGF13) on the X chromosome is associated with GEFS+. Female mice in which one *Fgf13* allele was deleted exhibited SRS (Puranam et al., 2015). Leucin-rich, glioma inactivated 1 (LGI1) is a secreted protein linked to human autosomal dominant epilepsy with auditory features (ADEAF). *Lgi1* deletion in mice results in early onset SRS and seizure-related death. Selective deletion of *Lgi1* in excitatory neurons, but not parvalbumin interneurons, contributes to the epileptic phenotype associated with LGI1 (Boillot et al., 2014; Chabrol et al., 2010). The gene *Epm2a* has been indicated in an autosomal recessive disorder known as Lafora Disease. Deletion of *Epm2a* can cause spontaneous myoclonic seizures with approximately 80% penetrance at the age of 9 months (Ganesh et al., 2002). Disruption of expression of doublecortin (Nosten-Bertrand et al., 2008), synapsin (Ketzef et al., 2011), CELF4 (Yang et al., 2007) or conditional expression of a constitutively active form of MAP/ERK kinases (Nateri et al., 2007) in the murine brain all led to SRS.

Besides genetically modified mice, SRS are also found in rats and mice with *de novo* mutations reported periodically in laboratories worldwide, like GAERS rat, WAG/Rij rat, lde/lde rat and *tg*, *tg*^{la}, *rkr, lh, du, stz, wgl* mice (Noebels, 2006). Among these strains, GAERS rat and WAG/Rij rat are well validated genetic models of human absence epilepsy. Spontaneous absence seizures featuring SWD first appear at P30–P40 in GAERS rat, whereas they are observed at around P60–P80 in WAG/Rij rat. SWD in both strains are fully manifested with age and last throughout their lifetime (Coenen & van Luijtelaar, 2003; De Sarro et al., 2015; Marescaux et al., 1992). The progression of absence seizures with age in WAG/Rij and GAERS rats resembles genetically-determined epileptogenesis similar to post-brain insult epileptogenesis (Russo et al., 2016).

SRS in acquired models of epilepsy

It is estimated that up to 50% of all epilepsy cases are initiated by neurological insults also known as acquired epilepsy. To model acquired epilepsy in rodents, an episode of prolonged seizures, namely status epilepticus (SE), is commonly induced to trigger SRS (Table 2).

Table 2 SRS in acquired models of epilepsy

Insult		Methods	Features
SE	Pilocarpine (in the presence or absence of lithium)	Systemic or intracerebral injection	High mortality in general and wide spread brain damage*
	Kainic acid (KA)	Systemic or intracerebral injection	Hippocampal restricted damage. Short latent period (e.g., 3–5 days, KA amygdala infusion in mouse)
	Bicuculine after a lesion induced by DSP-4	Microinjection into anterior piriform cortex of rat	30% developed SRS with mossy fiber sprouting
	Tetanus toxin	Unilateral intrahippocampal injection in P10 rat	Early-life brain insult triggered diverse epileptiform response in adult rats
	Febrile seizures	Hyperthermia in P10 rat	Mimic etiology of TLE. 35.2% rats developed SRS in adults
	Sustained electrical stimulation	In BLA or AB of rat	Overall 80% (BLA) and 67% (AB) rats developed SRS
TBI		CCI or LFP	<50% developed SRS following TBI with long latent period*
Ischemia/hypoxia		Unilateral carotid ligation with hypoxia in P7 rat or global hypoxia in P10 rat	100% rats developed SRS, which propagated along time
Methylazoxymethanol		In utero exposure	2 out of 11 rats developed SRS
Virus infection		Intracerebral infection with Theiler's murine encephalomyelitis virus	75% mice developed seizures 3–10 days post infection*
Kindling	Over electrical kindling	Repeated daily electrical stimulus for weeks and months	Labor intensive, SRS have not been well characterized
	Flurothyl kindling	Repeated flurothyl induced convulsive seizures for 8 days (once/day)	SRS were observed within the first week following flurothyl kindling then remitted*

*: model or strain dependent phenotype; SE: status epilepticus; TBI: traumatic brain injury; KA: Kainic acid; DSP-4: N-(2-Chloroethyl)-N-ethyl-2-bromobenzylamine hydrochloride; TLE: temporal lobe epilepsy; SRS: spontaneous recurrent seizures; BLA: basolateral amygdala; AB: angular bundle: CCI: controlled cortical impact; LFP: lateral fluid percussion.

Post-SE models

Kainic acid (KA, an ionotropic glutamate receptors agonist) and pilocarpine (a cholinergic muscarinic agonist) are two of the most commonly used chemicals to trigger SE (Ben-Ari, 1985; Ben-Ari et al., 1980; Turski et al., 1987, 1989). Systemic or intracerebral administration of KA causes SE followed by the emergence of SRS with remarkable histopathological correlation of hippocampal sclerosis in both rats and mice (Lévesque & Avoli, 2013). Compared to KA, pilocarpine-induced SE (in the presence or absence of lithium) results in higher mortality and wider spread brain damage in general along with SRS. The latency to onset of SRS and frequency of SRS varies depending on dose and administration route of chemicals as well as strains of animal. Convulsive SE can also be induced by microinjection of bicuculine into the anterior piriform cortex after a lesion of the locus coeruleus, which results in SRS in rat (Giorgi et al., 2006). In addition to chemically-induced convulsive SE, convulsive or non-convulsive SE can be induced by sustained electrical stimulation in the angular bundle or the basolateral amygdala of a rat, and can evoke SRS along with hippocampal sclerosis (Brandt et al., 2003; Gorter et al., 2001; Norwood et al., 2010). SE that occurred during early developmental stage can also cause SRS in adults. Unilateral injection of tetanus toxin into the hippocampus of P10 rats produces recurrent seizures for one week followed by epileptiform burst discharges (electrographic seizures on rare occasions) in adults (Jiang et al., 1998a; Lee et al., 1995). Both longitudinal and retrospective clinical studies reveal early life febrile SE causes temporal lobe epilepsy (TLE) in adults. Similarly, prolonged febrile seizures induced by hyperthermia in P10 rats render 35.2% of them epileptic in adulthood (Dubé et al., 2006).

Brain insults

SRS can also develop following direct brain insults such as traumatic brain injury (TBI), stroke and viral infection in both human and rodents in the absence of SE. TBI caused by controlled cortical impact (CCI) or lateral fluid-percussion injury (FPI) is able to elicit SRS in rats and mice (Bolkvadze & Pitkänen, 2012; D'ambrosio et al., 2004; Hunt et al., 2009; Kharatishvili et al., 2006). Rats that experienced global hypoxia at P10 or hypoxic-ischemic insult at P7 developed progressive SRS in adulthood (Kadam et al., 2010; Rakhade et al., 2011; Williams et al., 2004). Rats exposed to methylazoxymethanol in utero exhibited altered GluRs expression and developed sporadic SRS in adulthood (Harrington et al., 2007). Viral encephalitis of the CNS causes severe brain damage and epilepsy. Libbey et al. described the first mouse model of viral-induced epilepsy after intracerebral infection with Theiler's murine encephalomyelitis virus, where the seizures were transient and remitted after 10 days post infection (Libbey & Fujinami, 2011; Libbey et al., 2008).

Kindling models

Kindling is the process in which a train of repeated subconvulsive or subthreshold stimuli (electrical, audiogenic or chemical) renders a naïve animal more susceptible to subsequent stimuli. Kindling is a canonical model used for the study of epileptogenesis, yet it receives increasing criticism due to the lack of SRS. However, over-electrical kindling ultimately results in SRS (Kogure et al., 2000; McIntyre et al., 2002). Recent research revealed eight day consecutive flurothyl-kindling is sufficient to elicit SRS immediately after kindling, which remits weeks later (Kadiyala et al., 2016).

CONCLUDING REMARKS

Chronic rodent SRS recording is fundamental to preclinical study of epilepsy. A lack of standard methodology for SRS recording hampers the reproducibility of available models as well as the discovery of novel animal models of SRS. We recommend chronic 24/7 simultaneous video-EEG recording for rigorous study of SRS in rodents, and the recording period should vary from weeks to months depending on the model that is being used. Exclusive EEG recording often results in false positives because movement artifacts from grooming, drinking, and eating frequently generate epileptiform-like activity with rhythmic increases of frequency and amplitude (Figure 1B, right panel). Simultaneous analysis of behavior and EEG is necessary because exclusive video monitoring commonly fails to identify focal seizures or absence seizures since these lack overt behavioral manifestations.

While there are many ways to model SRS in rodents, the researcher first needs to decide what type of epilepsy they want to most closely recapitulate. Idiopathic or acquired epilepsy? TLE or absence seizures? Then the researcher needs to weigh the risks and benefits of each model that is chosen by studying the mortality and success rates and taking into consideration the developmental stage, length of latent period, frequency of SRS, electrographic and behavioral features of SRS, etc. Successful implication of rodent model of SRS will facilitate our knowledge of epilepsy and finally lead to discovery of potential biomarkers and therapies.

ACKNOWLEDGEMENTS

We thank Kamesh Krishnamurthy (Duke University, USA) for critical discussions and reading of the manuscript.

REFERENCES

Ben-Ari Y, Tremblay E, Ottersen OP. 1980. Injections of kainic acid into the amygdaloid complex of the rat: an electrographic, clinical and histological study in relation to the pathology of epilepsy. *Neuroscience,* **5**(3): 515-528.

Ben-Ari Y. 1985. Limbic seizure and brain damage produced by kainic acid: mechanisms and relevance to human temporal lobe epilepsy. *Neuroscience,* **14**(2): 375-403.

Boillot M, Huneau C, Marsan E, Lehongre K, Navarro V, Ishida S, Dufresnois B, Ozkaynak E, Garrigue J, Miles R, Martin B, Leguern E, Anderson MP, Baulac S. 2014. Glutamatergic neuron-targeted loss of *LGI1* epilepsy gene results in seizures. *Brain,* **137**: 2984-2996.

Bolkvadze T, Pitkänen A. 2012. Development of post-traumatic epilepsy after controlled cortical impact and lateral fluid-percussion-induced brain

injury in the mouse. *Journal of Neurotrauma,* **29**(5): 789-812.

Brandt C, Glien M, Potschka H, Volk H, Löscher W. 2003. Epileptogenesis and neuropathology after different types of status epilepticus induced by prolonged electrical stimulation of the basolateral amygdala in rats. *Epilepsy Research,* **55**(1-2): 83-103.

Brenner R, Chen QH, Vilaythong A, Toney GM, Noebels JL, Aldrich RW. 2005. BK channel β4 subunit reduces dentate gyrus excitability and protects against temporal lobe seizures. *Nature Neuroscience,* **8**(12): 1752-1759.

Brew HM, Gittelman JX, Silverstein RS, Hanks TD, Demas VP, Robinson LC, Robbins CA, McKee-Johnson J, Chiu SY, Messing A, Tempel BL. 2007. Seizures and reduced life span in mice lacking the potassium channel subunit Kv1.2, but hypoexcitability and enlarged Kv1 currents in auditory neurons. *Journal of Neurophysiology,* **98**(3): 1501-1525.

Brusa R, Zimmermann F, Koh DS, Feldmeyer D, Gass P, Seeburg PH, Sprengel R. 1995. Early-onset epilepsy and postnatal lethality associated with an editing-deficient *GluR-B* allele in mice. *Science,* **270**(5242): 1677-1680.

Burgess DL, Jones JM, Meisler MH, Noebels JL. 1997. Mutation of the Ca^{2+} channel β subunit gene *Cchb4* is associated with ataxia and seizures in the lethargic (*lh*) mouse. *Cell,* **88**(3): 385-392.

Chabrol E, Navarro V, Provenzano G, Cohen I, Dinocourt C, Rivaud-Péchoux S, Fricker D, Baulac M, Miles R, LeGuern E, Baulac S. 2010. Electroclinical characterization of epileptic seizures in leucine-rich, glioma-inactivated 1-deficient mice. *Brain,* **133**(9): 2749-2762.

Chao HT, Chen HM, Samaco RC, Xue MS, Chahrour M, Yoo J, Neul JL, Gong S, Lu HC, Heintz N, Ekker M, Rubenstein JLR, Noebels JL, Rosenmund C, Zoghbi HY. 2010. Dysfunction in GABA signalling mediates autism-like stereotypies and Rett syndrome phenotypes. *Nature,* **468**(7321): 263-269.

Chen CL, Westenbroek RE, Xu XR, Edwards CA, Sorenson DR, Chen Y, McEwen DP, O'malley HA, Bharucha V, Meadows LS, Knudsen GA, Vilaythong A, Noebels JL, Saunders TL, Scheuer T, Shrager P, Catterall WA, Isom LL. 2004. Mice lacking sodium channel *β*1 subunits display defects in neuronal excitability, sodium channel expression, and nodal architecture. *The Journal of Neuroscience: the Official Journal of the Society for Neuroscience,* **24**(16): 4030-4042.

Chen CL, Dickendesher TL, Oyama F, Miyazaki H, Nukina N, Isom LL. 2007. Floxed allele for conditional inactivation of the voltage-gated sodium channel β1 subunit *Scn1b*. *Genesis,* **45**(9): 547-553.

Chen YC, Parker WD, Wang KL. 2014. The role of T-type calcium channel genes in absence seizures. *Frontiers in Neurology,* **5**: 45.

Cheong E, Shin HS. 2013. T-type Ca^{2+} channels in absence epilepsy. *Biochimica et Biophysica Acta (BBA)-Biomembranes,* **1828**(7): 1560-1571.

Cho CH. 2012. Molecular mechanism of circadian rhythmicity of seizures in temporal lobe epilepsy. *Frontiers in Cellular Neuroscience,* **6**: 55.

Coenen AM, van Luijtelaar ELJM. 2003. Genetic animal models for absence epilepsy: a review of the WAG/Rij strain of rats. *Behavior Genetics,* **33**(6): 635-655.

D'ambrosio R, Fairbanks JP, Fender JS, Born DE, Doyle DL, Miller JW. 2004. Post-traumatic epilepsy following fluid percussion injury in the rat. *Brain,* **127**: 304-314.

D'Cruz JA, Wu C, Zahid T, El-Hayek Y, Zhang L, Eubanks JH. 2010. Alterations of cortical and hippocampal EEG activity in MeCP2-deficient mice. *Neurobiology of Disease,* **38**(1): 8-16.

De Sarro G, Russo E, Citraro R, Meldrum BS. 2015. Genetically epilepsy-prone rats (GEPRs) and DBA/2 mice: two animal models of audiogenic reflex epilepsy for the evaluation of new generation AEDs. *Epilepsy & Behavior,* 2015, doi: 10.1016/j.yebeh.2015.06.030.

Douglas CL, Vyazovskiy V, Southard T, Chiu SY, Messing A, Tononi G, Cirelli C. 2007. Sleep in *Kcna2* knockout mice. *BMC Biology,* **5**: 42.

Dubé C, Richichi C, Bender RA, Chung G, Litt B, Baram TZ. 2006. Temporal lobe epilepsy after experimental prolonged febrile seizures: prospective analysis. *Brain,* **129**: 911-922.

Dutton SB, Makinson CD, Papale LA, Shankar A, Balakrishnan B, Nakazawa K, Escayg A. 2013. Preferential inactivation of *Scn1a* in parvalbumin interneurons increases seizure susceptibility. *Neurobiology of Disease,* **49**: 211-220.

Fletcher CF, Lutz CM, O'Sullivan TN, Shaughnessy JD Jr, Hawkes R, Frankel WN, Copeland NG, Jenkins NA. 1996. Absence epilepsy in tottering mutant mice is associated with calcium channel defects. *Cell,* **87**(4): 607-617.

Ganesh S, Delgado-Escueta AV, Sakamoto T, Avila MR, Machado-Salas J, Hoshii Y, Akagi T, Gomi H, Suzuki T, Amano K, Agarwala KL, Hasegawa Y, Bai DS, Ishihara T, Hashikawa T, Itohara S, Cornford EM, Niki H, Yamakawa K. 2002. Targeted disruption of the *Epm2a* gene causes formation of Lafora inclusion bodies, neurodegeneration, ataxia, myoclonus epilepsy and impaired behavioral response in mice. *Human Molecular Genetics,* **11**(11): 1251-1262.

Giorgi FS, Mauceli G, Blandini F, Ruggieri S, Paparelli A, Murri L, Fornai F. 2006. Locus coeruleus and neuronal plasticity in a model of focal limbic epilepsy. *Epilepsia,* **47 Suppl 5**: 21-25.

Goldberg EM, Coulter DA. 2013. Mechanisms of epileptogenesis: a convergence on neural circuit dysfunction. *Nature Reviews Neuroscience,* **14**(5): 337-349.

Gorter JA, Van Vliet EA, Aronica E, Da Silva FHL. 2001. Progression of spontaneous seizures after status epilepticus is associated with mossy fibre sprouting and extensive bilateral loss of hilar parvalbumin and somatostatin-immunoreactive neurons. *European Journal of Neuroscience,* **13**(4): 657-669.

Han K, Holder JL Jr, Schaaf CP, Lu H, Chen HM, Kang H, Tang JR, Wu ZY, Hao S, Cheung SW, Yu P, Sun H, Breman AM, Patel A, Lu HC, Zoghbi HY. 2013. *SHANK3* overexpression causes manic-like behaviour with unique pharmacogenetic properties. *Nature,* **503**(7474): 72-77.

Harrington EP, Möddel G, Najm IM, Baraban SC. 2007. Altered glutamate receptor-transporter expression and spontaneous seizures in rats exposed to methylazoxymethanol in utero. *Epilepsia,* **48**(1): 158-168.

Hawkins NA, Kearney JA. 2012. Confirmation of an epilepsy modifier locus on mouse chromosome 11 and candidate gene analysis by RNA-Seq. *Genes, Brain and Behavavior,* **11**(4): 452-460.

Hirtz D, Thurman DJ, Gwinn-Hardy K, Mohamed M, Chaudhuri AR, Zalutsky R. 2007. How common are the "common" neurologic disorders? *Neurology,* **68**(5): 326-337.

Hitt BD, Jaramillo TC, Chetkovich DM, Vassar R. 2010. BACE1-/- mice exhibit seizure activity that does not correlate with sodium channel level or axonal localization. *Molecular Neurodegener,* **5**: 31.

Hofstra WA, de Weerd AW. 2009. The circadian rhythm and its interaction with human epilepsy: a review of literature. *Sleep Medicine Reviews,* **13**(6): 413-420.

Hunt RF, Scheff SW, Smith BN. 2009. Posttraumatic epilepsy after controlled cortical impact injury in mice. *Experimental Neurology,* **215**(2): 243-252.

Jiang MH, Lee CL, Smith KL, Swann JW. 1998a. Spine loss and other

persistent alterations of hippocampal pyramidal cell dendrites in a model of early-onset epilepsy. *The Journal of Neuroscience: the Official Journal of the Society for Neuroscience,* **18**(20): 8356-8368.

Jiang YH, Armstrong D, Albrecht U, Atkins CM, Noebels JL, Eichele G, Sweatt JD, Beaud AL. 1998b. Mutation of the Angelman ubiquitin ligase in mice causes increased cytoplasmic p53 and deficits of contextual learning and long-term potentiation. *Neuron,* **21**(4): 799-811.

Jiang YH, Pan YZ, Zhu L, Landa L, Yoo J, Spencer C, Lorenzo I, Brilliant M, Noebels J, Beaud AL. 2010. Altered ultrasonic vocalization and impaired learning and memory in Angelman syndrome mouse model with a large maternal deletion from *Ube3a* to *Gabrb3*. *PLoS One,* **5**(8): e12278.

Judson MC, Wallace ML, Sidorov MS, Burette AC, Gu B, van Woerden GM, King IF, Han JE, Zylka MJ, Elgersma Y, Weinberg RJ, Philpot BD. 2016. GABAergic neuron-specific loss of *Ube3a* causes angelman syndrome-like EEG abnormalities and enhances seizure susceptibility. *Neuron,* **90**(1): 56-69.

Jun K, Piedras-Rentería ES, Smith SM, Wheeler DB, Lee SB, Lee TG, Chin H, Adams ME, Scheller RH, Tsien RW, Shin HS. 1999. Ablation of P/Q-type Ca^{2+} channel currents, altered synaptic transmission, and progressive ataxia in mice lacking the α_{1A}-subunit. *Proceedings of the National Academy of Sciences of the United States of America,* **96**(26): 15245-15250.

Kadam SD, White AM, Staley KJ, Dudek FE. 2010. Continuous electroencephalographic monitoring with radio-telemetry in a rat model of perinatal hypoxia-ischemia reveals progressive post-stroke epilepsy. *The Journal of Neuroscience: the Official Journal of the Society for Neuroscience,* **30**(1): 404-415.

Kadiyala SB, Yannix JQ, Nalwalk JW, Papandrea D, Beyer BS, Herron BJ, Ferland RJ. 2016. Eight flurothyl-induced generalized seizures lead to the rapid evolution of spontaneous seizures in mice: a model of epileptogenesis with seizure remission. *The Journal of Neuroscience: the Official Journal of the Society for Neuroscience,* **36**(28): 7485-7496.

Kearney JA, Plummer NW, Smith MR, Kapur J, Cummins TR, Waxman SG, Goldin AL, Meisler MH. 2001. A gain-of-function mutation in the sodium channel gene *Scn2a* results in seizures and behavioral abnormalities. *Neuroscience,* **102**(2): 307-317.

Kearney JA, Yang Y, Beyer B, Bergren SK, Claes L, DeJonghe P, Frankel WN. 2006. Severe epilepsy resulting from genetic interaction between *Scn2a* and *Kcnq2*. *Human Molecular Genetics,* **15**(6): 1043-1048.

Ketzef M, Kahn J, Weissberg I, Becker AJ, Friedman A, Gitler D. 2011. Compensatory network alterations upon onset of epilepsy in synapsin triple knock-out mice. *Neuroscience,* **189**: 108-122.

Kharatishvili I, Nissinen JP, Mcintosh TK, Pitkänen A. 2006. A model of posttraumatic epilepsy induced by lateral fluid-percussion brain injury in rats. *Neuroscience,* **140**(2): 685-697.

Klaassen A, Glykys J, Maguire J, Labarca C, Mody I, Boulter J. 2006. Seizures and enhanced cortical GABAergic inhibition in two mouse models of human autosomal dominant nocturnal frontal lobe epilepsy. *The Journal of Neuroscience: the Official Journal of the Society for Neuroscience,* **103**(50): 19152-19157.

Kogure S, Kitayama M, Matsuda Y. 2000. Simultaneous kindling of the bilateral hippocampi: an advanced model for epilepsy research. *Epilepsia,* **41**(8): 929-932.

Laxer KD, Trinka E, Hirsch LJ, Cendes F, Langfitt J, Delanty N, Resnick T, Benbadis SR. 2014. The consequences of refractory epilepsy and its treatment. *Epilepsy & Behavior,* **37**: 59-70.

Lee CL, Hrachovy RA, Smith KL, Frost Jr JD, Swann JW. 1995. Tetanus toxin-induced seizures in infant rats and their effects on hippocampal excitability in adulthood. *Brain Research,* **677**(1): 97-109.

Lévesque M, Avoli M. 2013. The kainic acid model of temporal lobe epilepsy. *Neuroscience & Biobehavioral Reviews,* **37**(10): 2887-2899.

Libbey JE, Kirkman NJ, Smith MCP, Tanaka T, Wilcox KS, White HS, Fujinami RS. 2008. Seizures following picornavirus infection. *Epilepsia,* **49**(6): 1066-1074.

Libbey JE, Fujinami RS. 2011. Neurotropic viral infections leading to epilepsy: focus on Theiler's murine encephalomyelitis virus. *Future Virology,* **6**(11): 1339-1350.

Löscher W. 2011. Critical review of current animal models of seizures and epilepsy used in the discovery and development of new antiepileptic drugs. *Seizure,* **20**(5): 359-368.

Löscher W, Klitgaard H, Twyman RE, Schmidt D. 2013. New avenues for anti-epileptic drug discovery and development. *Nature Reviews Drug discovery,* **12**(10): 757-776.

Marescaux C, Vergnes M, Depaulis A. 1992. Genetic absence epilepsy in rats from strasbourg-a review. *Journal of Neural Transmission. Supplementum,* **35**: 37-69.

Martin MS, Dutt K, Papale LA, Dubé CM, Dutton SB, de Haan G, Shankar A, Tufik S, Meisler MH, Baram TZ, Goldin AL, Escayg A. 2010. Altered function of the *SCN1A* voltage-gated sodium channel leads to γ-aminobutyric acid-ergic (GABAergic) interneuron abnormalities. *Journal of Biological Chemistry,* **285**(13): 9823-9834.

McIntyre DC, Poulter MO, Gilby K. 2002. Kindling: some old and some new. *Epilepsy Research,* **50**(1-2): 79-92.

McNamara JO, Huang YZ, Leonard AS. 2006. Molecular signaling mechanisms underlying epileptogenesis. *Science's STKE,* **2006**(356): re12.

Minkeviciene R, Rheims S, Dobszay MB, Zilberter M, Hartikainen J, Fülöp L, Penke B, Zilberter Y, Harkany T, Pitkänen A, Tanila H. 2009. Amyloid β-induced neuronal hyperexcitability triggers progressive epilepsy. *The Journal of Neuroscience: the Official Journal of the Society for Neuroscience,* **29**(11): 3453-3462.

Miura K, Kishino T, Li E, Webber H, Dikkes P, Holmes GL, Wagstaff J. 2002. Neurobehavioral and electroencephalographic abnormalities in *Ube3a* maternal-deficient mice. *Neurobiology of Disease,* **9**(2): 149-159.

Nateri AS, Raivich G, Gebhardt C, Da Costa C, Naumann H, Vreugdenhil M, Makwana M, Brandner S, Adams RH, Jefferys JGR, Kann O, Behrens A. 2007. ERK activation causes epilepsy by stimulating NMDA receptor activity. *The EMBO Journal,* **26**(23): 4891-4901.

Noebels JL. 2006. CHAPTER 17-spontaneous epileptic mutations in the mouse A2-Pitkänen, Asla. schwartzkroin PA and Moshé SL. *In*: Models of Seizures and Epilepsy. Burlington: Academic Press, 223-232.

Norwood BA, Bumanglag AV, Osculati F, Sbarbati A, Marzola P, Nicolato E, Fabene PF, Sloviter RS. 2010. Classic hippocampal sclerosis and hippocampal-onset epilepsy produced by a single "cryptic" episode of focal hippocampal excitation in awake rats. *The Journal of Comparative Neurology,* **518**(16): 3381-3407.

Nosten-Bertrand M, Kappeler C, Dinocourt C, Denis C, Germain J, Tuy FPD, Verstraeten S, Alvarez C, Métin C, Chelly J, Giros B, Miles R, Depaulis A, Francis F. 2008. Epilepsy in *Dcx* knockout mice associated with discrete lamination defects and enhanced excitability in the hippocampus. *PLoS One,* **3**(6): e2473.

Ogiwara I, Miyamoto H, Morita N, Atapour N, Mazaki E, Inoue I, Takeuchi T, Itohara S, Yanagawa Y, Obata K, Furuichi T, Hensch TK, Yamakawa K.

2007. $Na_V1.1$ localizes to axons of parvalbumin-positive inhibitory interneurons: a circuit basis for epileptic seizures in mice carrying an *Scn1a* gene mutation. *The Journal of Neuroscience: the Official Journal of the Society for Neuroscience,* **27**(22): 5903-5914.

Palop JJ, Chin J, Roberson ED, Wang J, Thwin MT, Bien-Ly N, Yoo J, Ho KO, Yu GQ, Kreitzer A, Finkbeiner S, Noebels JL, Mucke L. 2007. Aberrant excitatory neuronal activity and compensatory remodeling of inhibitory hippocampal circuits in mouse models of Alzheimer's disease. *Neuron,* **55**(5): 697-711.

Papale LA, Beyer B, Jones JM, Sharkey LM, Tufik S, Epstein M, Letts VA, Meisler MH, Frankel WN, Escayg A. 2009. Heterozygous mutations of the voltage-gated sodium channel *SCN8A* are associated with spike-wave discharges and absence epilepsy in mice. *Human Molecular Genetics,* **18**(9): 1633-1641.

Peñagarikano O, Abrahams BS, Herman EI, Winden KD, Gdalyahu A, Dong HM, Sonnenblick LI, Gruver R, Almajano J, Bragin A, Golshani P, Trachtenberg JT, Peles E, Geschwind DH. 2011. Absence of CNTNAP2 leads to epilepsy, neuronal migration abnormalities, and core autism-related deficits. *Cell,* **147**(1): 235-246.

Pitkänen A, Lukasiuk K. 2011. Mechanisms of epileptogenesis and potential treatment targets. *Lancet Neurol,* **10**(2): 173-186.

Puranam RS, He XP, Yao LJ, Le T, Jang W, Rehder CW, Lewis DV, McNamara JO. 2015. Disruption of *Fgf13* causes synaptic excitatory-inhibitory imbalance and genetic epilepsy and febrile seizures plus. *The Journal of Neuroscience: the Official Journal of the Society for Neuroscience,* **35**(23): 8866-8881.

Racine RJ. 1972. Modification of seizure activity by electrical stimulation: II. Motor seizure. *Electroencephalography and Clinical Neurophysiology,* **32**(3): 281-294.

Rakhade SN, Klein PM, Huynh T, Hilario-Gomez C, Kosaras B, Rotenberg A, Jensen FE. 2011. Development of later life spontaneous seizures in a rodent model of hypoxia-induced neonatal seizures. *Epilepsia,* **52**(4): 753-765.

Reid CA, Kim T, Phillips AM, Low J, Berkovic SF, Luscher B, Petrou S. 2013. Multiple molecular mechanisms for a single $GABA_A$ mutation in epilepsy. *Neurology,* **80**(11): 1003-1008.

Russo E, Citraro R, Constanti A, Leo A, Lüttjohann A, van Luijtelaar G, De Sarro G. 2016. Upholding WAG/Rij rats as a model of absence epileptogenesis: hidden mechanisms and a new theory on seizure development. *Neuroscience & Biobehavioral Reviews,* **71**: 388-408.

Shahbazian M, Young JI, Yuva-Paylor LA, Spencer CM, Antalffy BA, Noebels JL, Armstrong DL, Paylor R, Zoghbi HY. 2002. Mice with truncated MeCP2 recapitulate many Rett syndrome features and display hyperacetylation of histone H3. *Neuron,* **35**(2): 243-254.

Singh NA, Otto JF, Dahle EJ, Pappas C, Leslie JD, Vilaythong A, Noebels JL, White HS, Wilcox KS, Leppert MF. 2008. Mouse models of human *KCNQ2* and *KCNQ3* mutations for benign familial neonatal convulsions show seizures and neuronal plasticity without synaptic reorganization. *Journal of Physiology,* **586**(14): 3405-3423.

Smart SL, Lopantsev V, Zhang CL, Robbins CA, Wang H, Chiu SY, Schwartzkroin PA, Messing A, Tempel BL. 1998. Deletion of the $K_V1.1$ potassium channel causes epilepsy in mice. *Neuron,* **20**(4): 809-819.

Song I, Kim D, Choi S, Sun M, Kim Y, Shin HS. 2004. Role of the α1G T-type calcium channel in spontaneous absence seizures in mutant mice. *The Journal of Neuroscience: the Official Journal of the Society for Neuroscience,* **24**(22): 5249-5257.

Tan HO, Reid CA, Single FN, Davies PJ, Chiu C, Murphy S, Clarke AL, Dibbens L, Krestel H, Mulley JC, Jones MV, Seeburg PH, Sakmann B, Berkovic SF, Sprengel R, Petrou S. 2007. Reduced cortical inhibition in a mouse model of familial childhood absence epilepsy. *Proceedings of the National Academy of Sciences of the United States of America,* **104**(44): 17536-17541.

Turski L, Cavalheiro EA, Czuczwar SJ, Turski WA, Kleinrok Z. 1987. The seizures induced by pilocarpine: behavioral, electroencephalographic and neuropathological studies in rodents. *Polish Journal of Pharmacology and Pharmacy,* **39**(5): 545-555.

Turski L, Ikonomidou C, Turski WA, Bortolotto ZA, Cavalheiro EA. 1989. Review: cholinergic mechanisms and epileptogenesis. The seizures induced by pilocarpine: a novel experimental model of intractable epilepsy. *Synapse,* **3**(2): 154-171.

Um JW, Nygaard HB, Heiss JK, Kostylev MA, Stagi M, Vortmeyer A, Wisniewski T, Gunther EC, Strittmatter SM. 2012. Alzheimer amyloid-β oligomer bound to postsynaptic prion protein activates fyn to impair neurons. *Nature Neuroscience,* **15**(9): 1227-1235.

Varvel NH, Jiang JX, Dingledine R. 2015. Candidate drug targets for prevention or modification of epilepsy. *Annual Review of Pharmacology and Toxicology*, **55**: 229-247.

Wagnon JL, Korn MJ, Parent R, Tarpey TA, Jones JM, Hammer MF, Murphy GG, Parent JM, Meisler MH. 2015. Convulsive seizures and SUDEP in a mouse model of *SCN8A* epileptic encephalopathy. *Human Molecular Genetics,* **24**(2): 506-515.

Wallace RH, Marini C, Petrou S, Harkin LA, Bowser DN, Panchal RG, Williams DA, Sutherland GR, Mulley JC, Scheffer IE, Berkovic SF. 2001. Mutant $GABA_A$ receptor γ2-subunit in childhood absence epilepsy and febrile seizures. *Nature Genetics,* **28**(1): 49-52.

Williams PA, Dou P, Dudek FE. 2004. Epilepsy and synaptic reorganization in a perinatal rat model of hypoxia-ischemia. *Epilepsia,* **45**(10): 1210-1218.

Yang Y, Mahaffey CL, Béerubé N, Maddatu TP, Cox GA, Frankel WN. 2007. Complex seizure disorder caused by *Brunol4* deficiency in mice. *PLoS Genetics,* **3**(7): e124.

Yu FH, Mantegazza M, Westenbroek RE, Robbins CA, Kalume F, Burton KA, Spain WJ, McKnight GS, Scheuer T, Catterall WA. 2006. Reduced sodium current in GABAergic interneurons in a mouse model of severe myoclonic epilepsy in infancy. *Nature Neuroscience,* **9**(9): 1142-1149.

Zamponi GW, Lory P, Perez-Reyes E. 2010. Role of voltage-gated calcium channels in epilepsy. *Pflügers Archiv-European Journal of Physiology,* **460**(2): 395-403.

Zeng LH, Rensing NR, Zhang B, Gutmann DH, Gambello MJ, Wong M. 2011. *Tsc2* gene inactivation causes a more severe epilepsy phenotype than *Tsc1* inactivation in a mouse model of tuberous sclerosis complex. *Human Molecular Genetics,* **20**(3): 445-454.

Zhang W, Peterson M, Beyer B, Frankel WN, Zhang ZW. 2014. Loss of MeCP2 from forebrain excitatory neurons leads to cortical hyperexcitation and seizures. *The Journal of Neuroscience: the Official Journal of the Society for Neuroscience,* **34**(7): 2754-2763.

Zwingman TA, Neumann PE, Noebels JL, Herrup K. 2001. Rocker is a new variant of the voltage-dependent calcium channel gene *Cacna1a*. *The Journal of Neuroscience: the Official Journal of the Society for Neuroscience,* **21**(4): 1169-1178.

Establishment of basal cell carcinoma animal model in Chinese tree shrew (*Tupaia belangeri chinensis*)

Li-Ping Jiang[1,2,#], Qiu-Shuo Shen[1,2,#], Cui-Ping Yang[1,2,*], Yong-Bin Chen[1,2,*]

[1] *Key Laboratory of Animal Models and Human Disease Mechanisms*, *Kunming Institute of Zoology*, *Chinese Academy of Sciences*, *Kunming Yunnan* 650223, *China*

[2] *Kunming College of Life Science*, *University of Chinese Academy of Sciences*, *Kunming Yunnan* 650204, *China*

ABSTRACT

Basal cell carcinoma (BCC) is the most common skin cancer worldwide, with incidence rates continuing to increase. Ultraviolet radiation is the major environmental risk factor and dysregulation of the Hedgehog (Hh) signaling pathway has been identified in most BCCs. The treatment of locally advanced and metastatic BBCs is still a challenge and requires a better animal model than the widely used rodents for drug development and testing. Chinese tree shrews (*Tupaia belangeri chinensis*) are closely related to primates, bearing many physiological and biochemical advantages over rodents for characterizing human diseases. Here, we successfully established a Chinese tree shrew BCC model by infecting tail skins with lentiviral SmoA1, an active form of Smoothened (Smo) used to constitutively activate the Hh signaling pathway. The pathological characteristics were verified by immunohistochemical analysis. Interestingly, BCC progress was greatly enhanced by the combined usage of lentiviral SmoA1 and shRNA targeting Chinese tree shrew *p53*. This work provides a useful animal model for further BCC studies and future drug discoveries.

Keywords: Chinese tree shrew; Basal cell carcinoma; Hedgehog

INTRODUCTION

Basal cell carcinoma (BCC) is the most common non-melanoma skin cancer (NMSC), accounting for over 80% of NMSC cases (Rubin et al., 2005). Exposure to ultraviolet radiation is the greatest oncogenic factor for this disease. Most BCCs occur in superficial sites, including the head, neck, trunk, and extremities (Bastiaens et al., 1998; Scrivener et al., 2002), whereas some sites, such as the axillae, breasts, perianal area, genitalia, palms, and soles, are readily ignored by dermatologists during medical examinations (de Giorgi et al., 2005; Rubin et al., 2005). Generally, human skin under both sun and non-sun exposure has the capability to form cancer, indicating that BCC formation could be a multifactor-induced oncogenic process with other genetic factors involved (De Giorgi et al., 2006). The most common histological BCC subtypes are nodular BCCs, followed by superficial BCCs and infiltrative BCCs (Bastiaens et al., 1998; Betti et al., 2012; Scrivener et al., 2002).

The incidence of BCC continues to increase worldwide (Lomas et al., 2012). Due to different standards, however, it is difficult to compare incidences among countries. Currently, Europe, North America, and Australia top the global incidence rates. For example, the rates have increased approximately 5% every year over recent decades in Europe (Lomas et al., 2012), and cases in the USA now exceed 2.8 millon patients, outnumbering the total rates of all other cancers (Asgari et al., 2015; Rogers et al., 2015; Siegel et al., 2016) and accounting for 3 000 deaths annually (Madan, 2010; Mohan & Chang, 2014). Although the incidence of BCC obviously increases with age, the incidence in adults younger than 40 has also increased year by year (Christenson et al., 2005; Demers et al., 2005). Currently, it costs the government more than $40 million (USD) to provide medical care annually in USA (Chen et al., 2001; Mudigonda et al., 2010). In Australia, one in two people by the

Received: 05 March 2017; Accepted: 25 June 2017

Foundation items: This study was supported by the National Key Research and Development Program of China (2016YFA0100900), the Strategic Priority Research Program of the Chinese Academy of Sciences (XDB13000000), the National Nature Science Foundation of China (U1502224, 81672764), and the Yunnan Applied Basic Research Projects (2014FA038, 2016FA009, 2014FB182). C.P.Y was also supported by the Chinese Academy of Sciences Western Light Program, Youth Innovation Promotion Association, CAS.

[#]Authors contributed equally to this work

[*]Corresponding authors, E-mail: ybchen@mail.kiz.ac.cn; cuipingyang@mail.kiz.ac.cn

DOI: 10.24272/j.issn.2095-8137.2017.045

age of 70 will be diagnosed with BCC (Lomas et al., 2012; Staples et al., 2006). In Africa and South America, the rates also have increased but relatively slowly (Abarca & Casiccia, 2002; Rawashdeh & Matalka, 2004).

The Hedgehog (Hh) signaling pathway is an evolutionarily conserved pathway known to play essential roles in embryonic development and adult tissue hemostasis and repair (Chen & Jiang, 2013). In general, the Hh ligand is bound to the secreted twelve-transmembrane receptor Patched-1 (Ptch1). Smoothened (Smo), a seven transmembrane receptor, is then activated by phosphorylation and other post-translational modifications, leading to accumulation in the primary cilium and induction of the Gli transcription factor to activate downstream gene expression (Yang et al., 2012). Malfunction of the Hh signaling pathway results in various developmental defects, including holoprosencephaly, cyclopia, limb abnormalities, and progression of tumors such as BCC and medulloblastoma (Teglund & Toftgård, 2010). Studies have demonstrated some Hh signaling component mutations associated with BCC development (De Zwaan & Haass, 2010; Lacour, 2002; Reifenberger et al., 2005). However, the predominant oncogenic mutations are those of the *Ptch1* and *Smo* genes, which can cause abnormal constitutive activation of the Hh signaling pathway (Bonilla et al., 2016; Sekulic & Von Hoff, 2016; Xie et al., 1998). Although activation of the Gli transcriptional factor sequestered by Sufu protein loss of function should promote BCC progression, inactivated Sufu in mouse skin shows few or no BCCs (Li et al., 2014), suggesting that Ptch1 or Smo might be a better target for establishing a BCC animal model.

There are many therapies for the treatment of BCC in cancer patients, including the modulation of Hh signaling activities for invasive BCC (Sekulic et al., 2012; Tang et al., 2012; Von Hoff et al., 2009). Vismodegib (GDC-0449), a Smo specific antagonist approved by the Food and Drug Administration (FDA) in 2012, is used to treat metastatic or locally advanced BCCs (Dlugosz et al., 2012). A recent study showed that an amino acid substitution at a conserved specific aspartic acid residue of a *SMO* mutation could confer BCC patients resistance to GDC-0449 treatment, suggesting that targeting *SMO* might be important for BCC treatment. As such, exploration of second-generation *SMO* inhibitors that are capable of overcoming acquired resistance is increasing (Yauch et al., 2009). Sonidegib (LDE225), another Smo antagonist approved by the FDA in 2015, is a clinical drug used for locally advanced BCC (Burness, 2015). It has also been reported that the antifungal drug itraconazole can suppress all known Smo drug-resistant mutants, thus inhibiting the Hh signaling pathway (Kim et al., 2013).

To further explore BCC pathogenesis, as well as develop new strategies for treating BCC, better animal models are required. Such models should conform to the conditions of patients and allow for: (1) the time of BCC induction to be defined and controllable; (2) the development of various stages and subgroups of human BCC; and (3) the inductivity of BCC in 100% of animals (Chen et al., 2009). To meet these requirements, many BCC models have been established. Most are transgenic mouse models, such as *Ptch1* knockout mice (Arad et al., 2008; Aszterbaum et al., 1999; Nitzki et al., 2010; Skvara et al., 2011; So et al., 2004), or include constitutive activation of other Hh signaling pathway key regulators, such as oncogenic *Smo*, *Gli1*, or *Gli2* mutation expressions driven by skin-specific keratin (K) 5, 6, or 14 promoters (Nitzki et al., 2012). In seven-week-old Sprague-Dawley rats, e.g., spontaneous BCC tumors were observed as single, reddish-brown subcutaneous masses located at the left inguinal region, basaloid cells showed lobular and cribriform growth with high mitotic rates, and cytokeratin 14 and cytokeratin 18 were expressed in nest tumor cells, thereby indicating that spontaneous BCC can occur in young rats (Lee et al., 2010). Nano-electro-ablation methods have been found to induce apoptosis efficiently in a Ptch1 (+/-) K14-Cre-ER *p53* fl/fl mouse BCC model (Nuccitelli et al., 2012). Protein kinase A (PKA) activation by cAMP agonist forskolin inhibited BCC growth, particularly drug resistant BCC for Smo inhibitors, which was performed and evaluated in tamoxifen-induced 30-day-old postnatal mice which were born from male K14-CreERT2 crossed with female homozygous R26-SmoM2 (Makinodan & Marneros, 2012). Furthermore, introduction of Smoothened constitutive active form SmoA1 in mouse cerebellar granule neuron precursors was shown to cause a 48% incidence rate of medulloblastoma (Hallahan et al., 2004).

Inactivation of tumor suppressor *p53* promotes tumorigenesis and is correlated with poor survival (Ghaderi & Haghighi, 2005; Lacour, 2002; Moles et al., 1993; Urano et al., 1995; Wang et al., 2017; Ziegler et al., 1993). Thus, the clues to the mutation of *p53* in human BCCs show that their ablation might also contribute to tumor formation (Wörmann et al., 2016; Wu et al., 2014). Therefore, to imitate spontaneous BCCs in humans and speed up progression in animals, disruption of *p53* could be an alternative.

Considering the distant relationship between humans and rodents, and the long period for non-human primate model establishment, we choose the Chinese tree shrew (*Tupaia belangeri chinensis*) as an animal model for BCC. The Chinese tree shrew, which belongs to Tupaiidae (Scandentia), is widely spread over Southeast Asia and Southwest China, including Yunnan province (Zhao et al., 2014). This tree shrew species possesses a variety of unique and notable physiological characteristics, including small adult body size, high brain-to-body mass ratio, short reproductive cycle and life span, low maintenance, and most importantly, a close affinity to primates (Fan et al., 2013). The recent elucidation of the genome of *Tupaia belangeri chinensis* confirmed the close genomic relationship between *Tupaia belangeri* and primates (Fan et al., 2013). As a favorable animal model, the tree shrew has been used for many human disease studies, including research on depression (Fuchs, 2005; Wang et al., 2011; 2012; 2013), drug addiction (Sun et al., 2012; Zhang et al., 2011), virus infection (Amako et al., 2010; Yan et al., 1996; Yang et al., 2005), bacterial infection (Li et al., 2012), breast cancer (Elliot et al., 1966; Ge et al., 2016; He et al., 2016; Xia et al., 2012), glioblastoma (Tong et al., 2017), thrombosis (Endo et al., 1997), metabolic diseases (Wu et al., 2013; 2016; Zhang et al., 2015; 2016), stem spermatogonium transgenics (Li et al., 2017), and myopia (Norton et al., 2006). Recently, pharmacological research through drug target prediction and genomic and

transcriptomic scale analysis has shown that more than half of the drug target proteins identified from the tree shrew genome demonstrate higher similarity to human targets than that of the mouse, as validated by the constitutive expression of proteinase-activated receptors (Zhao et al., 2014). The above studies indicate that over several years of research, the tree shrew has shown huge potential as an animal model for research of human diseases, including mental, nervous, infective, metabolic, and cancer diseases (Xiao et al., 2017; Xu et al., 2013; Yao, 2017), as well as drug safety (Zhao et al., 2014).

To establish a BCC model in the tree shrew, we constructed lentiviral vectors containing Hh signaling pathway constitutive activator SmoA1 tagged by GFP, which was used to trace the lentiviral infected tree shrew skin cells. We then infected the dorsal skins of 6-week-old tree shrews *in vivo* with both control and SmoA1 containing lentiviruses using one dose (10 μL) of the virus containing 5.6×10^5 transducing units (TU). Two weeks later, hematoxylin-eosin (HE) staining was performed to examine the pathological phenotypes of the skins. The results showed the human BCC-like phenotype and remarkable pathological changes compared with reciprocal biopsies from the control virus. Interestingly, when we injected the virus into the tree shrew tail skins, the BCC tumor formed more easily than that on other parts of skin after only one dose containing 5 μL of pCDH-SmoA1 virus (5.6×10^5 TU) and 5 μL of lentiviral shRNA targeting *p53* (2×10^5 TU). In summary, we successfully and efficiently established a BCC model using the tree shrew, which closely recapitulated the clinical phenomena. This animal model will help to better understand the fundamental mechanisms of BCC, and could be used for evaluating novel therapeutic strategies against BCC and pre-clinical drugs in the future.

MATERIALS AND METHODS

Animal use and care

Wild-type adult male tree shrews were provided by the Kunming Primate Research Center, Kunming Institute of Zoology (KIZ), Chinese Academy of Sciences (CAS). All experimental procedures and animal care and handling were performed under the standard guidelines approved by the Institutional Animal Care and Use Committee of the KIZ, CAS (SMKX2013023).

Plasmids construction and cell culture

A mSmoA1-6×myc fragment was collected from pGE-*mSmoA1* digested by double restriction endonuclease with *Hind* Ⅲ and *Sac II*, and was then cloned into pCDH empty expression vector digested by *EcoR I* and *BamH I* in blunting form. The short heparin RNA (shRNA) targeting sequences for tree shrew *p53* (*tsp53*) were 1#: 5′-CCTCAGCATCTTATCCGGGTG-3′ and 2#: 5′-TTTGTGCCTGTCCTGGAAGAG-3′, and the control scramble shRNA sequence was 5′-GCACTACCAGAGCTAACTCAG-3′. The shRNA oligos were synthesized by BGI-Shenzhen (Shenzhen, China). The synthesized complementary oligo DNA was annealed by 95 °C boiling water and ligated with pLKO.1 plasmid. The product was transformed into DH5α competent cells and plated on LB agar. Individual colonies were randomly collected and shaken at 37 °C, with the plasmids then extracted using a plasmid extraction kit (Tiangen, Beijing, China) and checked by enzyme digestion and sequencing. Primary culture of tree shrew skin derived progenitor/stem cells (SKPs) was performed according to a previously validated method (Biernaskie et al., 2007). Briefly, animals were euthanized by ethyl ether anesthesia and dissected for the generation of dorsal back skin and tail skin. All blood vessels, adipose, fascia, and muscle underlying the dermis were removed gently to reduce contamination by other cell types in the culture. The dissected skin tissues were minced into 1–2 mm^2 size pieces, transferred to a 15 mL conical tube for digestion, and submerged in 0.1% trypsin for 15–60 min at 37 °C. Afterwards, 10 mL of Dulbecco modified Eagle's medium (DMEM/F12) (Hyclone) supplemented with 10% fetal bovine serum (FBS) (Hyclone) was added to stop the trypsin digestion process. The samples were then centrifuged at 1 200 r/min and 4 °C for 6-8 min and resuspended in 1 mL of DMEM/F12 medium, and filtered through a 40 μm cell strainer. The flow-through samples were cultured continuously as SKP cells.

The HEK-293T cells were obtained from American type culture collection (ATCC, CAT#: CRL-3216) and cultured in DMEM high glucose (Hyclone), 10% FBS (Hyclone), 1% penicillin (Beyotime Biotechnology, China) and 1% streptomycin (Beyotime Biotechnology, China) in a 37 °C and 5% CO_2 incubator.

Lentiviral package and preparation

The lentiviruses were generated according to the manufacturer's protocols (Addgene, USA), with the viruses harvested at 48 h and 72 h after transfection and filtered with a 0.45 μm filter. The tree shrew SKPs were then infected with the viruses or the virus particles were concentrated by ultracentrifugation at 8 000 r/min and 4 °C for 3 h before *in vivo* infection. Polybrene (Sigma, USA) (final concentration 4 μg/mL) was added when the tree shrew SKPs were infected to promote infection efficiency as well as *in vivo* infection. Infected SKPs were screened with puromycin (Invitrogen, USA) after 72 h of infection, followed by cell amplification and identification.

Real-time quantitative PCR (qPCR)

The efficiency of ts*p53* (ts: tree shrew) shRNA was tested in tree shrew SKPs. Total RNA was isolated using Trizol reagent (Takara, Japan) and reverse transcription was performed using an iScript cDNA Synthesis Kit according to the manufacturer's instructions (Bio-Rad, USA). This was followed by quantitative real-time PCR using a SYBR Green Mix with Rox (Roche, USA). The primer sequences used were: tsGAPDH: 5′–ACGACCCCT TCATTGACTTG-3′and 5′-TCTCCATGGTGGTGAAGACA-3′; tsP53: 5′-CCACGGAAGACTGGTTCAAT-3′ and 5′-ACGTGCAGGTGA CAGACTTG-3′.

Lentiviral injection

After ketamine anesthetic (40 μg/g), the hair on the dorsum and tail of the tree shrews was shaved, with depilatory paste then applied to remove fine hair. Next, the pCDH-mSmoA1 lentivirus (5.6×10^5 TU), shRNA targeting tree shrew *p53* gene lentivirus (shp53, 2×10^5 TU), and control vector (pCDH-mSmoA1 group,

pCDH-mSmoA1 and shp53 group, and control group, respectively) were injected into a certain region of the dorsum and tail. At least 30 domesticated tree shrews (~6-weeks-old) were used. Both normal skin tissues and skin tumors were isolated and collected after animals were sacrificed at two weeks or two months on the dorsum and tail of the tree shrews, respectively. All tissues were fixed for immunohistochemical analysis or immediately frozen by liquid nitrogen and stored at –80 °C.

HE staining

Normal skin tissues and tumors were preserved in 10% phosphate- buffered formalin. Tissues were then processed for paraffin embedding and cut into 4 μm thick sections. Section samples were subjected to standard hematoxylin and eosin (HE) staining.

Statistical analysis

All data were presented as means±*SE* of a minimum of three replicates. For all analyses, we evaluated statistical differences using the Student's *t*-test. Each experiment was performed at least three times. Differences were considered significant if the *P* value was <0.05 (*: P<0.05, **: P<0.01, ***: P<0.001), compared with the control group.

RESULTS

We performed protein sequence alignment for the Smo protein among humans, tree shrews, and mice using Blast software (https://blast.ncbi.nlm.nih.gov/Blast.cgi). The results showed that the core transmembrane domains as well as the C-terminal of the human, mouse, and tree shrew Smo proteins were highly conserved, although the tree shrew Smo also contained an elongated N-terminal overhang, whose structural and functional roles need to be further validated. While we found that the oncogenic *SmoA1* mutation site (W539 in mice and W535 in humans) was highly conserved among all three species, as shown in Figure 1 (Taipale et al., 2000; Xie et al., 1998), we decided to induce BCC in tree shrew skins with the constitutive active form of SmoA1 for the following experiments (Chen et al., 2011). To validate the lentiviral titer and efficiency for tree shrew skin, we infected tree shrew SKPs with the viruses *in vitro*. As SmoA1 was tagged by green fluorescence protien (GFP), the green fluorescence percentage observed by the fluorescence microscope was used to validate infection efficiency (Figure 2A–C). The fluorescence analysis results showed that the SmoA1 lentivirus infected the tree shrew SKPs efficiently by more than 70% (Figure 2C). We also analyzed the Hh signaling pathway activity after lentiviral *SmoA1* expression, and found the *Ptch1* and *Gli1* mRNA expressions were up-regulated (Figure 2D).

The intracutaneous lentiviral injected dorsal areas of the tree shrew skin are shown in Figure 3B. All tree shrews were intracutaneously injected with 5.6×10^5 TU virus/injection site with either the control, SmoA1, or *p53* shRNA lentiviruses, respectively, or in combination. No significant weight lost was observed in the animals (data not shown). The total viral mixture volume was approximately 10 μL. Two weeks later, the pathologies of the lentivirus infected dorsal skins were analyzed by HE staining. We found that the pCDH-SmoA1 group exhibited human BCC-like pathological characteristics, such as hyperplasia of skin cells with hair follicle (HF) disruption, and pigmentation and nuclear explosion expansion (Figure 3C). However, black plaque did not develop into human-like BCC, even after a longer period. Since *p53* ablation has been frequently observed in BCC and other tumors, which could possibly speed up the process of BCC (Rady et al., 1992; Soussi & Béroud, 2001; Soussi et al., 2000; Wijnhoven et al., 2005), we constructed lentiviral expressing shRNAs targeting tree shrew *p53* with tdTomato expression driven by an individual PGK promoter, which was used to follow the shRNA expressing cells and tissues (Figure 4A). Fluorescence microscopy showed that positive red fluorescence approached 100% in tree shrew SKPs after lentiviral shp53-tdTomato infection (Figure 4B), and tree shrew *Tp53* mRNA knockdown efficiency by lentiviral shRNAs was confirmed by real-time PCR compared with scramble shRNA control (Figure 4C).

It has been documented previously that the vast majority of BCCs in a conditional mouse model (*K5–tTA*;*TRE–Gli2* bitransgenic mice) formed on the mice tails, ears, extremities, and dorsal skin (Hutchin et al., 2005). We tested BCC formation efficiency in the tail skins of tree shrews using the above lentiviruses. The results (Figure 4D) indicated that both SmoA1-GFP and shp53-tdTomato successfully infected the tree shrew tail skin. Furthermore, obvious BCC plaque and mass formation were found in the pCDH-SmoA1 group two months later, and the pCDH-mSmoA1 and shp53 groups showed the most malignancies. Statistically, ~40% of tree shrews showed BCC-like phenotypes after four weeks following the SmoA1 viral-injection alone, and reached 60% after 6–8 weeks. Interestingly, more than 70% of tree shrews showed BCC-like phenotypes two weeks after SmoA1 and *p53*-shRNA viral-injection, which reached to 100% after four weeks (Figure 4F). These data suggest that the Hh signaling pathway constitutively activated by SmoA1 overexpression induced tree shrew BCC pathogenesis, and knockdown of tumor suppressor *p53* could accelerate tree shrew BCC tumor progression.

DISCUSSION

Vismodegib has been used recently for metastatic or advanced BCC in clinical trials, showing good effect in phase I trials (Graham et al., 2011; Lorusso et al., 2011; Von Hoff et al., 2009), but only 30% of metastatic and 43% of locally advanced BCC patients treated with vismodegib have demonstrated a good response in Phase II trials (Sekulic et al., 2012). In Phase I study of sonidegib, 37% of BCC patients achieved partial or complete response, whereas 42% of BCC patients in Phase 2 responded well to treatment with 200 mg of sonidegib per day orally (Migden et al., 2015). Collectively, these studies suggest that downstream inhibitors of Hh signaling and a combination of therapies targeting other pathways using better animal models are required. Here, we showed that lentiviral injection of SmoA1 and shp53 could induce BCCs in tree shrew skins successfully.

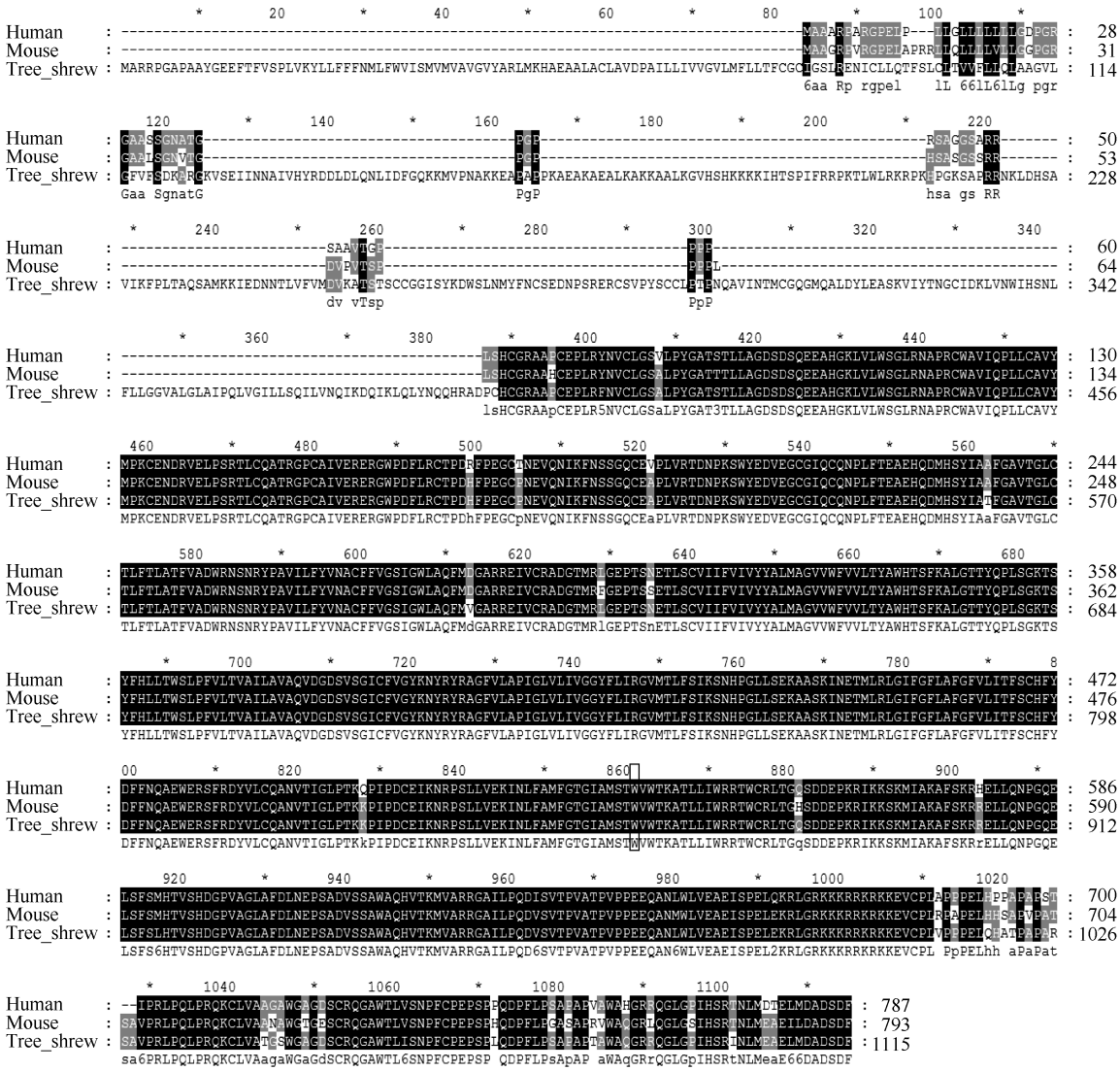

Figure 1 Comparison of human, tree shrew, and mouse Smoothened proteins

Protein sequence alignment results showed that *Smoothened* (*Smo*) was highly conserved among tree shrews (TSDB Protein sequence: TSDBP00001058), mice (GenBank Accession No: NM_176996.4), and humans (GenBank Accession No: NM_005631.4). The Smoothened A1 site was identical among the three species and is marked by a black frame. Ts: tree shrew.

In addition, a recent study indicated that the MK-4101 molecule can attenuate the Hh signaling pathway through inhibition of Gli, alteration of IGF, and Wnt signaling pathway activities, thus proving to be a promising therapeutic drug for BCC patients (Filocamo et al., 2016). A second-generation antifungal drug posaconazole, which showed distinct mechanisms from cyclopamine or cyclopamine competitive inhibitors, exhibits better drug-drug interaction and fewer side effects than current SMO inhibitors, and could provide a novel strategy for clinical drug combinational therapy (Chen et al., 2016).

In general, older adults suffering from BCC receive Hh signaling pathway inhibitor treatment. Premenopausal women are also subjected to menopause due to the reversal of chorionic hormone receptor inhibition (Simone et al., 2016). Furthermore, many dermatologists are not familiar with the side effects of such treatment, thus consulting professional practitioners about teratogenicity and sequelae of ovarian failure is required. New or persistent ulcers, nodules, or erythema after three months of treatment with Hh signaling pathway inhibitors have been found by biopsy (Simone et al., 2016; Zhu et al., 2014), therefore all skin should be monitored during the whole treatment process (Simone et al., 2016; Zhu et al., 2014). At the same time, non-BCC damage should also be given comprehensive treatment because synchronous occult amelanotic melanoma has been reported in 25% (3/12) of BCC patients (Simone et al., 2016; Zhu et al., 2014). Two BCC patients, five years after Hh signaling pathway inhibitor treatment, have survived by paying close attention to and interfering with various side effects (Jacobsen et al., 2017).

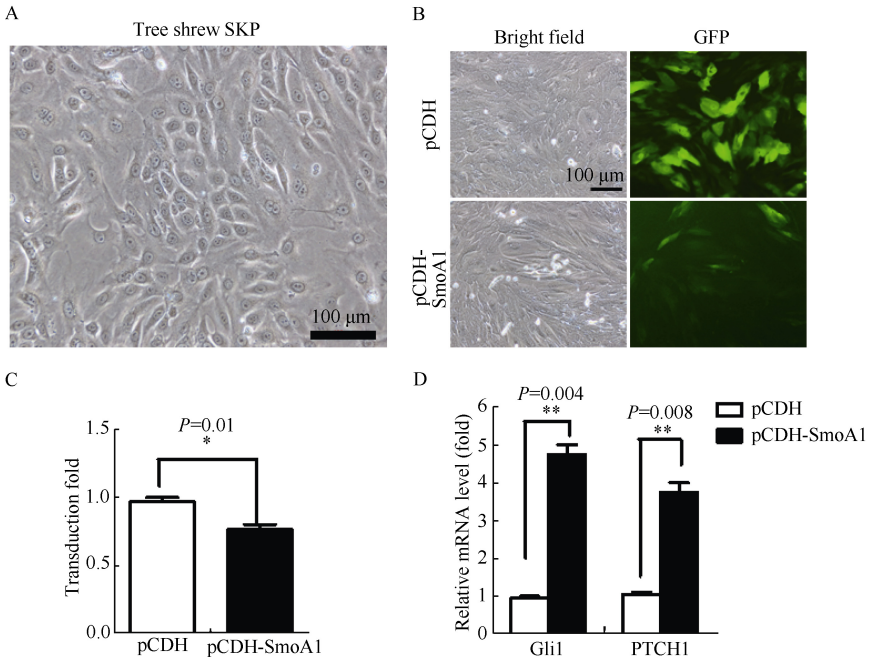

Figure 2 Lentivirus SmoA1 efficiently infected tree shrew SKPs

A: Representative image of tree shrew SKPs; B: SmoA1 lentivirus infected SKPs with high efficiency. pCDH empty vector was used as the control; C: Relative virus titer determination in SKPs by fluorescence microscopy between pCDH vector and pCDH-SmoA1 lentivirus groups; D: Relative mRNA expressions of *Gli1* and *Ptch1* were determined by real-time PCR, cells were SKPs infected with indicated lentiviruses. Data are presented as mean±*SE* (*: $P<0.5$; **: $P<0.1$).

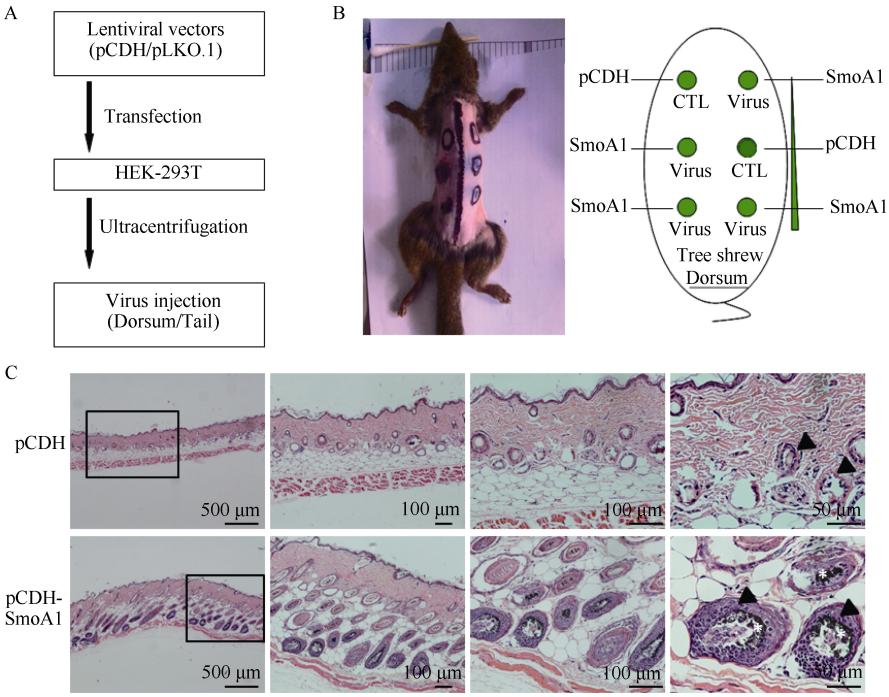

Figure 3 Over-expression of SmoA1 induced BCC-like hyperplasia in dorsal skins of the tree shrews *in vivo*

A: Flow chart for lentivirus preparation; B: Viral injection design in dorsal areas of tree shrew skin; C: Representative images under different magnifications (4×, 10×, 20×, 40×) with HE staining. Results showed BCC-like hyperplasia of skin cells with hair follicle (HF) disruption (arrow head), pigmentation (asterisk), and nuclear explosion expansion after viral injection two weeks later. The pCDH-vector served as the control viral injection.

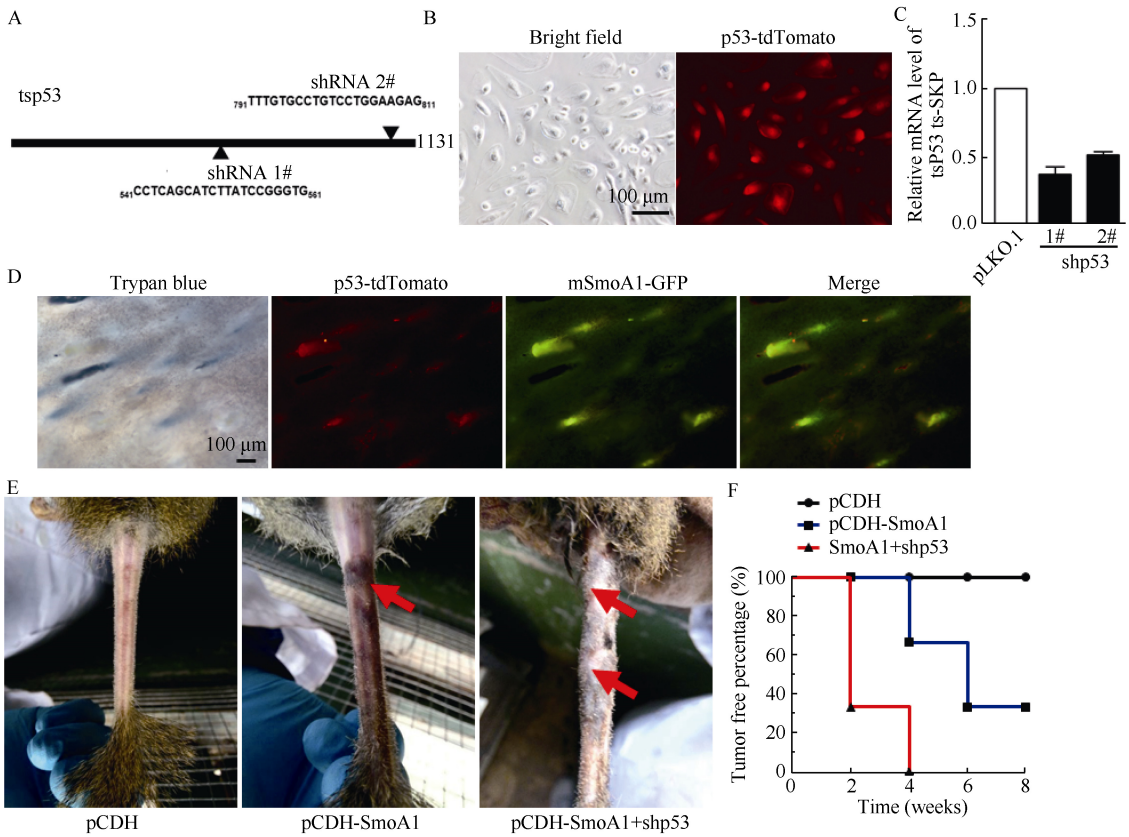

Figure 4 BCC formation in tree shrew tail skins by combined usage of SmoA1 and shp53 viruses

A: Diagram of two shRNAs targeting tree shrew *p53*; B: Lentivirus expressing shRNAs co-expressing tdTomato infected SKPs *in vitro* efficiently; C: shp53 knockdown efficiency was verified by real-time PCR, cells were SKPs infected with indicated viruses; D: The tree shrew tail skins formed BCC tumors efficiently. Trypan blue, tdTomato, and GFP indicate the locations of the injected viruses; E: Representative images of BCC originated from the tails of tree shrews with indicated treatment (empty vector, SmoA1 or/in combination with shp53, respectively); F: Percentage curve of tumor-free tree shrews shows that the combination of lentiviral SmoA1 and shp53 (median time: two weeks) accelerated BCC formation in tails compared with SmoA1 alone (median time: six weeks). *n*=6, separately.

Recent research, which established EGFP-tagged transgenic tree shrews following spermatogonial stem cell (SSC) transplantation, provided a good approach for the generation of multiple human disease models using the tree shrew by gene editing manipulation (Li et al., 2017). Although BCC was not observed in DMBA/TPA combination treated wild-type mice (Indra et al., 2007), it has been successfully generated in $Ptch^{flox/flox}CD4Cre^{+/-}$ mice (Uhmann et al., 2014). Thus, it would be interesting to combine DMBA/TPA with lentiviral SmoA1and p53-shRNA in tree shrew skins in the future.

PTEN (phosphatase and tensin homolog deleted on chromosome 10) plays critical roles in tissue homeostasis and cancer development, and is a commonly mutated tumor suppressor gene (Salmena et al., 2008). Earlier research showed that 100% of mice with complete *Pten* deficiency in their keratinocytes and a proportion with *Pten* heterozygosity, developed NMSC spontaneously (Suzuki et al., 2003). Deletions of *Pten* in BCC are an infrequent event (Quinn et al., 1994), implicating that *Pten* is a significant suppressor of non-melanoma skin tumorigenesis (Hertzler-Schaefer et al., 2014; Macdonald et al., 2014; Ming & He, 2009). To improve the BCC tree shrew model, loss of PTEN function as well as UV radiation might stimulate low-level Hh signaling caused by mutations in Hh pathway components via the up-regulation of the PI3K/AKT pathway and DNA damage-related signaling activation, respectively (Ming & He, 2009; Ouhtit et al., 1998).

BCCs are closely related to abnormal oncogenic activation of the Hh pathway, which can have different functions and mechanisms between different species, the closer relationship between different species, the closer functions and mechanisms of relative genes. These similar biological characteristics between animals and human allow for the mimicry of human tumor progression. However, there are limits to murine animal models. Genome analysis has verified that the tree shrew is closely related to primates (Fan et al., 2013) and is superior to murine species. Small body size, low-cost maintenance, short reproductive cycle and life span, and its close relationship to primates make the tree shrew a safer, more efficient, and more predictable animal model, therefore surpassing murine species in the testing of drug efficacy and safety and deciphering the

pathogenesis of BCC. Here we established, for the first time, a tree shrew BCC model that successfully simulated human BCC pathological features. However, the molecular markers of BCCs are needed to confirm this model at the molecular level. It would be interesting to use current clinical BCC-treatment drugs, such as vismodegib, to validate the efficiency and effects of the tree shrew BCC model. Furthermore, this model could be used to screen novel natural compounds that might function alone or in synergy with current clinical drugs to treat BCC.

REFERENCES

Abarca JF, Casiccia CC. 2002. Skin cancer and ultraviolet-B radiation under the Antarctic ozone hole: southern Chile, 1987-2000. *Photodermatology, Photoimmunology & Photomedicine,* **18**(6): 294-302.

Amako Y, Tsukiyama-Kohara K, Katsume A, Hirata Y, Sekiguchi S, Tobita Y, Hayashi Y, Hishima T, Funata N, Yonekawa H, Kohara M. 2010. Pathogenesis of hepatitis C virus infection in *Tupaia belangeri*. *Journal of Virology*, **84**(1): 303-311.

Arad S, Zattra E, Hebert J, Epstein EH, Jr., Goukassian DA, Gilchrest BA. 2008. Topical thymidine dinucleotide treatment reduces development of ultraviolet-induced basal cell carcinoma in *Ptch-1*$^{+/-}$ mice. *The American Journal of Pathology,* **172**(5): 1248-1255.

Asgari MM, Moffet HH, Ray GT, Quesenberry CP. 2015. Trends in basal cell carcinoma incidence and identification of high-risk subgroups, 1998-2012. *JAMA Dermatology,* **151**(9): 976-981.

Aszterbaum M, Beech J, Epstein EH, Jr. 1999. Ultraviolet radiation mutagenesis of hedgehog pathway genes in basal cell carcinomas. *Journal of Investigative Dermatology Symposium Proceedings,* **4**(1): 41-45.

Bastiaens MT, Hoefnagel JJ, Vermeer BJ, Bavinck JNB, Bruijn JA, Westendorp RGJ. 1998. Differences in age, site distribution, and sex between nodular and superficial basal cell carcinomas indicate different types of tumors. *Journal of Investigative Dermatology,* **110**(6): 880-884.

Betti R, Radaelli G, Crosti C, Ghiozzi S, Moneghini L, Menni S. 2012. Margin involvement and clinical pattern of basal cell carcinoma with mixed histology. *Journal of the European Academy of Dermatology and Venereology,* **26**(4): 483-487.

Biernaskie JA, Mckenzie IA, Toma JG, Miller FD. 2007. Isolation of skin-derived precursors (SKPs) and differentiation and enrichment of their Schwann cell progeny. *Nature Protocols,* **1**(6): 2803-2812.

Bonilla X, Parmentier L, King B, Bezrukov F, Kaya G, Zoete V, Seplyarskiy VB, Sharpe HJ, McKee T, Letourneau A, Ribaux PG, Popadin K, Basset-Seguin N, Chaabene RB, Santoni FA, Andrianova MA, Guipponi M, Garieri M, Verdan C, Grosdemange K, Sumara O, Eilers M, Aifantis I, Michielin O, de Sauvage FJ, Antonarakis SE, Nikolaev SI. 2016. Genomic analysis identifies new drivers and progression pathways in skin basal cell carcinoma. *Nature Genetics,* **48**(4): 398-406.

Burness CB. 2015. Sonidegib: first global approval. *Drugs,* **75**(13): 1559-1566.

Chen BZ, Trang V, Lee A, Williams NS, Wilson AN, Epstein EH, Jr., Tang JY, Kim J. 2016. Posaconazole, a second-generation triazole antifungal drug, inhibits the hedgehog signaling pathway and progression of basal cell carcinoma. *Molecular Cancer Therapeutics,* **15**(5): 866-876.

Chen JG, Fleischer AB, Jr., Smith ED, Kancler C, Goldman ND, Williford PM, Feldman SR. 2001. Cost of nonmelanoma skin cancer treatment in the United States. *Dermatologic Surgery,* **27**(12): 1035-1038.

Chen YB, Sasai N, Ma GQ, Yue T, Jia JH, Briscoe J, Jiang J. 2011. Sonic Hedgehog dependent phosphorylation by CK1α and GRK2 is required for ciliary accumulation and activation of smoothened. *PLoS Biology,* **9**(6): e1001083.

Chen YB, Jiang J. 2013. Decoding the phosphorylation code in Hedgehog signal transduction. *Cell Research,* **23**(2): 186-200.

Chen YH, Wang YH, Yu TH, Wu HJ, Pai CW. 2009. Transgenic zebrafish line with over-expression of Hedgehog on the skin: a useful tool to screen Hedgehog-inhibiting compounds. *Transgenic Research,* **18**(6): 855-864.

Christenson LJ, Borrowman TA, Vachon CM, Tollefson MM, Otley CC, Weaver AL, Roenigk RK. 2005. Incidence of basal cell and squamous cell carcinomas in a population younger than 40 years. *JAMA,* **294**(6): 681-690.

de Giorgi V, Salvini C, Massi D, Raspollini MR, Carli P. 2005. Vulvar basal cell carcinoma: retrospective study and review of literature. *Gynecologic Oncology,* **97**(1): 192-194.

de Giorgi V, Massi D, Lotti T. 2006. Basal-cell carcinoma. *The New England Journal of Medicine,* **354**(7): 769-771.

De Zwaan SE, Haass NK. 2010. Genetics of basal cell carcinoma. *Australasian Journal of Dermatology,* **51**(2): 81-92.

Demers AA, Nugent Z, Mihalcioiu C, Wiseman MC, Kliewer EV. 2005. Trends of nonmelanoma skin cancer from 1960 through 2000 in a Canadian population. *Journal of the American Academy of Dermatology,* **53**(2): 320-328.

Dlugosz A, Agrawal S, Kirkpatrick P. 2012. Vismodegib. *Nature Reviews Drug Discovery,* **11**(6): 437-438.

Elliot OS, Elliot MW, Lisco H. 1966. Breast cancer in a tree shrew (*Tupaia glis*). *Nature,* **211**(5053): 1105.

Endo H, Mifune H, Maeda S, Kimura J, Yamada J, Rerkamnuaychoke W, Chungsamarnyart N, Ogawa K, Kurohmaru M, Hayashi Y. 1997. Cardiac-like musculature of the intrapulmonary venous wall of the long-clawed shrew (Sorex unguiculatus), common tree shrew (Tupaia glis) and common marmoset (Callithrix jacchus). *Anatomical Record-advances in Integrative Anatomy & Evolutionary Biology*, **247**(1): 46-52.

Fan Y, Huang ZY, Cao CC, Chen CS, Chen YX, Fan DD, He J, Hou HL, Hu L, Hu XT, Jiang XT, Lai R, Lang YS, Liang B, Liao SG, Mu D, Ma YY, Niu YY, Sun XQ, Xia JQ, Xiao J, Xiong ZQ, Xu L, Yang L, Zhang Y, Zhao W, Zhao XD, Zheng YT, Zhou JM, Zhu YB, Zhang GJ, Wang J, Yao YG. 2013. Genome of the Chinese tree shrew. *Nature Communications,* **4**: 1426.

Filocamo G, Brunetti M, Colaceci F, Sasso R, Tanori M, Pasquali E, Alfonsi R, Mancuso M, Saran A, Lahm A, Di Marcotullio L, Steinkühler C, Pazzaglia S. 2016. MK-4101, a Potent inhibitor of the hedgehog pathway, is highly active against medulloblastoma and basal cell carcinoma. *Molecular Cancer Therapeutics,* **15**(6): 1177-1189.

Fuchs E. 2005. Social stress in tree shrews as an animal model of depression: an example of a behavioral model of a CNS disorder. *CNS Spectrums,* **10**(3): 182-190.

Ge GZ, Xia HJ, He BL, Zhang HL, Liu WJ, Shao M, Wang CY, Xiao J, Ge F, Li FB, Chen CS. 2016. Generation and characterization of a breast carcinoma model by PyMT overexpression in mammary epithelial cells of tree shrew, an animal close to primates in evolution. *International Journal of Cancer,* **138**(3): 642-651.

Ghaderi R, Haghighi F. 2005. Immunohistochemistry assessment of p53 protein in Basal cell carcinoma. *Iranian journal of Allergy, Asthma and*

Immunology, **4**(4): 167-171.

Giorgi VD, Salvini C, Massi D, Raspollini MR, Carli P. 2005. Vulvar basal cell carcinoma: retrospective study and review of literature. *Gynecologic Oncology*, **97**(1): 192-194.

Graham RA, Lum BL, Cheeti S, Jin JY, Jorga K, Von Hoff DD, Rudin CM, Reddy JC, Low JA, Lorusso PM. 2011. Pharmacokinetics of hedgehog pathway inhibitor vismodegib (GDC-0449) in patients with locally advanced or metastatic solid tumors: the role of alpha-1-acid glycoprotein binding. *Clinical cancer research : an official journal of the American Association for Cancer Research*, **17**(8): 2512-2520.

Hallahan AR, Pritchard JI, Hansen S, Benson M, Stoeck J, Hatton BA, Russell TL, Ellenbogen RG, Bernstein ID, Beachy PA, Olson JM. 2004. The SmoA1 mouse model reveals that notch signaling is critical for the growth and survival of sonic hedgehog-induced medulloblastomas. *Cancer Research,* **64**(21): 7794-7800.

He BL, Xia HJ, Jiao JL, Wang CY, Zhang HL. 2016. Pathological analysis of the induced breast tumor models in tree shrew. *Chinese Journal of Comparative Medicine,* **26**(3): 6-10. (in Chinese)

Hertzler-Schaefer K, Mathew G, Somani AK, Tholpady S, Kadakia MP, Chen YP, Spandau DF, Zhang X. 2014. Pten loss induces autocrine FGF signaling to promote skin tumorigenesis. *Cell Reports,* **6**(5): 818-826.

Hutchin ME, Kariapper MST, Grachtchouk M, Wang AQ, Wei LB, Cummings D, Liu JH, Michael LE, Glick A, Dlugosz AA. 2005. Sustained Hedgehog signaling is required for basal cell carcinoma proliferation and survival: conditional skin tumorigenesis recapitulates the hair growth cycle. *Genes & Development,* **19**(2): 214-223.

Indra AK, Castaneda E, Antal MC, Jiang M, Messaddeq N, Meng XJ, Loehr CV, Gariglio P, Kato S, Wahli W, Desvergne B, Metzger D, Chambon P. 2007. Malignant transformation of DMBA/TPA-induced papillomas and nevi in the skin of mice selectively lacking retinoid-X-receptor α in epidermal keratinocytes. *Journal of Investigative Dermatology,* **127**(5): 1250-1260.

Jacobsen AA, Kydd AR, Strasswimmer J. 2017. Practical management of the adverse effects of Hedgehog pathway inhibitor therapy for basal cell carcinoma. *Journal of the American Academy of Dermatology,* **76**(4): 767-768.

Kim J, Aftab BT, Tang JY, Kim D, Lee AH, Rezaee M, Kim J, Chen BZ, King EM, Borodovsky A, Riggins GJ, Epstein EH, Jr., Beachy PA, Rudin CM. 2013. Itraconazole and arsenic trioxide inhibit Hedgehog pathway activation and tumor growth associated with acquired resistance to smoothened antagonists. *Cancer Cell,* **23**(1): 23-34.

Lacour JP. 2002. Carcinogenesis of basal cell carcinomas: genetics and molecular mechanisms. *British Journal of Dermatology,* **146**(S61): 17-19.

Lee HY, Na YR, Seok SH, Baek MW, Kim DJ, Park SH, Lee HK, Lee BH, Park JH. 2010. Spontaneous basal cell carcinoma in a 7-week-old Sprague-Dawley rat. *Veterinary Pathology,* **47**(1): 137-139.

Li CH, Yan LZ, Ban WZ, Tu Q, Wu Y, Wang L, Bi R, Ji S, Ma YH, Nie WH, Lv LB, Yao YG, Zhao XD, Zheng P. 2017. Long-term propagation of tree shrew spermatogonial stem cells in culture and successful generation of transgenic offspring. *Cell Research,* **27**(2): 241-252.

Li SA, Lee WH, Zhang Y. 2012. Two bacterial infection models in tree shrew for evaluating the efficacy of antimicrobial agents. *Zoological Research,* **33**(1): 1-6.

Li ZJ, Mack SC, Mak TH, Angers S, Taylor MD, Hui CC. 2014. Evasion of p53 and G_2/M checkpoints are characteristic of Hh-driven basal cell carcinoma. *Oncogene,* **33**(20): 2674-2680.

Lomas A, Leonardi-Bee J, Bath-Hextall F. 2012. A systematic review of worldwide incidence of nonmelanoma skin cancer. *British Journal of Dermatology,* **166**(5): 1069-1080.

LoRusso PM, Rudin CM, Reddy JC, Tibes R, Weiss GJ, Borad MJ, Hann CL, Brahmer JR, Chang I, Darbonne WC, Graham RA, Zerivitz KL, Low JA, Von Hoff DD. 2011. Phase I trial of hedgehog pathway inhibitor vismodegib (GDC-0449) in patients with refractory, locally advanced or metastatic solid tumors. *Clinical Cancer Research*, **17**(8): 2502-2511.

Macdonald FH, Yao D, Quinn JA, Greenhalgh DA. 2014. PTEN ablation in Ras^{Ha}/Fos skin carcinogenesis invokes p53-dependent p21 to delay conversion while p53-independent p21 limits progression via cyclin D1/E2 inhibition. *Oncogene,* **33**(32): 4132-4143.

Madan V, Lear JT, Szeimies RM. 2010. Non-melanoma skin cancer. *The Lancet,* **375**(9715): 673-685.

Makinodan E, Marneros AG. 2012. Protein kinase A activation inhibits oncogenic Sonic hedgehog signalling and suppresses basal cell carcinoma of the skin. *Experimental Dermatology,* **21**(11): 847-852.

Migden MR, Guminski A, Gutzmer R, Dirix L, Lewis KD, Combemale P, Herd RM, Kudchadkar R, Trefzer U, Gogov S, Pallaud C, Yi TT, Mone M, Kaatz M, Loquai C, Stratigos AJ, Schulze HJ, Plummer R, Chang ALS, Cornélis F, Lear JT, Sellami D, Dummer R. 2015. Treatment with two different doses of sonidegib in patients with locally advanced or metastatic basal cell carcinoma (BOLT): a multicentre, randomised, double-blind phase 2 trial. *The Lancet Oncology,* **16**(6): 716-728.

Ming M, He YY. 2009. PTEN: new insights into its regulation and function in skin cancer. *Journal of investigative Dermatology,* **129**(9): 2109-2112.

Mohan SV, Chang ALS. 2014. Advanced basal cell carcinoma: epidemiology and therapeutic innovations. *Current Dermatology Reports,* **3**(1): 40-45.

Moles JP, Moyret C, Guillot B, Jeanteur P, Guilhou JJ, Theillet C, Basset-Sèguin N. 1993. p53 gene mutations in human epithelial skin cancers. *Oncogene,* **8**(3): 583-588.

Mudigonda T, Pearce DJ, Yentzer BA, Williford P, Feldman SR. 2010. The economic impact of non-melanoma skin cancer: a review. *Journal of the National Comprehensive Cancer Network,* **8**(8): 888-896.

Nitzki F, Zibat A, König S, Wijgerde M, Rosenberger A, Brembeck FH, Carstens PO, Frommhold A, Uhmann A, Klingler S, Reifenberger J, Pukrop T, Aberger F, Schulz-Schaeffer W, Hahn H. 2010. Tumor stroma-derived Wnt5a induces differentiation of basal cell carcinoma of *Ptch*-mutant mice via CaMKII. *Cancer Research,* **70**(7): 2739-2748.

Norton TT, Amedo AO, Siegwart JT, Jr. 2006. Darkness causes myopia in visually experienced tree shrews. *Investigative Opthalmology & Visual Science,* **47**(11): 4700.

Nuccitelli R, Tran K, Athos B, Kreis M, Nuccitelli P, Chang KS, Epstein EH, Jr., Tang JY. 2012. Nanoelectroablation therapy for murine basal cell carcinoma. *Biochemical and Biophysical Research Communications,* **424**(3): 446-450.

Ouhtit A, Nakazawa H, Armstrong BK, Kricker A, Tan E, English DR. 1998. UV-radiation-specific p53 mutation frequency in normal skin as a predictor of risk of basal cell carcinoma. *Journal of the National Cancer Institute,* **90**(7): 523-531.

Quinn AG, Sikkink S, Rees JL. 1994. Basal cell carcinomas and squamous cell carcinomas of human skin show distinct patterns of chromosome loss. *Cancer Research,* **54**(17): 4756-4759.

Rady P, Scinicariello F, Wagner RF, Jr., Tyring SK. 1992. p53 mutations in basal cell carcinomas. *Cancer Research,* **52**(13): 3804-3806.

Rawashdeh MA, Matalka I. 2004. Basal cell carcinoma of the maxillofacial region: site distribution and incidence rates in Arab/Jordanians, 1991 to 2000. *Journal of Oral and Maxillofacial Surgery,* **62**(2): 145-149.

Reifenberger J, Wolter M, Knobbe CB, Köhler B, Schönicke A, Scharwächter C, Kumar K, Blaschke B, Ruzicka T, Reifenberger G. 2005. Somatic mutations in the *PTCH*, *SMOH*, *SUFUH* and *TP53* genes in sporadic basal cell carcinomas. *British Journal of Dermatology,* **152**(1): 43-51.

Rogers HW, Weinstock MA, Feldman SR, Coldiron BM. 2015. Incidence Estimate of Nonmelanoma Skin Cancer (Keratinocyte Carcinomas) in the U.S. Population, 2012. *JAMA Dermatology,* **151**(10): 1081-1086.

Rubin AI, Chen EH, Ratner D. 2005. Basal-cell carcinoma. *The New England journal of medicine*, **353**(21): 2262-2269.

Salmena L, Carracedo A, Pandolfi PP. 2008. Tenets of PTEN tumor suppression. *Cell,* **133**(3): 403-414.

Scrivener Y, Grosshans E, Cribier B. 2002. Variations of basal cell carcinomas according to gender, age, location and histopathological subtype. *British Journal of Dermatology,* **147**(1): 41-47.

Sekulic A, Migden MR, Oro AE, Dirix L, Lewis KD, Hainsworth JD, Solomon JA, Yoo S, Arron ST, Friedlander PA, Marmur E, Rudin CM, Chang ALS, Low JA, Mackey HM, Yauch RL, Graham RA, Reddy JC, Hauschild A. 2012. Efficacy and safety of vismodegib in advanced basal-cell carcinoma. *The New England Journal of Medicine,* **366**(23): 2171-2179.

Sekulic A, Von Hoff D. 2016. Hedgehog pathway inhibition. *Cell,* **164**(5): 831.

Siegel RL, Miller KD, Jemal A. 2016. Cancer statistics, 2016. *CA*: *A Cancer Journal for Clinicians,* **66**(1): 7-30.

Simone PD, Schwarz JM, Strasswimmer JM. 2016. Four-year experience with vismodegib hedgehog inhibitor therapy. *Journal of the American Academy of Dermatology*, **74**(6): 1264-1265

Skvara H, Kalthoff F, Meingassner JG, Wolff-Winiski B, Aschauer H, Kelleher JF, Wu X, Pan SF, Mickel L, Schuster C, Stary G, Jalili A, David OJ, Emotte C, Antunes AMC, Rose K, Decker J, Carlson I, Gardner H, Stuetz A, Bertolino AP, Stingl G, De Rie MA. 2011. Topical treatment of Basal cell carcinomas in nevoid Basal cell carcinoma syndrome with a smoothened inhibitor. *The Journal of Investigative Dermatology,* **131**(8): 1735-1744.

So PL, Lee K, Hebert J, Walker P, Lu Y, Hwang J, Kopelovich L, Athar M, Bickers D, Aszterbaum M, Epstein EH, Jr. 2004. Topical tazarotene chemoprevention reduces Basal cell carcinoma number and size in Ptch1+/- mice exposed to ultraviolet or ionizing radiation. *Cancer Research,* **64**(13): 4385-4389.

Soussi T, Béroud C. 2001. Assessing *TP53* status in human tumours to evaluate clinical outcome. *Nature Reviews Cancer,* **1**(3): 233-239.

Soussi T, Dehouche K, Béroud C. 2000. p53 website and analysis of p53 gene mutations in human cancer: forging a link between epidemiology and carcinogenesis. *Human mutation,* **15**(1): 105-113.

Staples MP, Elwood M, Burton RC, Williams JL, Marks R, Giles GG. 2006. Non-melanoma skin cancer in Australia: the 2002 national survey and trends since 1985. *Medical Journal of Australia,* **184**(1): 6-10.

Sun YM, Yang JZ, Sun HY, Ma YY, Wang JH. 2012. Establishment of tree shrew chronic morphine dependent model. *Zoological Research,* **33**(1): 14-18. (in Chinese)

Suzuki A, Itami S, Ohishi M, Hamada K, Inoue T, Komazawa N, Senoo H, Sasaki T, Takeda J, Manabe M, Mak TW, Nakano T. 2003. Keratinocyte-specific pten deficiency results in epidermal hyperplasia, accelerated hair follicle morphogenesis and tumor formation. *Cancer Research,* **63**(3): 674-681.

Taipale J, Chen JK, Cooper MK, Wang BL, Mann RK, Milenkovic L, Scott MP, Beachy PA. 2000. Effects of oncogenic mutations in *Smoothened* and *Patched* can be reversed by cyclopamine. *Nature,* **406**(6799): 1005-1009.

Tang JY, Mackay-Wiggan JM, Aszterbaum M, Yauch RL, Lindgren J, Chang K, Coppola C, Chanana AM, Marji J, Bickers DR, Epstein EH, Jr. 2012. Inhibiting the hedgehog pathway in patients with the basal-cell nevus syndrome. *The New England Journal of Medicine,* **366**(23): 2180-2188.

Teglund S, Toftgård R. 2010. Hedgehog beyond medulloblastoma and basal cell carcinoma. *Biochimica et Biophysica Acta (BBA)-Reviews on Cancer,* **1805**(2): 181-208.

Tong YH, Hao JJ, Tu Q, Yu HL, Yan LZ, Li Y, Lv LB, Wang F, Iavarone A, Zhao XD. 2017. A tree shrew glioblastoma model recapitulates features of human glioblastoma. *Oncotarget,* **8**(11): 17897-17907.

Uhmann A, Heß I, Frommhold A, König S, Zabel S, Nitzki F, Dittmann K, Lühder F, Christiansen H, Reifenberger J, Schulz-Schaeffer W, Hahn H. 2014. DMBA/TPA treatment is necessary for BCC formation from patched deficient epidermal cells in $Ptch^{flox/flox}CD4Cre^{+/-}$ mice. *Journal of Investigative Dermatology,* **134**(10): 2620-2629.

carcinoma. *The Journal of Investigative Dermatology,* **104**(6): 928-932.

Von Hoff DD, LoRusso PM, Rudin CM, Reddy JC, Yauch RL, Tibes R, Weiss GJ, Borad MJ, Hann CL, Brahmer JR, Mackey HM, Lum BL, Darbonne WC, Marsters JC, Jr., de Sauvage FJ, Low JA. 2009. Inhibition of the hedgehog pathway in advanced basal-cell carcinoma. *New England Journal of Medicine,* **361**(12): 1164-1172.

Wang GY, Wood CN, Dolorito JA, Libove E, Epstein EH, Jr. 2017. Differing tumor-suppressor functions of Arf and p53 in murine basal cell carcinoma initiation and progression. *Oncogene,* **36**(26): 3772-3780, doi: 10.1038/onc.2017.12.

Wang J, Zhou QX, Tian M, Yang YX, Xu L. 2011. Tree shrew models: a chronic social defeat model of depression and a one-trial captive conditioning model of learning and memory. *Zoological Research,* **32**(1): 24-30.

Wang J, Zhou QX, Lü LB, Xu L, Yang YX. 2012. A depression model of social defeat etiology using tree shrews. *Zoological Research,* **33**(1): 92-98. (in Chinese)

Wang J, Chai AP, Zhou QX, Lv LB, Wang LP, Yang YX, Xu L. 2013. Chronic clomipramine treatment reverses core symptom of depression in subordinate tree shrews. *PLoS One,* **8**(12): e80980.

Wijnhoven SWP, Zwart E, Speksnijder EN, Beems RB, Olive KP, Tuveson DA, Jonkers J, Schaap MM, Van Den Berg J, Jacks T, Van Steeg H, De Vries A. 2005. Mice expressing a mammary gland-specific R270H mutation in the *p53* tumor suppressor gene mimic human breast cancer development. *Cancer Research,* **65**(18): 8166-8173.

Wörmann SM, Song L, Ai JY, Diakopoulos KN, Kurkowski MU, Görgülü K, Ruess D, Campbell A, Doglioni C, Jodrell D, Neesse A, Demir IE, Karpathaki AP, Barenboim M, Hagemann T, Rose-John S, Sansom O, Schmid RM, Protti MP, Lesina M, Algül H. 2016. Loss of P53 function activates JAK2-STAT3 signaling to promote pancreatic tumor growth, stroma modification, and gemcitabine resistance in mice and is associated with patient survival. *Gastroenterology,* **151**(1): 180-193.e12.

Wu DW, Lee MC, Wang J, Chen CY, Cheng YW, Lee H. 2014. DDX3 loss by p53 inactivation promotes tumor malignancy via the MDM2/Slug/E-cadherin pathway and poor patient outcome in non-small-cell lung cancer. *Oncogene,* **33**(12): 1515-1526.

Wu XY, Li YH, Chang Q, Zhang LQ, Liao SS, Liang B. 2013. Streptozotocin induction of type 2 diabetes in tree shrew. *Zoological Research,* **34**(2): 108-115. (in Chinese)

Wu XY, Xu HB, Zhang ZG, Chang Q, Liao SS, Zhang LQ, Li YH, Wu DD, Liang B. 2016. Transcriptome profiles using next-generation sequencing reveal liver changes in the early stage of diabetes in tree shrew (*Tupaia belangeri chinensis*). *Journal of Diabetes Research,* **2016**:6238526.

Xia HJ, Wang CY, Zhang HL, He BL, Jiao JL, Chen CS. 2012. Characterization of spontaneous breast tumor in tree shrews (*Tupaia belangeri chinenesis*). *Zoological Research,* **33**(1): 55-59. (in Chinese)

Xiao J, Liu R, Chen CS. 2017. Tree shrew (*Tupaia belangeri*) as a novel laboratory disease animal model. *Zoological Research,* **38**(3): 127-137. .

Xie JW, Murone M, Luoh SM, Ryan A, Gu QM, Zhang CH, Bonifas JM, Lam CW, Hynes M, Goddard A, Rosenthal A, Epstein EH, Jr., De Sauvage FJ. 1998. Activating *Smoothened* mutations in sporadic basal-cell carcinoma. *Nature,* **391**(6662): 90-92.

Xu L, Zhang Y, Liang B, Lü LB, Chen CS, Chen YB, Zhou JM, Yao YG. 2013. Tree shrews under the spot light: emerging model of human diseases. *Zoological Research,* **34**(2): 59-69. (in Chinese)

Yan RQ, Su JJ, Huang DR, Gan YC, Yang C, Huang GH. 1996. Human hepatitis B virus and hepatocellular carcinoma. II. Experimental induction of hepatocellular carcinoma in tree shrews exposed to hepatitis B virus and aflatoxin B1. *Journal of Cancer Research and Clinical Oncology,* **122**(5): 289-295.

Yang CP, Chen WL, Chen YB, Jiang J. 2012. Smoothened transduces Hedgehog signal by forming a complex with Evc/Evc2. *Cell Research,* **22**(11): 1593-1604.

Yang EB, Cao J, Su JJ, Chow P. 2005. The tree shrews: useful animal models for the viral hepatitis and hepatocellular carcinoma. *Hepatogastroenterology,* **52**(62): 613-616.

Yao YG. 2017. Creating animal models, why not use the Chinese tree shrew (*Tupaia belangeri chinensis*)? *Zoological Research,* **38**(3): 118-126.

Yauch RL, Dijkgraaf GJP, Alicke B, Januario T, Ahn CP, Holcomb T, Pujara K, Stinson J, Callahan CA, Tang T, Bazan JF, Kan ZY, Seshagiri S, Hann CL, Gould SE, Low JA, Rudin CM, de Sauvage FJ. 2009. *Smoothened* mutation confers resistance to a Hedgehog pathway inhibitor in medulloblastoma. *Science,* **326**(5952): 572-574.

Zhang LQ, Zhang ZG, Li YH, Liao SS, Wu XY, Chang Q, Liang B. 2015. Cholesterol induces lipoprotein lipase expression in a tree shrew (*Tupaia belangeri chinensis*) model of non-alcoholic fatty liver disease. *Scientific Reports,* **5**(1): 15970.

Zhang LQ, Wu XY, Liao SS, Li YH, Zhang ZG, Chang Q, Xiao RY, Liang B. 2016. Tree shrew (*Tupaia belangeri chinensis*), a novel non-obese animal model of non-alcoholic fatty liver disease. *Biology Open,* **5**(10): 1545-1552.

Zhang QY, Fan XN, Cao Y. 2011. Expression of cannabinoid and opioid receptors in nervous as well as immune systems of *Macaca mulatta* and *Tupaia belangeri*. *Zoological Research,* **32**(1): 31-39. (in Chinese)

Zhao F, Guo XL, Wang YJ, Liu J, Lee WH, Zhang Y. 2014. Drug target mining and analysis of the Chinese tree shrew for pharmacological testing. *PLoS One,* **9**(8): e104191.

Zhu GA, Sundram U, Chang AL. 2014. Two different scenarios of squamous cell carcinoma within advanced Basal cell carcinomas: cases illustrating the importance of serial biopsy during vismodegib usage. *JAMA Dermatology,* **150**(9): 970-973.

Ziegler A, Leffell DJ, Kunala S, Sharma HW, Gailani M, Simon JA, Halperin AJ, Baden HP, Shapiro PE, Bale AE. 1993. Mutation hotspots due to sunlight in the p53 gene of nonmelanoma skin cancers. *Proceedings of the National Academy of Sciences of the United States of America,* **90**(9): 4216-4220.

Regeneration of adhesive tail pad scales in the New Zealand gecko (*Hoplodactylus maculatus*) (Reptilia; Squamata; Lacertilia) can serve as an experimental model to analyze setal formation in lizards generally

Lorenzo Alibardi[1], Victor Benno Meyer-Rochow[2,3,*]

[1] *Comparative Histolab and Department of Bigea*, *Dipartimento di Biologia*, *University of Bologna*, *Bologna* 40126, *Italy*

[2] *Research Institute of Luminous Organisms*, *Tokyo* 100-1623, *Japan*

[3] *Department of Genetics and Physiology*, *Oulu University*, *Oulu*, *FIN* 90140, *Finland*

ABSTRACT

During the regeneration of the tail in the arboreal New Zealand gecko (*Hoplodactylus maculatus*) a new set of tail scales, modified into pads bearing setae 5–20 μm long, is also regenerated. Stages of the formation of these specialized scales from epidermal pegs that invaginate the dermis of the regenerating tail are described on the basis of light and electron microscopic images. Within the pegs a differentiating clear layer interfaces with the spinulae and setae of the Oberhäutchen according to a process similar to that described for the digital pads. A layer of clear cytoplasm surrounds the growing tiny setae and eventually cornifies around them and their spatular ends, later leaving the new setae free-standing on the epidermal surface. The fresh adhesive pads help the gecko to maintain the prehensile function of its regenerated tail as together with the axial skeleton (made of a cylinder of elastic cartilage) the pads allow the regenerated tail to curl around twigs and small branches just like the original tail. The regeneration of caudal adhesive pads represents an ideal system to study the cellular processes that determine setal formation under normal or experimental manipulation as the progressive phases of the formation of the setae can be sequentially analyzed.

Keywords: Gecko lizard; Regeneration; Epidermis; Tail pad scales; Adhesion; Prehensile function; Ultrastructure

INTRODUCTION

The regeneration of the tail in lizards involves the regrowth of a variety of tissues, of which the skin with its regenerated (neogenic) scales is one type (Alibardi & Meyer-Rochow, 1988, 1989; Bellairs & Bryant, 1985; Maderson et al., 1978). The new scales are formed through an initial morphogenetic process that is different from the process of scale formation during development, since the initial regenerating (wound) epidermis undergoes invagination and in the dermis forms pegs that ultimately give rise to the new scales (Alibardi, 1995; Bryant & Bellairs, 1967; Liu & Maneely, 1969; Wu et al., 2014). The regenerated scales in numerous lizard species appear to be of similar shapes and patterns of arrangement, and they are usually smaller than the original scales, allowing the regenerated tail to be distinguished from the original tail.

In some geckos, specialized scales are also regenerated like, for instance, the large, dorsal plate-like scales in *Teratoscincus* (Werner, 1967), or the caudal adhesive pads in *Lygodactylus* (Maderson, 1971) and various Carphodactyline geckos (Bauer, 1998). In the latter scales, especially present on the ventral side of the tail, the external layer exhibits micro-ornamentation, brought about by the so-called Oberhäutchen, and features long bristles like those present in the digital pads that allow caudal adhesion and permit arboreal climbing in these geckos (Hiller, 1972; Maderson, 1966). Studies on scale regeneration have indicated six main stages in the histology of the epidermis: stage 1 indicative of the resting phase, and stages 2–6 covering the renewal period. During scale regeneration these stages are repeated and the new scales pass through similar differentiating stages to those normally occurring during the shedding cycle, forming an external corneous wound epidermis (lacunar cells), followed by a clear layer, the Oberhäutchen, and then a beta-, meso- and alpha-layer (Figure 1A, B).

Received: 05 March 2017; Accepted: 20 May 2017

*Corresponding author, E-mail: vbmeyrow@gmail.com

DOI: 10.24272/j.issn.2095-8137.2017.046

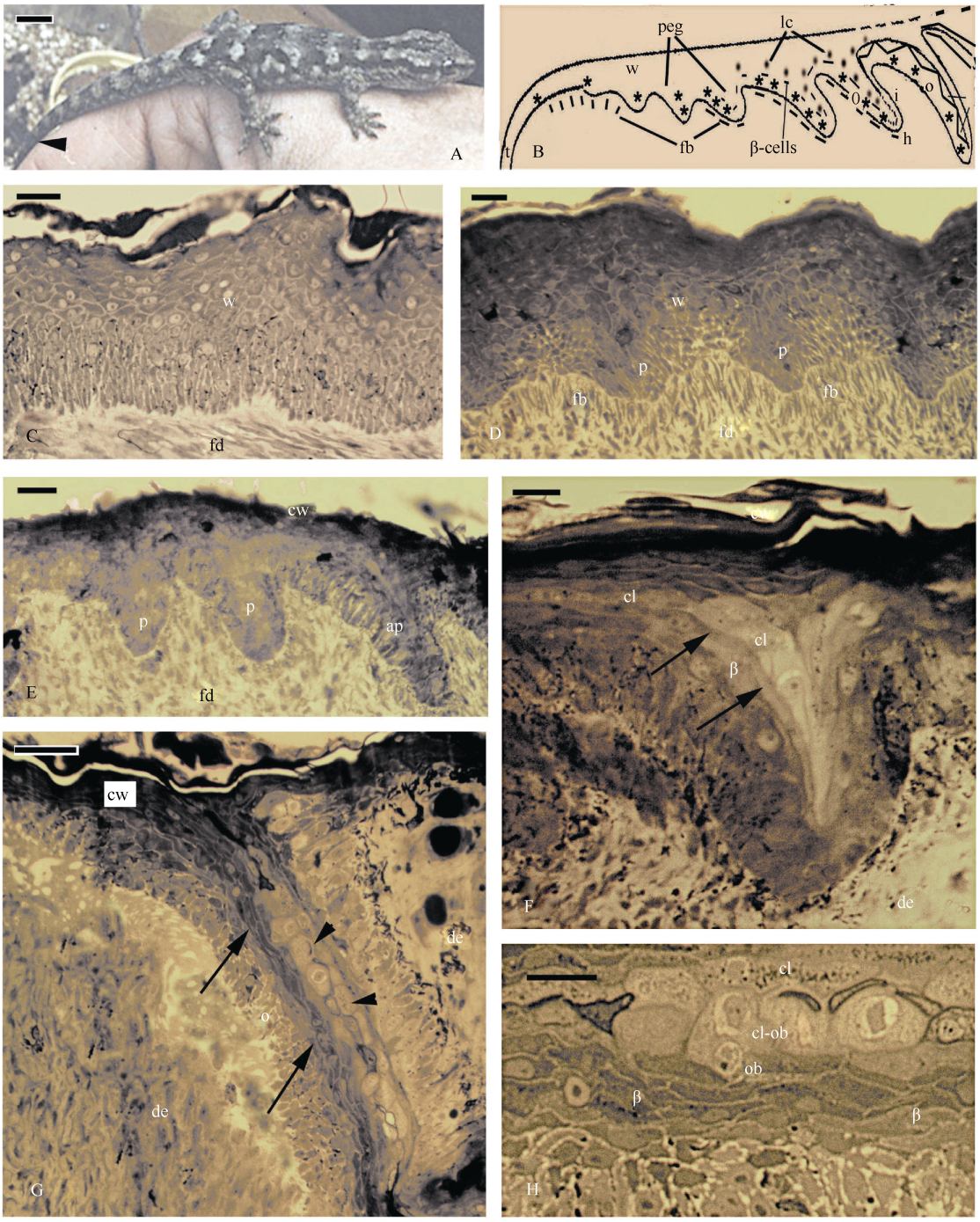

Figure 1 Images and histological aspect of the regenerating tail skin of *Hoplodactylus maculatus*

A: Experimental animal; B: Schematic drawing showing the proximal to distal sequence of scale regeneration (see text); C: Linear, multilayered apical wound epidermis. Bar=10 μm; D: Formation of epidermal pegs in the more proximal epidermis. Bar=20 μm; E: The pegs become asymmetric in more proximal regions (refers in general to Figure 1B). Bar=20 μm; F: In the middle of the elongating asymmetric peg, new epidermal layers are formed, starting with a pale layer of clear cells, followed underneath by Oberhäutchen and beta-cells (arrows). Bar=10 μm; G: In the interior of an elongating peg, the pale, roundish clear layer cells (arrowheads) are in contact with denser cells of the Oberhäutchen and beta layers (arrows). Bar=20 μm; H: Detail of the darker Oberhäutchen and beta-cells adjacent to clear cells, presenting some granular material. Bar=10 μm. cl: clear cells; cl-ob: clear cells perhaps containing tiny elongation of the Oberhäutchen, appearing as granules; cw: corneous layer of the wound epidermis; de: dermis; o: forming outer (dorsal) side of the regenerated scale; fb: fibroblasts; lc: lacunar cells; ob: Oberhäutchen cells; p: epidermal pegs; w: wound epidermis.

Histological studies on the regeneration of caudal pads in *Lygodactylus picturensis* have shown the formation of setae in the lamellae of these modified scales (Maderson, 1971), but this study did not provide cytological details on the process of setal formation, in particular on the interaction between clear and Oberhäutchen cells in forming the setae as described for the digital pads (Alibardi, 1999, 2009; Alibardi et al., 2011; Hiller, 1972). However, to possess this information is important, since it is believed that the knowledge of the proteins forming the cytoskeleton in clear cells is essential to understand how these same cells can mould the spinulae and setae of the Oberhäutchen cells, forming the species-specific micro-ornamentation and setal branching patterns in geckos and other lizards that are equipped with such adhesive pads.

In order to verify some cytological details of setal regeneration in the caudal pads, we used samples of the New Zealand gecko (*Hoplodactylus maculates*), collected by us in the field. The geckos possessed regenerated scales at the tip of the new tail (Bauer, 1998), suggesting that the regenerated tail can also make use of these pads for adhesion and movement among a tree's branches. In order to fulfil its role in climbing, the tail must be capable to curl nearly as well as the original tail, and indeed this does occur since the regenerated axial skeleton of the regenerated tail is composed of a tube of elastic cartilage (Alibardi & Meyer-Rochow, 1989). In the present study, we focus on the regenerating tail skin, which allows us to find some stages of setal regeneration and to conclude that this is a promising experimental system to analyze details of setal formation in lizards generally.

MATERIAL AND METHODS

A total of six individuals of the New Zealand gecko, *H. Maculatus*, with regenerating tails of 3–4 mm (*n*=4) and about 10 mm (*n*=2) were used in the present study (Figure 1A). Details of animal collection and fixation were previously provided (Alibardi & Meyer-Rochow, 1988, 1989). Autotomy, a natural mechanism of tail release following grabbing of the tail, was induced, and the regenerating tail was collected at 40 days (*n*=4) and 60 days (*n*=2) of regeneration when scalation was visible. Permission to carry out the research and approval of the experimental protocol was obtained from the institutional Ethics Committee on Animal Care and Welfare of the University of Waikato (Hamilton; New Zealand).

In these samples, the regenerating tail showed stages of epidermal differentiation spanning from the beginning of scale formation to completely formed scales over most of the surface of the regenerated scales. Among the normal caudal scales a few differentiated pad lamellae were also present, in particular noticeable at 60 days of regeneration. Briefly, for plastic embedding, small pieces of tail tissues from four individuals were initially fixed in 2.5% glutaraldehyde in cacodylate buffer for about eight hours, osmicated, dehydrated and included in Epon. For wax embedding, the tissues from two individuals were fixed in 10% buffered formaldehyde for about 12 hours, dehydrated, cleared with xylene, and embedded in wax.

Sections 2–3 μm thick form plastic-embedded tissues were collected using an ultramicrotome (Nova, LKB, Bromma, Sweden), dried on a glass slide and stained with 1% toluidine blue solution. Interesting levels of the tissues, showing most likely the presence of differentiating Oberhäutchen and beta-cells, were sectioned at 40–80 nm thickness with an ultramicrotome and were collected on 200 mesh copper grids, stained for 30 minutes at room temperature with 2% uranyl acetate, washed and stained for 6 minutes in lead citrate according to standard procedures. The sections were observed under a Zeiss C10 transmission electron microscope at a high tension of 60 kV. Images were collected on a digital camera and imported into a computer, allowing representative section images to be used in composing figures.

Wax sections of 6–8 μm thickness, obtained with the help of a rotary microtome (Reichert, Germany), were dried on glass slides for some hours and stained with 1% toluidine blue for a minute. Pictures were taken under a light microscope equipped with a digital camera, imported into a computer and selected to compose the figures.

RESULTS

Histology of the regeneration of pad scales

The four available specimens with poorly scaled regenerating tails of 3–4 mm in length, showed some stages (2–4) of the scale regeneration sequence (indicated in Figure 1B). Initially the thick wound epidermis toward the tip of the tail was linear or undulated (Figure 1C), but in more proximal regions epidermal pegs were formed and they became asymmetric (with a longer, distal side) toward the tail stump (Figure 1D, E). Inside these pegs, underneath the dark corneous layer of the wound epidermis, the differentiation of clear and darker beta-cells started in the middle of the elongated peg, indicative of stages 3–4 of the shedding cycle (Figure 1F). The Oberhäutchen layer was sandwiched between the clear and darker beta-cells, representing the first line of cells contacting the hyperthrophic and pale clear cells (Figure 1G, H).

This early stage of differentiation (stage 3–4: Maderson, 1966, 1970) did not allow us to detect the tiny spinulae and setae originating from Oberhäutchen cells, but small granulations and seemingly irregular filaments were seen inside the pale cells, giving a granular appearance to their cytoplasm (Figure 1G). The external, corneous wound epidermis covering the entire regenerated epidermis in more proximal regions was detached from the pegs, being evidence of the beginning of the shedding process at stage 5 of the shedding cycle (Figure 1F, G). No further stage of setal formation was apparent, but this same material, analyzed under the electron microscope, revealed some important details (see further below).

An examination of the two advanced regenerated tails, about 10 mm long (60 days regeneration), one sectioned sagittally and the other transversely, showed that they were completely scaled and contained an axial tube of elastic cartilage surrounding the ependymal tube (Figure 2A, B). Toward the tip of the tail on its ventral side (this was determined by an examination of the regenerating cartilage in relation to the vertebrae of the tail stump), the presence of lamellar pads

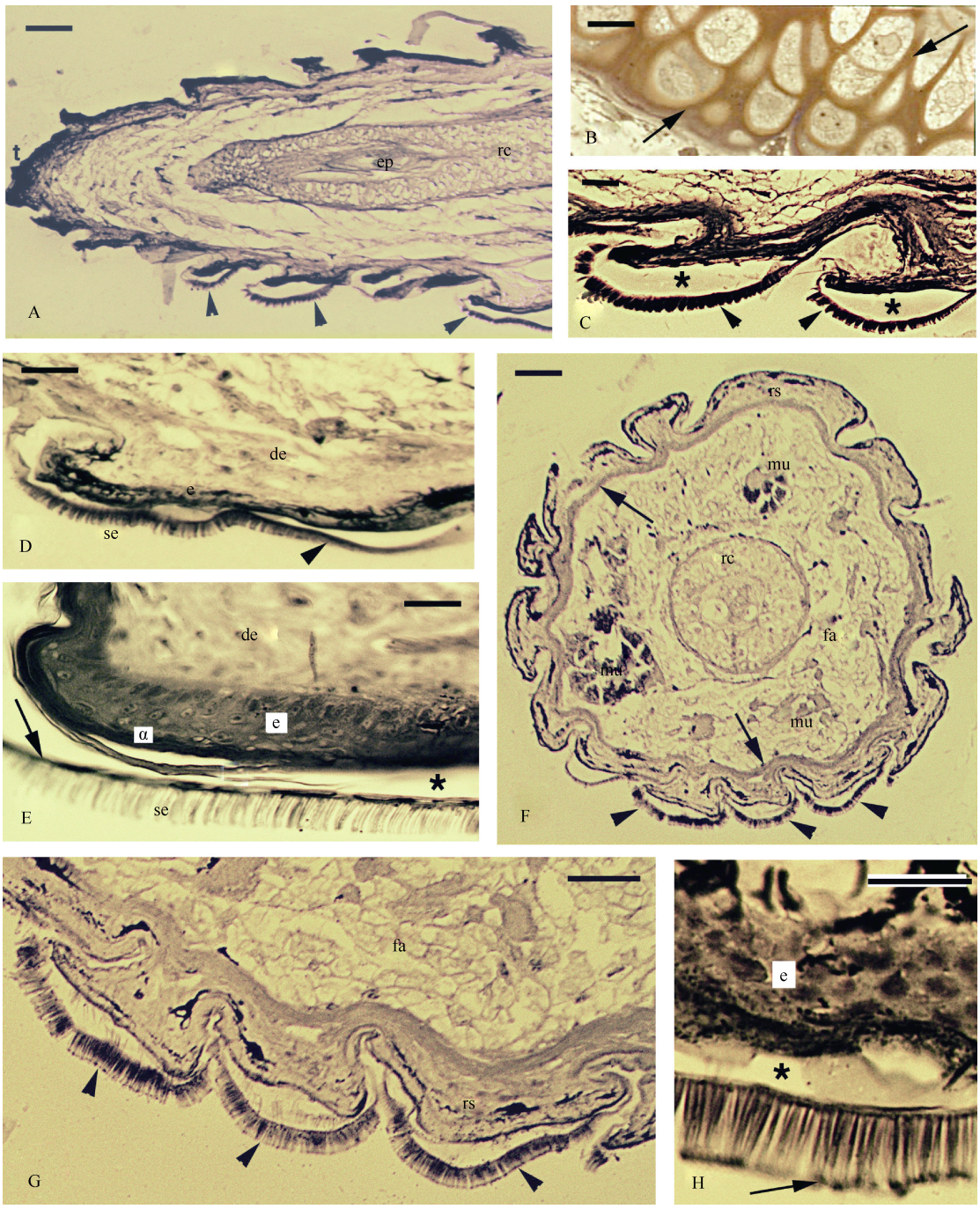

Figure 2 Histological aspect of regenerating tail with formed tail pad lamellae

A: Apical region of the regenerated tail with complete scaling. Arrowheads indicate some ventral pad lamellae. Bar=100 μm; B: Detail of the large chondrocytes forming the regenerated elastic cartilage (arrows on the scanty extracellular matrix). Bar=10 μm; C: Detail of the external setae (arrowheads) of two pads. Bar=20 μm; D: Detail of a pad lamella showing the disappearing of setae (arrowhead) in the Oberhäutchen-beta layer region at about half of the outer surface. Bar=50 μm; E: Higher magnification detail of the epidermis and setae of a caudal pad showing the setae resting upon a mature Oberhäutchen-beta-layer (arrow) artifactually detached from the underlying alpha-layer (asterisk). Bar=20 μm; F: Cross-sectioned regenerated tail toward the distal tip, showing three ventral pads (arrowheads). The dense deep dermis seen underneath the scales is indicated with arrows. Bar=100 μm; G: Detail of the setae (arrowheads) in three pads. Bar=50 μm; H: Further details of the setae with their expanded tips (arrow). Bar=20 μm. de: dermis; e: epidermis; ep: ependymal canal (regenerated spinal cord); fa: fat tissue; mu: regenerated muscles; rc: regenerated cartilaginous tube; rs: regenerated scales; se: setae; *: the artifactual detachment of the beta layer bearing the setae from the remaining epidermis.

bearing bristles among the normal scales was noted, whose outer (dorsal) surface appeared decorated with indentations not seen in the remaining scales (Figure 2A, C, D). A closer look at higher magnification showed that all these pads appeared at the post-shedding, resting stage or stage 2 of the shedding cycle with completely mature setae and beta-layer, while the alpha layer was still uncompleted (Figure 2E).

The localization of the lamellar pads was better appreciated in cross sections, which confirmed that these modified and indented scales were restricted to the ventral side, forming three or four rows of scales (Figure 2A, F, G). The maximal length of the setae was approx. 20 μm. The enlargements of their terminal tips were probably related to the apical branching into thinner setae and the development of adhesive spatulae (Figure 2H).

In summary, while at the early stages of scale regeneration (40 days regeneration) only the beginning of setal formation was detected, at the later stage (60 days regeneration) mature setae were present.

Ultrastructure of setal formation

Although the progressive formation of setae in its entirety was not seen in the available material, careful examination of the epidermis at stages 3–4 of the shedding cycle detected in the elongated pegs the pale cytoplasm of clear cells, which surrounded the numerous, tiny spinulae and the setae formed from the Oberhäutchen layer. The more proximal, normal scales showed a completely formed beta-layer (stage 5, close to shedding) merged to the Oberhäutchen from which protruding spinulae of 0.2 by 1.0 μm were present (data not shown). Only short setae were seen in the sparse pads sectioned in the available material and they were slightly thicker and clearly longer than the spinulae, e.g., 0.3–0.6 μm versus 4–5 μm or more (Figure 3A). Among the spinulae or the setae, the pale cytoplasm of the clear cells with a loose meshwork of cytoskeletal filaments mainly composed of keratin (diameter=10 nm; inset of Figure 3A) was apparent. In other regions of the tail pad lamella, the cytoplasm of the clear cells became dense and fibrous, especially around each seta (Figure 3B, C). In the regenerated and more proximal scales, after shedding of the corneous wound epidermis (Figure 1F, G), the cytoplasm of the clear cells was either totally or partially degenerated among the spinulae or the longer setae, which were therefore free-standing on the skin surface (Figure 3C inset, D). As in other geckos (Bauer,1998; Hiller, 1972; Maderson, 1971), the beta-layer sustaining the mature setae also in *H. maculatus* appeared subdivided into two darker strata and one pale stratum sandwiched between them (Figure 3D).

In summary, in the regenerating scales at stages 3–4 the formation of setae in the caudal pads resembled the typical process that occurs during the formation of digital scales with mature setae at the late stages resting upon a merged Oberhäutchen and beta-layer.

DISCUSSION

Although the available stages of regeneration in the adhesive caudal pads were incomplete to describe the entire process of setal differentiation, the combination of light and electron microscopic observations revealed the novel finding that the formation of setae in the caudal pads largely resembled that of the digital pads earlier described by Hiller (1972), Alibardi (1999, 2009) and Alibardi et al. (2011). Thin setae, 0.3–0.6 μm in diameter and 5–20 μm in length, with terminal branches into thin spatulae, were present, as also previously reported (but based solely on scanning electron microscopy (SEM) images (Bauer, 1998) in some ventral scales at the tip of the tail of *H. maculatus*. However, mainly tiny setae were apparent and only in a few cases the thicker basal parts of mature setae 0.9–1.2 μm thick or their characteristic small spatula ends were detected. Whether functionally and chemically the regenerated setae are identical to the original setae of normal scales is something that we cannot say without further studies.

As for the digital setae (Alibardi, 1999; Alibardi et al., 2011; Hiller, 1972), also those of the regenerating tail pads utilize the guidance of the cytoplasm of the clear cells (Figure 4) to extensively branch into very tiny setal ends (spatulae) that likely gift these caudal pads with adhesion properties with the same efficiency as the digital pads. The large pale cells occupying the position of the clear cells (indicated as cl-ob in Figure 1G), resemble the beta-glandular cells previously described in geckos (beta-glands, cf., Maderson, 1970). However the tiny granulations present in these cells (Figure 1H) may actually represent very thin intra-cytoplasmic branching of Oberhäutchen setae within the cytoplasm of the clear cells, but the lack of the sequence of differentiating cells precluded a clarification of this important issue (Figure 4). The presence of very large and roundish pale cells, referred to as clear cells and containing granulations, was also described during setal formation in the gecko *Tarentula mauritanica* (Hiller, 1972). The nature of this intimate, almost symbiotic penetration of numerous setae into the cytoplasm of the clear cells could be confirmed by our ultrastructural observations (Figure 3A), and is schematically represented in Figure 4.

The ultrastructural study has also shown that in tail pads the fibrous cytoskeletal material formed in the clear cells surrounds the setae during their formation and eventually becomes cornified. In normal caudal scales, the maturation of the corneous layer and its shed occur through the detachment of the corneous clear layer from the Oberhäutchen, but in the case of the setae formed in the caudal pads it appears that the corneous and dead clear layer degenerates between the numerous setae after the other corneous layers of the wound epidermis have been shed (Figure 3D, Figure 4A, C). It remains unclear, however, whether shedding in this specialized tail scale type occurs by the detachment of the clear Oberhäutchen layer as in the digital scales, or is instead due to the degeneration of the cytoplasm of the clear cells. Whatever the scenario, the disappearance of the clear layer allows the setae to become free and exposed to the substrate effectuating adhesion.

CONCLUSION

The present study demonstrates that the process of setal

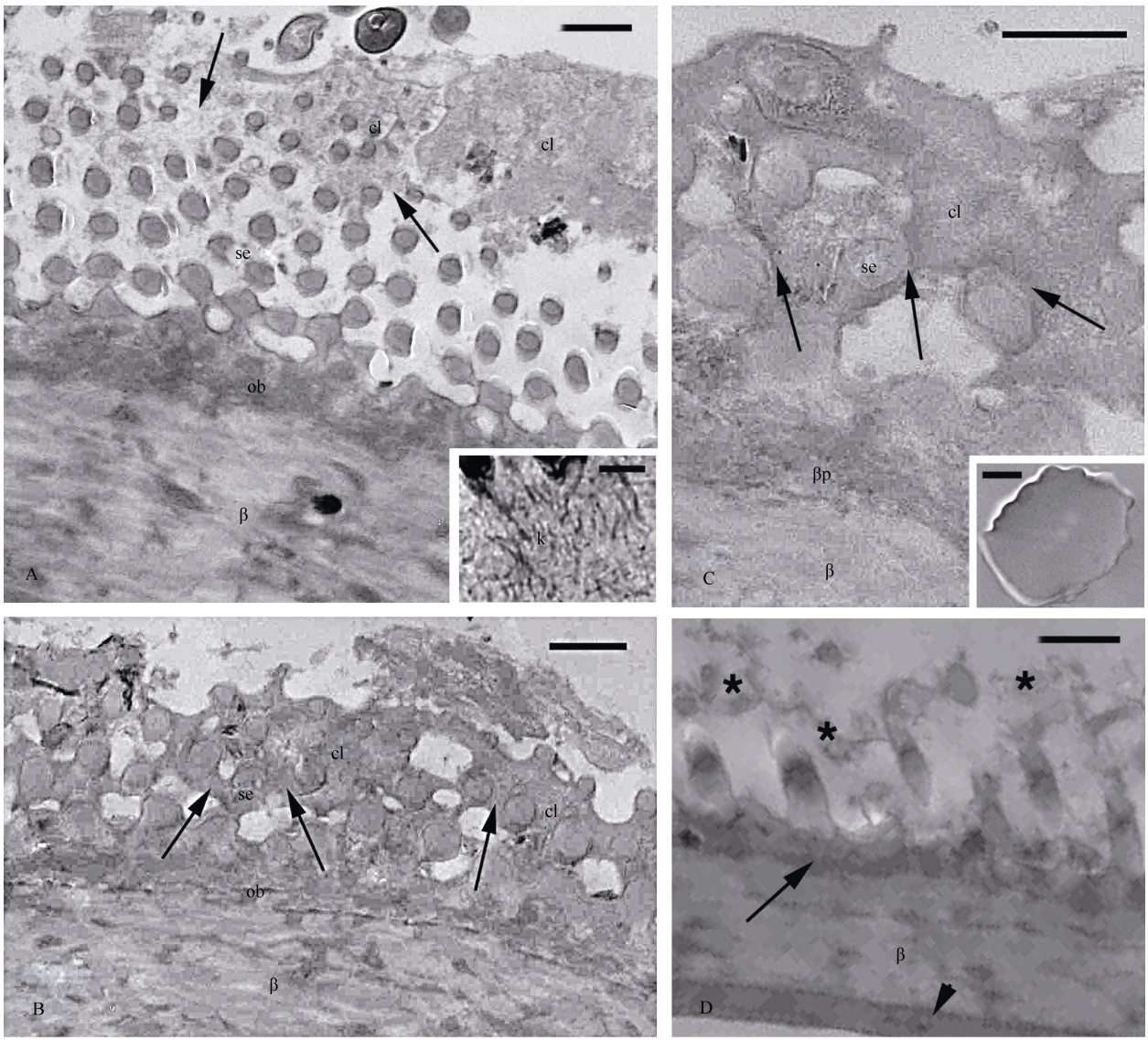

Figure 3 Electron microscopy images (TEM) aspect of formed setae in regenerated scales

A: Group of setae sectioned mainly transversally, and embedded within the pale cytoplasm of clear cells (arrows). Bar=1 μm. The inset shows the filaments of likely keratin (k) forming the cytoskeleton of clear cells. Bar=100 nm; B: Additional image of the setae embedded in the denser corneous cytoplasm of the clear layer (arrows). Bar=1 μm; C: Further detail of the dense fibrous cytoplasm of cornified clear cells that surround the setae (arrows). Bar=1 μm. The inset shows a cross-sectioned and mature seta. Bar=250 nm; D: Detail of Oberhäutchen with spinulae isolated from the degenerated clear layer cytoplasm (*). The spinulae rest on a denser material (arrow) that alternates between a paler and compact beta-layer, which shows a denser basal layer (arrowhead). Bar=1 μm. β: beta-layer; βp: beta-packets (accumulating corneous beta-material); cl: clear cell; ob: Oberhäutchen; se: setae.

formation in regenerating caudal pads in geckos can serve as a useful experimental system to analyze details of setal formation generally since the regeneration of scales and pads follows a proximal-distal direction of differentiation, along which all the stages of the typical renewal phase of the epidermal shedding cycle are present (Alibardi, 1995; Maderson, 1971). However, the interest in adhesive pads goes beyond that, because there are potential applications for using information gained from such scales and their setal properties in biomimetics to produce the next generation of dry adhesives. The study of regenerating adhesive pads during tail regeneration in geckos (at 40 and 60 days in *H. maculatus*) is ethically and ecologically acceptable, as it does not require any sacrifice of animals (except for the tail, which, however, will have regenerated and regained its full function within a few months after its loss), and at the same time would allow to perfectly stage all the phases of setal formation and enable a detailed investigations of the functional properties of the adhesive pads and their setae.

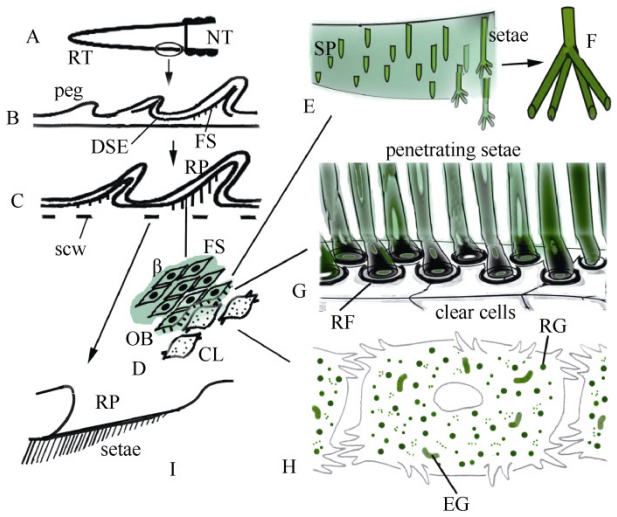

Figure 4 Schematic drawing illustrating the formation of setae in the caudal pads of the gecko

A: Regenerating tail. The oval details the skin illustrated in B–C, showing the formation of the epidermal pegs and the progressive differentiation of the epidermis; D: Showing a detail of the differentiating clear and Oberhäutchen as well as beta-cells along the shedding line; E: Showing the formation of spinuale that mature into setae on the right with the apical branching into thinner ends (F); G: Showing that the setae are penetrating into the cytoplasm of clear cells whereas the cytoplasm forms rings of fibrous material around the setae; H: Showing the granulated appearance of the large clear cells perhaps containing setae inclusions; I: Showing a mature caudal pad. DSE: differentiating epidermis along the shedding line; EG: elongated granules; FS: forming setae; NT: normal tail; OB: Oberhäutchen; RF: cytoskeletal ring of clear cell cytoplasm surrounding the growing setae; RG: roundish granules; RP: regenerated pad lamella; RT: regenerating tail; SCW: shedding corneous wound epidermis; SP: forming spinulae from the Oberhäutchen layer.

ACKNOWLEDGEMENTS

The study was completely self-supported (Comparative Histolab), while L.A.'s trip to New Zealand and stay at V.B.M-R.'s lab at the University of Waikato were largely supported by a New Zealand University Grants Committee Scholarship.

REFERENCES

Alibardi L, Meyer-Rochow VB, 1988. Ultrastructure of the neural component of the regenerating spinal cord of three species of New Zealand lizards (*Leiolopisma nigriplantare maccanni, Lampropholis delicata* and *Hoplodactylus maculatum*). *New Zealand Journal of Zoology*, **15**(4): 535-550.

Alibardi L, Meyer-Rochow VB, 1989. Comparative fine structure of the axial skeleton inside the regenerated tail of lizards and the tuatara (*Sphenodon punctatus*). *Gegembaurs Morphologisches Jahrbuch*, **135**(5): 705-716.

Alibardi L. 1995. Electron microscopic analysis of the regenerating scales in lizard. *Bollettino di Zoologia*, **62**(2): 109-120.

Alibardi L. 1999. Keratohyalin-like granules in embryonic and regenerating epidermis of lizards and *Sphenodon punctatus* (Reptilia, Lepidosauria). *Amphibia-Reptilia*, **20**(1): 11-23.

Alibardi L. 2009. Cell Biology of adhesive setae in gecko lizards. *Zoology*, **112**(6): 403-424.

Alibardi L, Edward DP, Patil L, Bouhenni R, Dhinojwala A, Niewiarowski PH. 2011. Histochemical and ultrastructural analysis of adhesive setae of lizards indicate that they contain lipids in addition to keratins. *Journal of Morphology*, **272**(6): 758-768.

Bauer AM, 1998. Morphology of the adhesive tail tips of Carphodactyline geckos (Reptilia: Diplodactylidae). *Journal of Morphology*, **235**(1): 41-58.

Bellairs Ad'A., Bryant SV, 1985. Autotomy and regeneration in reptiles. *In:* Gans, C, Billet F, Maderson PFA. Biology of the Reptilia. New York: John Wiley & Sons, 302-410.

Bryant SV, Bellairs Ad'A. 1967. Tail regeneration in the lizards *Anguis fragilis* and *Lacerta dugesii*. *Zoological Journal of the Linnéan Society*. (London), **46**(310): 297-305.

Hiller U. 1972. Licht- und elektronenmikroskopische Untersuchungen zur Haftborstenentwicklung bei *Tarentola mauritanica* L. (Reptilia, Gekkonidae). *Zeitschrft für Morphologie der Tiere*, **73**(3): 263-278.

Liu HC, Maneely RB. 1969. Observations on the developing and regenerating tail epidermis of *Hemidactylus bowringi* (Gray). *Acta Anatomica*, **72**(4): 549-583.

Maderson PFA. 1966. Histological changes in the epidermis of the Tokay (*Gekko gecko*) during the sloughing cycle. *Journal of Morphology*, **119**(1): 39-50.

Maderson PFA. 1970. Lizard glands and lizard hands: models for evolutionary study. *Forma et Functio*, **3**: 179-204.

Maderson PFA. 1971. The regeneration of caudal epidermal specializations in *Lygodactylus picturatus keniensis* (Gekkonidae, Lacertilia). *Journal of Morphology*, **134**(4): 467-478.

Maderson PFA, Baranowitz S, Roth SI. 1978. A histological study of the long term response to trauma of squamate integument. *Journal of Morphology*, **157**(2): 121-136.

Werner YL. 1967. Regeneration of specialized scales in tails of *Teratoscincus* (Reptilia: Gekkonidae). *Senckenbergiana Biologica*, **48**(2): 117-124.

Wu P, Alibardi L, Chuong CM. 2014. Lizard scale regeneration and development: a model system to analyze mechanisms of skin appendages morphogenesis in amniotes. *Regeneration*, **1**: 16-26.

Pseudogenization of the *Humanin* gene is common in the mitochondrial DNA of many vertebrates

Ian S. Logan*

22 *Parkside Drive*, *Exmouth*, *Devon*, *UK*

ABSTRACT

In the human the peptide Humanin is produced from the small *Humanin* gene which is embedded as a gene-within-a-gene in the 16S ribosomal molecule of the mitochondrial DNA (mtDNA). The peptide itself appears to be significant in the prevention of cell death in many tissues and improve cognition in animal models. By using simple data mining techniques, it is possible to show that 99.4% of the human *Humanin* sequences in the GenBank database are unaffected by mutations. However, in other vertebrates, pseudogenization of the *Humanin* gene is a common feature; occurring apparently randomly in some species and not others. The persistence, or loss, of a functional *Humanin* gene may be an important factor in laboratory animals, especially if they are being used as animal models in studies of Alzheimer's disease (AD). The exact reason why *Humanin* underwent pseudogenization in some vertebrate species during their evolution remains to be determined. This study was originally planned to review the available information about *Humanin* and it was a surprise to be able to show that pseudogenization has occurred in a gene in the mtDNA and is not restricted solely to chromosomal genes.

Keywords: mtDNA; Humanin; Pseudogenization; NUMT

INTRODUCTION

The peptide Humanin was first described in 2001 (Hashimoto et al., 2001) when it was observed during a study on Alzheimer's disease (AD) that the death of cells was prevented by the presence of the peptide. A further paper from the same research group (Terashita et al., 2003) described how the sequence of the peptide appeared to be produced by a hitherto unrecognised gene-within-a-gene in the *MT-RNR2* gene of the human mitochondrial DNA (mtDNA). Subsequently, Bodzioch et al. (2009) described that the *Humanin* gene was responsible for the production of Humanin, but also suggested that the peptide might be produced from chromosomal DNA as sequences very similar to mitochondrial *Humanin* could be found in the fragmentary copies of the mtDNA that exist in nuclear chromosomal DNA. This report also mentioned that sequences similar to the *Humanin* gene, as found in the human, are '*relatively well-conserved in mtDNA, where they can be traced down the whole evolutionary tree'.* Recent reports have not really settled the point as to whether Humanin is produced by the *Humanin* gene, the nuclear mitochondrial DNA segment (NUMT) copies, or both, but have concentrated more on the actions of Humanin as a protective agent, especially in AD (Cohen et al., 2015; Hashimoto et al., 2013; Matsuoka, 2015; Tajima et al., 2002), as a retrograde signal peptide passing information about the mitochondrion to the rest of the cell (Lee et al., 2013) and as an agent improving cognition (Murakami et al., 2017; Wu et al., 2017). Synthetic Humanin can now be purchased for research purposes from several companies, and is available with the standard amino acid sequence, or with the 14th amino acid altered from Serine to Glycine, the S14G form, a change which appears to increase the potency of the peptide (Li et al., 2013).

Mitochondria are small organelles found in all developing eukaryotic cells. Each mitochondrion contains a few small rings of double-stranded DNA. Human mtDNA is described as containing 16 569 numbered nucleotide bases, a fairly typical number for a vertebrate, and was the first mitochondrial DNA molecule to be fully sequenced (Anderson et al., 1981). This complete mtDNA sequence was later updated to eliminate the errors (revised Cambridge Reference Sequence [rCRS]; Andrews et al., 1999; Bandelt et al., 2014). The GenBank database (Benson et al., 2005) now holds over 36 000 human mtDNA sequences submitted by research institutes and some private individuals, as well as about 11 000 mtDNA sequences from other vertebrates. The rCRS (GenBank Accession No. NC_012920) describes the mtDNA as having 13 genes for

Received: 20 May 2017; Accepted: 05 July 2017

*Corresponding author, E-mail: ianlogan22@btinternet.com

DOI: 10.24272/j.issn.2095-8137.2017.049

peptides that form part of the OXPHOS system, 22 genes for the production of transfer RNA sequences, a hypervariable control region, several small non-coding sequences situated between the other parts, and most importantly for the present discussion, two genes for the production of RNA sequences (*MT-RNR1,* for the RNA 12S molecule & *MT-RNR2,* for the RNA 16S molecule) which are structural components used in the building of ribosomes. The *Humanin* gene is located at region 2 633–2 705 in the rCRS and encodes a 24 amino acid peptide. But as this is in the centre of the *MT-RNR2* gene, the nucleotide bases of the *Humanin* gene also have the separate function of being a part of the ribosomal RNA 16S molecule.

In this paper simple mining techniques (Yao et al., 2009; Zaki et al., 2007) have been used to look at the *Humanin* gene in the mitochondrial sequences of the human and other vertebrates available in the GenBank database. The study showed that pseudogenization of the *Humanin* gene does not occur in the human, but is a common feature in other vertebrates. Moreover, the study shows the surprise finding that pseudogenization has occurred in a gene in the mtDNA and is not restricted solely to chromosomal genes.

DATASET AND METHODS

The mitochondrial sequences held in the GenBank database formed the dataset for this study. This database holds about 36 000 different human mtDNA sequences. The individual page on the database for each sequence can be found using a direct link of the form: https://www.ncbi.nlm.nih.gov/nuccore/NC_012920. This particular link connects to the page for the rCRS; and the page for any other sequence can be found by replacing NC_012920 with another Accession No..

A list of the human mtDNA sequences can be found by searching the GenBank database with a query string such as: "homo sapiens" [organism] "complete genome" mitochondrion. Although this list should contain the details of different mtDNA sequences, note in particular that many sequences from the Human Diversity Genome Project are duplicated and in some instances triplicated.

The GenBank database also contains the mitochondrial sequences for approximately 11 000 other vertebrate samples. About 4 000 of these sequences are described as Reference Sequences and have Accession No. in the range NC_000000–NC_999999 (Pruitt et al., 2007). Each Reference Sequence comes from a different species, so the mtDNA sequences available on the GenBank database can be considered as coming from about 4 000 different species of vertebrate.

Unfortunately, GenBank does not give details of the parts of the *MT-RNR2* gene in the description accompanying a mtDNA sequence, so it is necessary to identify the *Humanin* sequence by searching for it. However, as the *Humanin* gene is well conserved throughout vertebrates the sequences are able to be identified fairly easily.

Initially, the sequences described in this study were found by visual examination of the FASTA file for each sequence, but subsequently a pattern matching computer program (in Javascript) was developed (Supplementary Program 1, available online). This program requires as its input the *MT-RNR2* gene in FASTA format. The 73 bases of the *Humanin* gene as given in the rCRS are then compared by stepping-along the *MT-RNR2* gene; and a best-fit is found. A non-matching comparison typically finds about 30 bases in common (i.e., about 40%), but a *Humanin* sequence will match about 50 bases (i.e., about 70%), even for a distant species, and much better for other mammalian species.

The results of this study are presented in three parts: firstly, the variants found in the 36 000+ human mtDNA sequences available for study in the GenBank database; secondly, the *Humanin* sequences found in other vertebrates; and thirdly, the NUMT sequences found in the human and some non-human species.

For clarity, the mtDNA variants are listed in a format of “rCRS allele position derived allele”, instead of the proposed nomenclature of the HVGS (http://varnomen.hgvs.org/). For instance, mtDNA variant T2638C may also be written as m.2638T>C according to HVGS nomenclature, and protein variant P3S written as p.P3S.

RESULTS

Variants identified in the human *Humanin* mtDNA sequences

The nucleotide sequence for the *Humanin* gene in the rCRS (GenBank Accession No. NC_012920) was predicted to encode a peptide of 24 amino acid residues, together with a stop codon (MAPRGFSCLLLLTSEIDLPVKRRAX), and this sequence was found in 99.4 % of all the human mtDNA sequences. Data mining of all the human mtDNA genomes in GenBank showed 17 variants are known so far, of which five variants are associated with different mitochondrial haplogroups A2f1 (T2638C, *n*=17, no change in the amino acid sequence), N1b (C2639T, *n*=96, this variant leads to an amino acid change P3S), U6a7a1a (A2672G, *n*=16, this variant changes the amino acid sequence at S14G and produces the well-known potent form of Humanin), G2701A (H13a1a2b, *n*=8, no change in the amino acid sequence), N1a1a (G2702A, *n*=71, this variant changes the amino acid sequence at A24T); and are common enough for them to be used as defining variants in the phylogenetic tree (van Oven & Kayser, 2009) (Supplementary Table 1, available online).

The other 12 variants all occur at low frequencies (1–6 sequences each); and in many of the sequences the presence of a mutation should be considered as ‘unverified’. An expanded table of these results is given in the Supplementary Table 1 (available online).

The *Humanin* sequences found in non-human vertebrates

Data mining of the non-human vertebrate mtDNA sequences showed *Humanin* sequences are present in all vertebrates. However, many of the sequences show pseudogenization and these sequences are not able to produce functional peptides. A pseudogene is recognizable because of the absence of a start codon, the presence of a premature stop codon, or a deletion/insertion causing a frameshift in the sequence.

Amongst our closest relatives are chimpanzees (*Pan troglodytes*) and gorillas (*Gorilla gorilla*), and their *Humanin* sequences are able to produce functional peptide, albeit the sequences differ from that of human by one residue (Figure 1). Some other small mammals showed they should be able to produce functional peptide, e.g., the Guinea pig (*Cavia porcellus*) and Northern tree shrew (*Tupaia belangeri*) (Yao, 2017). However, it was unexpected to find that the Macaques (*Macaca mulatta*) show pseudogenization as there is loss of the start codon.

Homo sapiens	MAPRGFSCLLLLTSEIDLPVKRRAX
Pan troglodytes	MAPRGFSCLLLSTSEIDLPVKRRAX
Gorilla gorilla	MAPRGFSCLLLLTSEIDLPVKRRTX
Macaca mulatta	KAPRGFNCLLLLTSEIDLPAKRRTX
Mus musculus	TAKRGSNCLLSLISEIDLSVKRLKX
Cavia porcellus	MARRGFICLLLYVSEIDLPVKKREX
Tupaia belangeri	MATRGFNCLLLSISEIDLPVKRRGX
Felis catus	TATRGLYCLLLPIREIDLPVKRREX
Capra hircus	TATRGFYCLLLPISEIDLPVKRREX
Danio rerio	MAKRGLNCLPHQVSEIDLSVQKRIX
Lepidotrigla microptera	MAXRGLNCLLFXVNEIDLPVQKRGX
Dopasia gracilis	MAKWGPSCLPWLISEIDLPVQKLVX
Corvus corax	MAKRGLNCLLQAIGEIDLPVQKQGX
Myxine glutinosa	MDXRKPNCLLFPINEINLSVQRQRX
Ichthyomyzon unicuspis	KVTRRHNCLLIPINEIDLPVQRRVX
Neoceratodus forsteri	MATRGFNCLPHFTSEIDLPVQKRAX

Figure 1 Alignment of Humanin peptide sequences
Residues that differ from that of the human are marked in red. The change in a start codon from Methionine is marked with a box. For sequence information, please refer to Supplementary Table 1 (available online).

Most rat and mouse species were shown to have functional genes, but importantly some common mice species (e.g., House mouse (*Mus musculus*)) were found to have undergone pseudogenization. Other common mammals, such as the cat (*Felis catus*) and the goat (*Capra hircus*), were also shown to have undergone pseudogenization. Amongst the bony fishes, the zebrafish (*Danio rerio*) appeared able to produce Humanin, but many other fishes, such as *Lepidotrigla microptera* 'Triglidae' cannot. Some other vertebrate classes may also be able to produce Humanin, such as the lizards (*Dopasia gracilis*) and birds (*Corvus corax*), but whether the peptides are fully functional is uncertain. The most distant vertebrates from ourselves are the lungfish (*Neoceratodus forsteri*), hagfish (*Myxine glutinosa*) and lampreys (*Ichthyomyzon unicuspis*); and whereas hagfish and lampreys show pseudogenization of their *Humanin* sequences, the lungfishes may have retained the ability to make a functional peptide.

The Tuatara (*Sphenodon puctatus*), an ancestor of the snake and found only in New Zealand (Subramanian et al., 2015) is also shown to have a functional gene. But in this species the peptide is one amino acid longer; and it is possible that the gene underwent pseudogenization, only for a later deletion to make the gene functional once again.

Supplementary Table 2 (available online) describes the *humanin* gene in 80 non-human vertebrate species. It is noteworthy that the ability to make the enhanced S14G form of Humanin was identified only in human sequences.

NUMT sequences in the human, Rhesus macaque, mouse and Golden hamster

As mentioned earlier, the question as to whether NUMT sequences are used to make Humanin is not resolved. But this data mining study showed that in the human there are two NUMT sequences that appear identical to the *Humanin* gene as found in the mtDNA, and a third sequence which is only altered at one amino acid. Also, in the Rhesus macaque (*Macaca mulatta*), the mouse and the Golden hampster (*Mesocricetus auratus*), the *Humanin* gene was shown to have undergone pseudogenization. However, it was also found that a possibly functional NUMT can be found in the chromosomes of each species, suggesting that the pseudogenization may have been a reasonably recent event in the evolutionary past of these species. The details of these sequences are given in the Supplementary Table 3 (available online).

DISCUSSION

Most of the recent papers dealing with the Humanin peptide have centred on its ability to act as a protective agent, especially in AD (Hashimoto et al., 2001), a retrograde signal peptide (Lee et al., 2013), or as an agent improving cognition (Murakami et al., 2017; Wu et al., 2017), but little has been said about the underlying biology of the *Humanin* gene. In this paper some of the basic points about *Humanin* have been examined by looking at the available sequences of human mtDNA and that of many other vertebrates found in the GenBank database.

In the mtDNA of vertebrates the *Humanin* gene is a gene-within-a-gene as it can be considered as a normal DNA gene and as such has a start-codon, a number of codons which code for amino acids, and finally a stop-codon, which is often represented by a single Thymine nucleotide. However, the bases of the *Humanin* gene are also part of a large RNA structure that is used in the building of ribosomes. Therefore, the *Humanin* gene is both a DNA gene and a RNA gene and as such it can be expected there will be evolutionary pressure to maintain the gene so that it continues to function successfully in both forms. The presumption therefore is that the nucleotide bases of the *Humanin* gene will respond to this evolutionary pressure by showing a low mutation rate. Indeed, the results presented here do suggest that the *Humanin* gene has been strongly conserved throughout vertebrate evolution, and has continued to be functional, for example, in both the human and the lamprey, which have an evolutionary period of separation of over 360 million years (Xu et al., 2016).

In the human, for which there were over 36 000 mtDNA sequences available for study, it appeared that 99.4% of the sequences did not show any mutational differences from that of the rCRS, but in 230 sequences mutations were observed. However, it is likely that the peptide functions normally in most people with mutations, e.g., the mutation C2639T, which is found in people of Haplogroup N1b, changes the 3rd amino acid from a proline to a serine, and a change this close to the end of a peptide usually has little effect. At the other end of the peptide

the mutation G2702A changes the 24th amino acid from a glycine to an adenine and similarly can be expected again to have little effect. Indeed, changes to the 3rd and 24th amino acids feature prominently in the sequences from other vertebrates.

However of much greater significance is the mutation A2672G, which causes the change of the 14th amino acid from a serine to a glycine. This change S14G is considered to increase the potency of the peptide (Li et al., 2013), and it appears that a few people in the world are able to produce this special form of Humanin naturally. Interestingly, this mutation for the most part is associated with the Haplogroup U6a7a1a, which contains members of an extended Acadian family found in Canada (Secher et al., 2014).

As for other vertebrates, there are mtDNA sequences from over 4 000 species in the GenBank database, and it has been possible to identify the *Humanin* gene unambiguously in all the sequences examined. However, and unexpectedly, many species show pseudogenization of the *Humanin* gene. For example, the human, chimpanzees, gorillas and many other monkeys do have functional genes, but the macaque monkeys, which are widely used in research, do not. Rats, guinea pigs and the northern tree shrew appear able to produce humanin, but some mice, cats and goats do not. So overall, it appears that there is a somewhat random pattern to the evolutionary success of the *Humanin* gene, with it surviving in some species, while undergoing pseudogenization in other apparently closely related species.

However, as with any apparently random pattern, there are features that may well be worthwhile considering further. In the case of the *Humanin* gene there does not appear to be any overt link to the size of an animal, it longevity or its innate intelligence. But it would seem that the presence of a potentially functional *Humanin* gene is commonly found in primates and birds. However, whether this indicates an evolutionary conserved advantage, or is just a feature of the short evolutionary history of these two groups remains to be determined.

The term pseudogene was used for the first time 40 years ago (Jacq et al., 1977) in a study looking at the genome of the African clawed toad, when it was found the genome had multiple copies of a gene. These copies were considered to have no function and were termed pseudogenes. It has since been shown that the genomes of vertebrates contain many different types of pseudogene (Mighell et al., 2000), of which duplication of genes and NUMTs are two of the types. Many pseudogenes are so fragmentary or degraded by subsequent mutations that they are clearly non-functional, but as mentioned earlier, it is possible that some chromosomal copies of the *Humanin* gene are the exception and might still be expressed. Another type of pseudogene formation occurs when a gene is affected by a mutation, or some other process, so that it stops functioning and this process is called pseudogenization. Typically this will occur as the result of loss of the start codon or the introduction of a premature stop codon. Duplication of a gene, and the subsequent loss of functioning of one copy forms another type of pseudogene, but this does not appear to apply to the *Humanin* gene, at least in the human genome (Stark et al., 2017).

The pseudogenization of the *Humanin* gene as detailed here may not solely be an interesting point of evolution, but may also have a significance in studies that use animal models. There have been many studies looking at the effect of Humanin in disease, in particular in AD, which have used animal models, and the results obtained from studies may well have been affected by whether the animals had functional copies of the *Humanin* gene, or pseudogenes. Also, research to find new animal models for many diseases is an important field (Xiao et al., 2017; Yao, 2017), and it would now seem that sequencing of the mtDNA, and in particular the *Humanin* gene, should become routine in any animal under consideration.

Overall, there is still much to be discovered about Humanin. In our own species, and in our close relatives, the peptide appears to be useful; and has been preserved. However, many other species do appear to have kept the ability to produce a Humanin-like peptide, but whether the peptide have the same function as in the human is as yet unknown. This study has also shown there are the many species where pseudogenization has taken place and the *Humanin* pseudogene continues as a sequence of nucleotide bases that form part of the structure of ribosomes.

Why the *humanin* gene has undergone pseudogenization in some species has not been determined. But it would appear that in many species there has been little evolutionary pressure to preserve their ability to make Humanin; and it is only in some species, including ourselves, that it appears to give some evolutionary advantage.

This paper has looked at *Humanin* by reviewing the evidence about the gene available from several sources, and suggests a number of places where experimental work is needed to confirm the findings. It is also possible that future practical work may show that this peptide, in its original or in a synthetic form, may have a therapeutic use in the treatment of conditions such as Alzheimer's disease.

ACKNOWLEDGEMENTS

The author is very grateful to Yong-Gang Yao (Kunming Institute of Zoology, CAS) for his many helpful comments, especially those concerning the presentation of the material in this paper.

REFERENCES

Anderson S, Bankier AT, Barrell BG, de Bruijn MHL, Coulson AR, Drouin J, Eperon IC, Nierlich DP, Roe BA, Sanger F, Schreier PH, Smith AJH, Staden R, Young IG. 1981. Sequence and organization of the human mitochondrial genome. *Nature*, **290**(5806): 457-465.

Andrews RM, Kubacka I, Chinnery PF, Lightowlers RN, Turnbull, DM, Howell N. 1999. Reanalysis and revision of the Cambridge reference sequence for human mitochondrial DNA. *Nature Genetics*, **23**(2): 147.

Bandelt HJ, Kloss-Brandstätter A, Richards MB, Yao YG, Logan I. 2014. The case for the continuing use of the revised Cambridge Reference Sequence (rCRS) and the standardization of notation in human mitochondrial DNA studies. *Journal of Human Genetics*, **59**(2): 66-77.

Benson DA, Karsch-Mizrachi I, Lipman DJ, Ostell J, Wheeler DL. 2005. GenBank. *Nucleic Acids Research,* **33**(S1): D34-D38.

Bodzioch M, Lapicka-Bodzioch K, Zapala B, Kamysz W, Kiec-Wilk B, Dembinska-Kiec A. 2009. Evidence for potential functionality of nuclearly-encoded humanin isoforms. *Genomics*, **94**(4): 247-256.

Cohen A, Lerner-Yardeni J, Meridor D, Kasher R, Nathan I, Parola AH. 2015. Humanin Derivatives Inhibit Necrotic Cell Death in Neurons. *Molecular Medicine*, **21**(1): 505-514.

Hashimoto Y, Niikura T, Tajima H, Yasukawa T, Sudo H, Ito Y, Kita Y, Kawasumi M, Kouyama K, Doyu M, Sobue G, Koide T, Tsuji S, Lang J, Kurokawa K, Nishimoto I. 2001. A rescue factor abolishing neuronal cell death by a wide spectrum of familial Alzheimer's disease genes and Aβ. *Proceedings of the National Academy of Sciences of the United States of America*, **98**(11), 6336–6341.

Hashimoto Y, Nawa M, Kurita M, Tokizawa M, Iwamatsu A, Matsuoka M. 2013. Secreted calmodulin-like skin protein inhibits neuronal death in cell-based Alzheimer's disease models via the heterotrimeric Humanin receptor. *Cell Death and Disease*, **4**(3): e555.

Jacq C, Miller JR, Brownlee GG. 1977. A pseudogene structure in 5S DNA of Xenopus laevis. *Cell*, **12**(1): 109-120.

Lee C, Yen K, Cohen P. 2013. Humanin: a harbinger of mitochondrial-derived peptides? *Trends in Endocrinology & Metabolism*, **24**(5): 222-228.

Li X, Zhao WC, Yang HQ, Zhang JH, Ma JJ. 2013. S14G-humanin restored cellular homeostasis disturbed by amyloid-beta protein. *Neural Regeneration Research,* 2013. **8**(27): 2573-2780.

Matsuoka M. 2015. Protective effects of Humanin and calmodulin-like skin protein in Alzheimer's disease and broad range of abnormalities. *Molecular Neurobiology*, **51**(3): 1232-1239.

Mighell AJ, Smith NR, Robinson PA, Markham AF. 2000. Vertebrate pseudogenes. *Federation of European Biochemical Societies Letters*, **468**(2-3): 109-114.

Murakami M, Nagahama M, Maruyama T, Niikura T. 2017. Humanin ameliorates diazepam-induced memory deficit in mice. *Neuropeptides*, **62**: 65-70.

Pruitt KD, Tatusova T, Maglott DR. 2007. NCBI reference sequences (RefSeq): a curated non-redundant sequence database of genomes, transcripts and proteins. *Nucleic Acids Research*, **35**(Database issue): D61- D65.

Romeo M, Stravalaci M, Beeg M, Rossi A, Fiordaliso F, Corbelli A, Salmona M, Gobbi M, Cagnotto A, Diomede L. 2017. Humanin Specifically Interacts with Amyloid-β Oligomers and Counteracts Their in vivo Toxicity. *Journal of Alzheimer's Disease*, **57**(3): 857-871.

Secher B, Fregel R, Larruga JM, Cabrera VM, Endicott P, Pestano JJ, González AM. 2014. The history of the North African mitochondrial DNA haplogroup U6 gene flow into the African, Eurasian and American continents. *BioMed Central Evolutionary Biology*, **14**: 109.

Stark TL, Liberles DA, Holland BR, O'Reilly MM. 2017. Analysis of a mechanistic Markov model for gene duplicates evolving under subfunctionalization. *BioMed Central Evolutionary Biology,* **17**(1): 38.

Subramanian S, Mohandesan E, Millar CD, Lambert DM. 2015. Distance-dependent patterns of molecular divergences in Tuatara mitogenomes. *Scientific Reports*. **5**: 8703.

Tajima H, Niikura T, Hashimoto Y, Ito Y, Kita Y, Terashita K, Yamazaki K, Koto A, Aiso S, Nishimoto I. 2002. Evidence for in vivo production of Humanin peptide, a neuroprotective factor against Alzheimer's disease-related insults. *Neuroscience Letters*, **324**(3): 227-231.

Terashita K, Hashimoto Y, Niikura T, Tajima H, Yamagishi Y, Ishizaka M, Kawasumi M, Chiba T, Kanekura K, Yamada M, Nawa M, Kita Y, Aiso S, Nishimoto I. 2003. Two serine residues distinctly regulate the rescue function of Humanin, an inhibiting factor of Alzheimer's disease-related neurotoxicity: functional potentiation by isomerization and dimerization. *Journal of Neurochemistry,* **85**(6): 1521-1538.

van Oven M, Kayser M. 2009. Updated comprehensive phylogenetic tree of global human mitochondrial DNA variation. *Human Mutation*, **30**(2): E386-E394.

Wu M, Shi H, He YX, Yuan L, Qu XS, Zhang J, Wang ZJ, Cai HY, Qi JS. 2017 Colivelin Ameliorates Impairments in Cognitive Behaviors and Synaptic Plasticity in APP/PS1 Transgenic Mice. *Journal of Alzheimer's Disease*, **59**(3): 1067-1078.

Xiao J, Liu R, Chen CS. 2017. Tree shrew (Tupaia belangeri) as a novel non-human primate laboratory disease animal model. *Zoological Research*, **38**(3): 127-137.

Xu Y, Zhu SW, Li QW. 2016. Lamprey: a model for vertebrate evolutionary research. *Zoological Research,* **37**(5): 263-269.

Yao YG, Salas A, Logan I, Bandelt HJ. 2009. mtDNA data mining in GenBank needs surveying. *American Journal of Human Genetics*, **85**(6): 929-933.

Yao, YG. 2017. Creating animal models, why not use the Chinese tree shrew (Tupaia belangeri chinensis)? *Zoological research*, **38** (3): 118-126.

Zaki MJ, Karypis G, Yang J. 2007. Data Mining in Bioinformatics (BIOKDD). *Algorithms for Molecular Biology*, **2**: 4.

A new record of the capped langur (*Trachypithecus pileatus*) in China

DEAR EDITOR,

The distribution of the capped langur (*Trachypithecus pileatus*) in China has become controversial since Shortridge's langur (*Trachypithecus shortridgei*) was upgraded to a full species. The capped langur is considered to be distributed in northeast India, Bangladesh, Bhutan, and northwest Myanmar only (Brandon-Jones et al., 2004; Choudhury, 2008, 2014; Das et al., 2008; Groves, 2001). In our field survey, however, we obtained photos of the capped langur, demonstrating its existence in China.

Following the species promotion of Shortridge's langur (Brandon-Jones et al., 2004; Groves, 2001) and the delimiting of its distribution range to northwestern Yunnan in China and northeastern Myanmar (Brandon-Jones et al., 2004; Cui et al., 2016; Das et al., 2008; Groves, 2001; Htun et al., 2008), with a new record in southeastern Tibet (Wu et al., 2016), the capped langur has been deleted from the checklist of mammals in China (Jiang et al., 2015). Despite this, Dr. George Schaller has suggested that capped langurs might exist in the northeastern section of the Yarlung-Zangbo River (Choudhury, 2008).

Recently, we conducted the Second National Survey of Terrestrial Wildlife Resources in southern Tibet along the southern slopes of the Himalayas in China (Figure 1) from 2013 to 2015 based on community interviews, field surveys (line transects), and camera traps in Dingjie, Yadong, Luozha, Cuona, Longzi, and Motuo counties. These counties encompass the potential distribution area of the langurs based on information from local forestry and conservation government departments in Tibet and previously published literature on langur species (Choudhury, 2008, 2014; Mittermeier et al., 2013; Smith & Xie, 2009; Wang, 2003). In this study, we aimed to: (1) determine if the capped langur exists in China, and (2) clarify its distribution in the southern Himalaya region.

Community interviews were conducted from June to August 2015. Following snowball sampling (Newing et al., 2011), we interviewed local leaders, forest patrollers, and regional forest managers. The interviewees were asked to describe the characteristics of the langur, and then identify the species from photos of several local langurs and macaques. The date, location, and group size of the langurs were recorded if the interviewees could correctly describe and identify the langur they encountered. We interviewed 41 people in 12 villages of the five surveyed counties, including 34 men and seven women. We conducted field surveys in habitats with low human disturbance near the villages where the community interview obtained positive feedback. We set line transects in subtropical and evergreen broad-leaved forest (suitable habitat for langur species) to corroborate the interview data. We set ten line transects in Cuona County, two in Dingjie County, and two in Yadong County from July to August 2015. The transects in Cuona County had a mean length of 8.6 km (range 2.8–15.7 km), with elevation ranging from 2 336 to 3 000 m a.s.l.. The transects in the other two counties had a mean length of 28.9 km (range 7.3–97.3 km), with the elevation ranging from 2 100 to 3 000 m a.s.l.. The transect lines covered two types of woodland (evergreen broad-leaved forest, mixed broadleaf-conifer forest). We recorded all primate individuals and the latitude and longitude where they were found. To obtain valuable image information, we set 32 camera traps (Ltl 6210, Shenzhen Ltl Acorn Electronics Co. Ltd) in Gedang, Deyang Gully, and Xigong River of Motuo County from 16 October 2013 to 25 April 2014 (over 180 days). The camera traps were also placed in potential langur habitats (evergreen broad-leaved forest, mixed broadleaf-conifer forest).

One local person from Lai village and two from Xian village in Cuona County correctly described and identified the capped langur from other langurs and macaques, and also provided information that the capped langur population near the villages consisted of about 20–30 individuals (Table 1). Importantly, we obtained valuable photos of the capped langur subspecies *T. p. tenebricus* taken by local villagers in Lai village at noon (1200h) on 12 April 2014 (Figure 2A). Species identifications were consistent with the description of capped langurs in previous studies (Brandon-Jones et al., 2004; Choudhury, 2014; Groves, 2001). In the photos, at least four capped langur individuals (three adults and one infant) could be identified (Supplementary Figure S1 A, B). These photos provided strong evidence of the existence of the capped langur in Tibet, China. However, we did

Received: 15 March 2017; Accepted: 09 June 2017

Foundation items: This study was supported by the Second National Survey of Terrestrial Wildlife Resources of the State Forestry Administration of China (*Semnopithecus schistaceus* Project, No. 176 Geographic Unit Project), the National Natural Science Foundation of China (31400361), the Science and Technology Planning Project of Guangdong Province, China (2013B061800042), and the National Key Program (2016YFC0503200) from the Ministry of Science and Technology of China

DOI: 10.24272/j.issn.2095-8137.2017.038

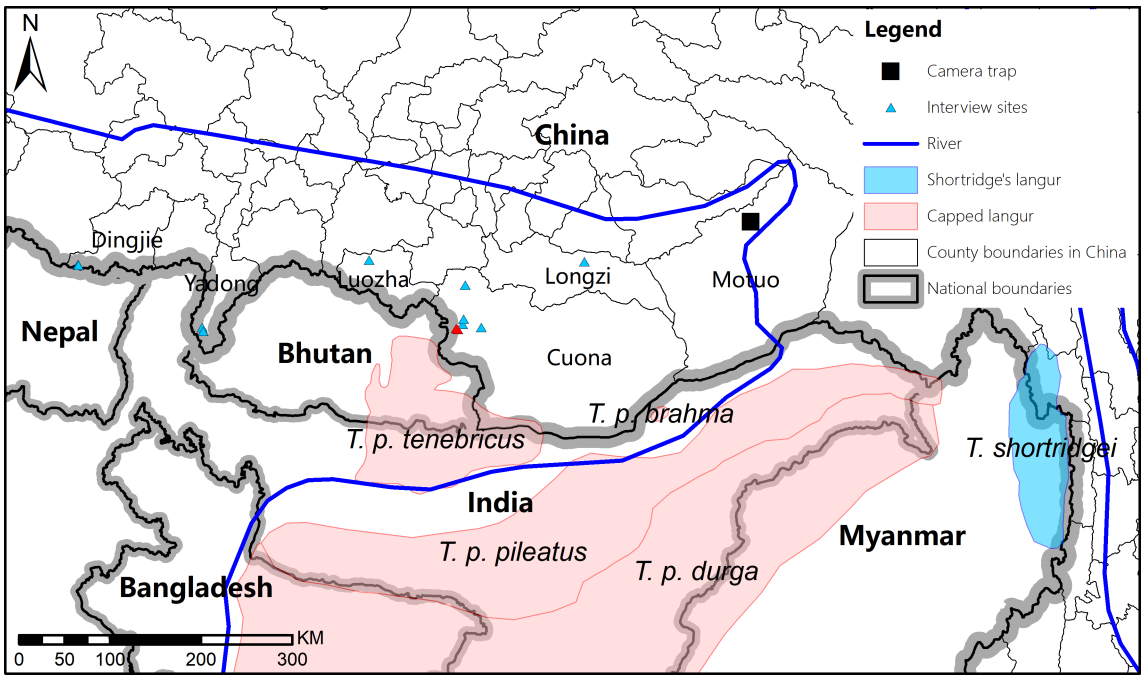

Figure 1 Map of langur survey area, including the counties within our study area

Blue triangles indicate field survey sites; red triangles show areas where capped langurs were found; black square indicates the location in Motuo County where a langur species (possibly Shortridge's langur) was found; light orange and light blue areas indicate the former distribution areas of capped and Shortridge's langurs, respectively (data from IUCN red list site).

Table 1 Details on the towns and villages in southern Tibet, China, where interviews were conducted between June and August 2015

Location	County	Number of Interviewees (*n*)
Chentang Town	Dingjie	4
Nadang Township	Dingjie	5
Chunpi Village	Yadong	3
Xia Yadong Township	Yadong	3
Zara Township	Luozha	3
Yumai Township	Luozha	3
Lampug Township	Cuona	3
Qudromo Township	Cuona	3
Marmang Township	Cuona	3
Lai Township	Cuona	4
Xian Village	Cuona	3
Gyiba Township	Cuona	1

not find any capped langur individuals during the field survey. Previously, the distribution of the capped langur was considered to be northeast India, Bangladesh, Bhutan, and northwest Myanmar, with subspecies *T. p. tenebricus* distributed north of Brahmaputra River (lower part of the Yarlung-Zangbo River), including Bhutan and the Assam State of India, which neighbor Cuona County (Choudhury, 2008, 2014; Das et al., 2008). The habitat and topography in these regions provide the possibility of langur dispersal, with the lower range of the southern Himalayas a potential habitat for this species.

Although no photo evidence was provided, a recent study indicated that Shortridge's langur is also distributed in southeastern Tibet (Wu et al., 2016). In the present study, a langur species (possibly Shortridge's langur) was twice captured by our camera trap (E94.90436°, N29.20175°, 1 429 m a.s.l.) in Deyang Gully, west of Xirang Township in Motuo County in January and March 2014 (Figure 2B and Supplementary Figure S2 A–C; three adults and an infant). However, as these pictures only caught the profiles of the species of interest, we cannot confirm with certainty that these are Shortridge's langurs. According to Choudhury (2014), the capped langur subspecies *T. p. brahma* is also distributed near Motuo County. Thus, the langur species we found in the Deyang Gully might also be *T. p. brahma* due to their similar gray coats. Further studies are needed to confirm the classification status of the langur species in Deyang Gully.

In our study, we confirmed the existence of the capped langur in China. As capped langurs are endangered, with small populations, the threat of habitat degradation and expanding human activities highlights the need for increasing conservation effort. Traditionally, Chinese mammalogists have used the Chinese name of "戴帽叶猴" for Shortridge's langur (*T. shortridgei*) (Jiang et al., 2015; Smith & Xie, 2009), which might cause confusion regarding the new record of capped langur (*T. pileatus*) in China. It is suggested that Shortridge's langur be named as "萧氏叶猴" and the capped langur be named as "戴帽叶猴".

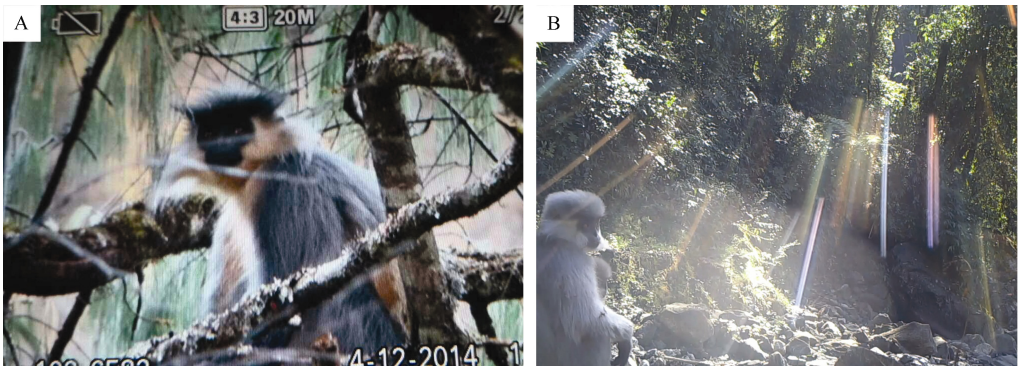

Figure 2 Photos of capped langur in Cuona County (A) and a langur species (possibly Shortridge's langur) in Motuo County (B)

ACKNOWLEDGEMENTS

We thank Wen-Wen Zhang and Ke Rong from the Northeast Forestry University, Wei-Shi Liu from the Chinese Academy of Forestry, and the local forestry administrations for assistance with the community interviews. We also thank the anonymous reviewers for their constructive suggestions for improving the quality of this manuscript.

Yi-Ming Hu[1,2,3,#], Zhi-Xin Zhou[1,#], Zhi-Wen Huang[1], Ming Li[2], Zhi-Gang Jiang[2], Jian-Pu Wu[4], Wu-Lin Liu[4], Kun Jin[5,*], Hui-Jian Hu[1,*]

[1] *Guangdong Key Laboratory of Animal Conservation and Resource Utilization*, *Guangdong Public Laboratory of Wild Animal Conservation and Utilization, Guangdong Institute of Applied Biological Resources*, *Guangzhou Guangdong* 510260, *China*

[2] *Institute of Zoology*, *Chinese Academy of Sciences*, *Beijing* 100101, *China*

[3] *University of the Chinese Academy of Sciences*, *Beijing* 100049, *China*

[4] *Forestry Inventory and Planning Institute of the Tibet Autonomous Region*, *Lhasa Tibet* 850000, *China*

[5] *Research Institute of Forest Ecology Environment and Protection*, *Chinese Academy of Forestry*, *Beijing* 100091, *China*

[#]Authors contributed equally to this work

[*]Corresponding authors, E-mail: jk2002@caf.ac.cn; 13922339577@139.com

REFERENCES

Brandon-Jones D, Eudey AA, Geissmann T, Groves CP, Melnick DJ, Morales JC, Shekelle M, Stewart CB. 2004. Asian primate classification. *International Journal of Primatology,* **25**(1): 97-164.

Choudhury A. 2008. Primates of Bhutan and observations of hybrid langurs. *Primate Conservation,* **23**(1): 65-73.

Choudhury A. 2014. Distribution and current status of the capped langur *Trachypithecus pileatus* in India, and a review of geographic variation in its subspecies. *Primate Conservation,* **28**(1): 143-157.

Cui LW, Li YC, Ma C, Scott MB, Li JF, He XY, Li DH, Sun J, Sun WM, Xiao W. 2016. Distribution and conservation status of Shortridge's capped langurs *Trachypithecus shortridgei* in China. *Oryx,* **50**(4): 732-741.

Das J, Molur S, Bleisch W. 2008[2016-05-17]. *Trachypithecus pileatus*. The IUCN red list of threatened species 2008: e.T22041A9350087. http://dx.doi.org/10.2305/IUCN.UK.2008.RLTS.T22041A9350087.en.

Groves C. 2001. Primate Taxonomy. Washington DC: Smithsonian Institution Press.

Htun S, Yongcheng L, Richardson M. 2008[2016-03-17]. *Trachypithecus shortridgei*. The IUCN red list of threatened species 2008: e.T39869A10268796. http://dx.doi.org/10.2305/IUCN.UK.2008.RLTS.T39869A10268796.en.

Jiang ZG, Ma Y, Wu Y, Wang YX, Zhou KY, Liu SY, Feng ZJ. 2015. China's Mammal Diversity and Geographic Distribution. Beijing: Science Press. (in Chinese)

http://dx.doi.org/10.2305/IUCN.UK.2008.RLTS.T39840A10275563.en.

Mittermeier RA, Rylands AB, Wilson DE. 2013. Handbook of the Mammals of the World, Volume 3: Primates. Barcelona: Lynx Edicions.

Newing H, Eagle C, Puri R, Watson C. 2011. Conducting Research in Conservation: A Social Science Perspective. Abingdon: Routledge.

Smith AT, Xie Y. 2009. A Guide to the Mammals of China. Changsha: Hunan Education Publishing House. (in Chinese)

Wang YX. 2003. A Complete Checklist of Mammal Species and Subspecies in China-A Taxonomic and Geographic Reference. Beijing: China Forestry Publishing House.

Wu JP, Luo H, Zhu XL, Li BZ, Liu WL, Ci P. 2016. Monitoring mammals and birds with camera traps at different altitudes of Medog, Tibet. *Biodiversity Science,* **24**(3): 351-354. (in Chinese)

Rediscovery of the sun bear (*Helarctos malayanus*) in Yingjiang County, Yunnan Province, China

DEAR EDITOR,

The sun bear, *Helarctos malayanus* (Raffles, 1821), is a forest-dependent bear species distributed in tropical Southeast Asia. The species was previously reported from scattered localities in southwestern China, which is at the northeastern edge of its global range. Due to the scarcity of reliable recent records, some authorities cast doubt on the continued existence of sun bear in China. Here we present the rediscovery of this species in Yingjiang County, western Yunnan Province, China, near the international border with Myanmar's Kachin State.

The sun bear, *Helarctos malayanus* (Raffles, 1821), is the rarest species in the family Ursidae in China, and is listed as a Category I species on the National Key Protected Animal List. The latest Red List of China's Vertebrates (Jiang et al., 2016) evaluated the sun bear as Critically Endangered (CR), though globally it is categorized as Vulnerable (VU) species by the International Union for Conservation of Nature (IUCN) Red List, indicating the species has undergone a suspected >30% decline in the global population (Fredriksson et al., 2008).

Globally, the sun bear occurs in northeast India, Bangladesh, and throughout Southeast Asia including the islands of Sumatra and Borneo. The sun bear is the most arboreal of all bear species and is found predominantly in lowland dipterocarp rainforest (Smith & Xie, 2008). Due to habitat destruction and poaching for their body parts as traditional medicine, the sun bear is now extinct in Singapore (Fredriksson et al., 2008) and has possibly become extinct more recently in Bangladesh (Islam et al., 2010). Studies in Vietnam (Cano & Tellería, 2013), Borneo (Meijaard, 1999) and Sumatra (Wong et al., 2013) also reported declines in both abundance and distribution, and the species has been extirpated from much of its former range.

Literature on the presence of sun bear in China is scanty, and the IUCN Red List stipulated that its current distribution in China is unknown. Richard Lydekker (1849–1915), a British naturalist, was the first to report the occurrence of sun bear in the Tibetan area of China. However, his specimen of two skulls and a skin of unknown provenance came from a wildlife trader (i.e., Rowland Ward Ltd.), and the author pointed out that the skin has external features of an Asiatic black bear (*Ursus thibetanus*) rather than that of a sun bear (Lydekker, 1906). Ernest Henry Wilson (1876–1930), another English who spent 11 years exploring southwestern China collecting plants, subsequently analyzed the trade routes and patterns of wildlife products of the area, and expressed his skepticism about the provenance for Lydekker's specimen, and argued that the skulls probably originated from the warmer regions of Yunnan Province while the skin was that of a Asiatic Black Bear (Wilson, 1913).

The first unequivocal record of sun bear occurrence in southern Yunnan came from Wang (1987), who collected a female specimen from the Red River Basin in 1972. Yin & Liu (1993) reported the collection of two sun bear specimens from Tibet during 1987–1990, and reported that sun bears occurred at an altitudinal range of 3 000-3 500 m a.s.l. in Mangkang County. It is of note that the highest known elevational record for sun bear is at 2 143 m a.s.l. in Sumatra (Fredriksson et al., 2008), the Tibet records thus warrant some investigation. Ma et al. (1994) and Hu (1995) reported the capture of a sun bear in Jingxi County of Guangxi Province, by the Sino-Vietnamese border, but these authors did not provide detailed information of this record. A number of publications reported the existence of sun bears in Sichuan Province and the northwestern part of Yunnan, but these reports are not supported by solid evidence such as specimens or photos (Jiang et al., 2015; Shi & Zhao, 1982; Smith & Xie, 2008). The current status and distribution of sun bear in China is unknown though it was listed in recent publications (Pan et al., 2007; Wang, 2003), and some scientists suspected the species may already be extinct in China (Smith & Xie, 2008).

At 1927h on 23 October 2016, we obtained a 10 sec video footage of a bear species by a camera trap installed in a community forest in Yingjiang County, Dehong Dai and Jingpo Autonomous Prefecture, Yunnan Province (Supplementary Video, available online). Despite the poor light, we could clearly identify the subject animal as a sun bear with the following diagnostic features: head broad with a short snout; muzzle very short and pale in color; face pale in contrast to the black body; ears set low on sides of head, very small and rounded without ear tuft; coat black, very short and dense; crescent-shaped pale-colored chest mark; limbs relatively slender and long, forelimbs bowed, forefeet turned inward.

The site of discovery is a disturbed montane rainforest at 1 000 m a.s.l. at N24°32', E97°34', adjacent to Tongbiguan Provincial Nature Reserve (Tongbiguan NR) less than 1 km from the international border with Kachin State of Myanmar.

Received: 05 May 2017; Accepted: 03 July 2017
DOI:10.24272/j.issn.2095-8137.2017.044

Camera traps from the same locality recorded several sympatric mammal species, including wild boar (*Sus scrofa*), red muntjac (*Muntiacus vaginalis*), Chinese serow (*Capricornis milneedwardsii*) and yellow-throated marten (*Martes flavigula*). We also camera-trapped the Asiatic black bear approximately 1.8 km east of the sun bear site in the same forest block, suggesting the two ursid species are sympatric in the western part of Yingjiang County.

Our sun bear record from Yingjiang produced the first image of the species for China, and represents a rediscovery of this species in Yunnan after an absence of 45 years. Although the site of discovery is very close to the boundary of Tongbiguan NR, the community forest is subject to high human disturbances, and under threats from being cleared for agriculture, as well as hydro-dam and road construction. We urge relevant government agencies to reconsider the necessity of all development plans of the general area to avoid further forest degradation, and step up protection and restoration efforts of natural forest surrounding Tongbiguan NR to reconnect fragmented lowland forest blocks, so as to enhance the future survival of tropical wildlife such as the highly threatened sun bear.

ACKNOWLEDGEMENTS

We would like to express our gratitude to the Yingjiang County Propaganda Department and the Forestry Bureau, and local villagers for their hospitality, encouragement and support. We thank Quan Li of Kunming Institute of Zoology, Chinese Academy of Sciences, for checking bear specimens in his institution's collection, Will Duckworth and Lorraine Scotson for verification of sun bear identification.

Fei Li[1], Xi Zheng[1], Xue-Long Jiang[2], Bosco Pui Lok Chan[1,*]

[1] *Kadoorie Conservation China*, *Kadoorie Farm & Botanic Garden*, *Hong Kong* 999077, *China.*

[2] *State Key Laboratory of Genetic Resources and Evolution*, *Kunming Institute of Zoology*, *Chinese Academy of Sciences*, *Kunming Yunnan* 650223, *China*

[*]Corresponding author, E-mail: boscokf@kfbg.org

REFERENCES

Cano LS, Tellería JL. 2013. Local ecological knowledge as a tool for assessing the status of threatened vertebrates: a case study in Vietnam. *Oryx,* 47(2): 177-183.

Fredriksson G, Steinmetz R, Wong S, Garshelis DL. 2008. Helarctos malayanus. The IUCN Red List of Threatened Species 2008: e.T9760A13014055. http://dx.doi.org/10.2305/IUCN.UK.2008.RLTS.T9760A13014055.en.

Hu JC. 1995. The bear resource and its protection in Southwest China. *Journal of Sichuan Teachers College* (*Natural Science*)*,* 16(4): 274-278. (in Chinese)

Islam A, Muzaffar SB, Aziz A, Kabir M, Uddin M, Chakma S, Chowdhury SU, Rashid A, Chowdhury GW, Mohsanin S, Jahan I, Saif S, Hossain B, Chakma D, Kamruzzaman. 2010. Baseline survey of Bears in Bangladesh 2008-2010. Wildlife Trust of Bangladesh.

Jiang ZG, Ma Y, Wu Y, Wang YX, Zhou KY, Liu SY, Feng ZJ. 2015. China's Mammal Diversity and Geographic Distribution. Beijing: Science Press, 159. (in Chinese)

Jiang ZG, Jiang JP, Wang YZ, Zhang E, Zhang YY, Li LL, Xie F, Cai B, Cao L, Zheng GM, Dong L, Zhang ZW, Ding P, Luo ZH, Ding CQ, Ma ZJ, Tang SH, Cao WX, Li CW, Hu HJ, Ma Y, Wu Y, Wang YX, Zhou KY, Liu SY, Chen YY, Li JT, Feng ZJ, Wang Y, Wang B, Li C, Song XL, Cai L, Zang CX, Zeng Y, Meng ZB, Fang HX, Ping XG. 2016. Red list of China's vertebrates. *Biodiversity Science,* 24(5): 500-551. (in Chinese)

Lydekker R. 1906. On the Occurrence of the Bruang in the Tibetan Province. *Proceedings of the Zoological Society of London,* 66: 997-999.

Ma YQ, Hu JC, Zhai QL. 1994. Bears of China. Chengdu: Sichuan Science and Technology Press, 1-146. (in Chinese)

Meijaard E. 1999. Human-imposed threats to sun bears in Borneo. *Ursus,* 11: 185-192.

Pan QH, Wang YX, Yan K. 2007. A Field Guide to the Mammals of China. Beijing: China Forestry Publishing House, 96. (in Chinese)

Shi BN, Zhao EM. 1982. Sichuan Fauna Economica, Volume I: Overview. Chengdu: Sichuan People's Publishing House, 84. (in Chinese)

Smith AT, Xie Y. 2008. A Guide to the Mammals of China. Princeton: Princeton University Press, 423-425.

Wang YX. 1987. Biological Resource Survey Report of Honghe Region, southern Yunnan, Volume I. Kunming: Publishing House of Yunnan Minority Nationalities, 13-14. (in Chinese)

Wang YX. 2003. A Complete Checklist of Mammal Species and Subspecies in China-A Taxonomic and Geographic Reference. Beijing: China Forestry Publishing House, 75-76. (in Chinese)

Wilson EH. 1913. A Naturalist in Western China, with Vasculum, Camera, and Gun: Being Some Account of Eleven Years' Travel, Exploration, and Observation in the More Remote Parts of the Flowery Kingdom, Volume II. London: Methuen & Go., Ltd., 184-188.

Wong WM, Leader-Williams N, Linkie M. 2013. Quantifying changes in sun bear distribution and their forest habitat in Sumatra. *Animal Conservation,* 16(2): 216-223.

Yin BG, Liu WL. 1993. Wildlife and its Conservation in Xizang. Beijing: China Forestry Publishing House, 65. (in Chinese)

Identification of a novel mtDNA lineage B3 in chicken (*Gallus gallus domesticus*)

DEAR EDITOR,

In this study, we sequenced the complete mitochondrial DNA genome (mitogenome) of the Zhengyang Yellow chicken (*Gallus gallus domesticus*) by next-generation sequencing technology. Samples were taken from Zhumadian city, Henan Province, China. The complete mitogenome was 16 785 bp in size, and had a nucleotide composition of 30.3% (A), 23.7% (T), 32.5% (C), and 13.5% (G), with a high AT content of 54.0%. The assembled mitogenome exhibited typical mitochondrial DNA (mtDNA) structure, including a non-coding control region, two rRNA genes, 13 protein-coding genes, and 22 tRNA genes. Phylogenetic analysis indicated that this mitogenome defined a novel sub-haplogroup B3 within haplogroup B. These results should provide essential information for chicken domestication and insight into the evolution of genomes.

Zhengyang yellow chicken (*Gallus gallus domesticus*) is an indigenous breed from Zhengyang County of Zhumadian in Henan Province, China (China National Commission of Animal Genetic Resources, 2011), and is noted for its yellow-colored shank, beak, and feathers. This chicken possesses many valuable and stable genetic traits that could be used as a gene bank for cultivating and creating new breeds in China. Here, for the first time, we sequenced and characterized the complete mtDNA genome of the Zhengyang yellow chicken.

Blood samples were collected from a Zhengyang yellow chicken farm in Zhumadian city, Henan Province, China. Genomic DNA was extracted from whole blood by standard phenol/chloroform methods. In addition, PCR for mtDNA fragments, library construction and next-generation sequencing, and *de novo* assembly were conducted as per previous publication (Chen et al., 2016). We followed caveats for quality control in mtDNA genome study in domestic animals (Shi et al., 2014). We scored the variants relative to the GenBank reference sequence under Accession No. AP003321 (Nishibori et al., 2005), and manually checked the bam file exported by Torrent Suite 5.0.2 to confirm the scored variants using Integrative Genomics Viewer (Thorvaldsdóttir et al., 2013).

The complete mitochondrial genome of the Zhengyang yellow chicken was 16 785 bp in length (GenBank Accession No. KX987152), with a base composition of 30.3% for A, 23.7% for T, 32.5% for C, and 13.5% for G, showing a high A+T content of 54.0%. Furthermore, the genome contained a typical structure, including a non-coding control region (D-loop), two ribosomal RNA genes, 13 protein-coding genes, and 22 tRNA genes. The arrangement of all genes was identical to that of *Gallus gallus* mtDNA (e.g., Huang et al., 2016; Liu et al., 2016). All proteins started with ATG, except for *COX1* (GTG). In addition, apart from eight tRNA genes ($tRNA^{Gln}$, $tRNA^{Ala}$, $tRNA^{Asn}$, $tRNA^{Cys}$, $tRNA^{Tyr}$, $tRNA^{Ser}$, $tRNA^{Pro}$, and $tRNA^{Glu}$) and one protein-coding gene (*ND6*), all other mitogenome genes were encoded on the H strand. Different genes shared different stop codons; for example, *ND1*, *COX2*, *ATPase8*, *ATPase6*, *ND3*, *ND4L*, *ND5*, *Cytb*, and *ND6* used TAA as a stop codon, *ND2* used TAG, *COX1* used AGG, and *COX3* and *ND4* used an incomplete stop codon ''T– –''.

Phylogenetic analysis was performed using complete mtDNA sequences containing major haplogroups and sub-haplogroups, as defined by Miao et al. (2013) and Peng et al. (2015). The aligned sequences were analyzed by maximum parsimony using MEGA 5.0 with 1 000 bootstrap replicates (Tamura et al., 2011). Our results showed that the Zhengyang yellow chicken sequence was clustered with sequences belonging to haplogroup B (Figure 1). This newly generated sequence characterized a novel sub-haplogroup B3 within haplogroup B (Miao et al., 2013; Peng et al., 2015) (Supplementary Figure S1). This sub-haplogroup B3 was determined by an additional coding region variation at site 16 359. After searching the published chicken mtDNA datasets, we found seven chicken mtDNAs containing this variation, but they did not belong to B3 (data not shown).

Haplogroup B is common in chicken mtDNA datasets (Liu et al., 2006; Miao et al., 2013), but no geographic distribution information for sub-haplogroup B3, which was defined by both D-loop variants and coding region variations, currently exists. Identification of more B3 mtDNAs (by genotyping the variation at site 16 359 in those haplogroup B samples defined by the D-loop mutation motif) will provide additional information regarding the geographic origin and dispersal of this lineage in domestic chicken.

Received: 09 March 2017; Accepted: 28 April 2017

Foundation items: This work was supported by the Guangdong Natural Science Foundation (2014A030307018), Science and Technology Planning Project of Guangdong Province (2016A030303068), and Animal Branch of the Germplasm Bank of Wild Species (GBOWS)

DOI: 10.24272/j.issn.2095-8137.2017.039

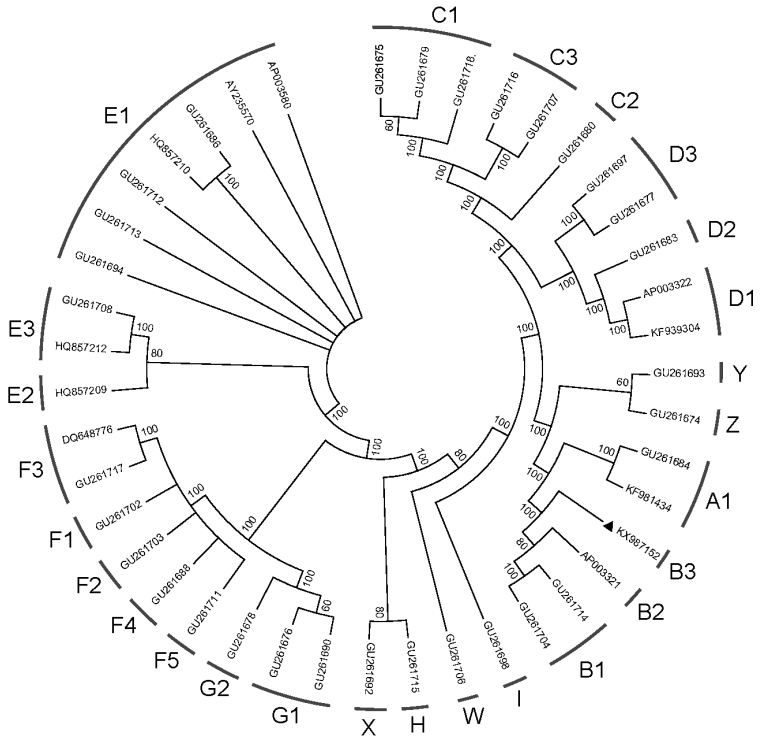

Figure 1 Phylogenetic tree based on mitochondrial genome analyses of 42 chicken samples using maximum parsimony

ACKNOWLEDGEMENTS

The authors thank the Bureau of Animal Husbandry of Zhengyang County for their assistance in sampling.

Xun-He Huang[1,#], Gui-Mei Li[2,3,#], Xing Chen[4], Ya-Jiang Wu[5], Wei-Na Li[1], Fu-Sheng Zhong[1], Wen-Zhi Wang[4,6], Zhao-Li Ding[2,3,*]

[1] *School of Life Sciences*, *Jiaying University*, *Meizhou Guangdong* 514015, *China*

[2] *Kunming Biological Diversity Regional Center of Large Apparatus and Equipments*, *Chinese Academy of Sciences*, *Kunming Yunnan* 650223, *China*

[3] *Public Technical Service Center*, *Kunming Institute of Zoology*, *Chinese Academy of Science*, *Kunming Yunnan* 650223, *China*

[4] *State Key Laboratory of Genetic Resources and Evolution*, *Kunming Institute of Zoology*, *Chinese Academy of Sciences*, *Kunming Yunnan* 650223, *China*

[5] *State Key Laboratory for Conservation and Utilization of Bio-resource in Yunnan*, *Yunnan University*, *Kunming Yunnan* 650091, *China*

[6] *Forensic Science Service of Yunnan Endangered Species Scientific Commission*, *Kunming Yunnan* 650223, *China*

[#]Authors contributed equally to this work

[*]Corresponding author, E-mail: dingzl@mail.kiz.ac.cn

REFERENCES

Chen X, Ni G, He K, Ding ZL, Li GM, Adeola AC, Murphy RW, Wang WZ, Zhang YP. 2016. An improved *de novo* pipeline for enrichment of high diversity mitochondrial genomes from Amphibia to high-throughput sequencing. *bioRxiv,* doi: 10.1101/080689.

China National Commission of Animal Genetic Resources. 2011. Animal Genetic Resources in China Poultry. Beijing: China Agriculture Press. (in Chinese)

Huang XH, Zhong FS, Li WN, Chen JB, Zhang AX, Yao QF. 2016. Complete mitochondrial genome of the Wuhua three-yellow chicken (*Gallus gallus domesticus*). *Mitochondrial DNA Part A,* **27**(2): 1311-1312.

Liu LL, Xie HB, Yang YS, Yu QF, He JH. 2016. The complete mitochondrial genome of the Xuefeng black-boned chicken. *Mitochondrial DNA Part A,* **27**(1): 30-31.

Liu YP, Wu GS, Yao YG, Miao YW, Luikart G, Baig M, Beja-Pereira A, Ding ZL, Palanichamy MG, Zhang YP. 2006. Multiple maternal origins of chickens: out of the Asian jungles. *Molecular Phylogenetics and Evolution,* **38**(1): 12-19.

Miao YW, Peng MS, Wu GS, Ouyang YN, Yang ZY, Yu N, Liang JP, Pianchou G, Beja-Pereira A, Mitra B, Palanichamy MG, Baig M, Chaudhuri TK, Shen YY, Kong QP, Murphy RW, Yao YG, Zhang YP. 2013. Chicken domestication: an updated perspective based on mitochondrial genomes. *Heredity,* **110**(3): 277-282.

Nishibori M, Shimogiri T, Hayashi T, Yasue H. 2005. Molecular evidence for hybridization of species in the genus *Gallus* except for *Gallus varius*.

Animal Genetics, **36**(5): 367-375.

Peng MS, Fan L, Shi NN, Ning T, Yao YG, Murphy RW, Wang WZ, Zhang YP. 2015. DomeTree: a canonical toolkit for mitochondrial DNA analyses in domesticated animals. *Molecular Ecology Resources,* **15**(5): 1238-1242.

Shi NN, Fan L, Yao YG, Peng MS, Zhang YP. 2014. Mitochondrial genomes of domestic animals need scrutiny. *Molecular Ecology,* **23**(22): 5393-5397.

Tamura K, Peterson D, Peterson N, Stecher G, Nei M, Kumar S. 2011. MEGA5: molecular evolutionary genetics analysis using maximum likelihood, evolutionary distance, and maximum parsimony methods. *Molecular Biology and Evolution,* **28**(10): 2731-2739.

Thorvaldsdóttir H, Robinson JT, Mesirov JP. 2013. Integrative Genomics Viewer (IGV): high-performance genomics data visualization and exploration. *Briefings in Bioinformatics,* **14**(2): 178-192.

Journal correction

In the paper “Tree shrew (*Tupaia belangeri*) as a novel non-human primate laboratory disease animal model” (*Zoological Research*, 2017, 38(3): 127-137), the title “Tree shrew (*Tupaia belangeri*) as a novel non-human primate laboratory disease animal model*”* should be corrected as *“*Tree shrew (*Tupaia belangeri*) as a novel laboratory disease animal model*”*.

The online versions have been corrected. We apologize to the readers for the mistake.

Comment on “The role of wildlife (wild birds) in the global transmission of antimicrobial resistance genes”

DEAR EDITOR,

We read with interest the article by Wang and colleagues regarding the role of wildlife in the transmission of antimicrobial resistance (AMR) (Wang et al., 2017). Although we appreciate the efforts in reviewing this important topic, we would like to comment on some statements that we believe are not up-to-date or properly cited.

The authors mentioned only two reports of *Escherichia coli* carrying plasmid-mediated colistin resistance gene *mcr-1* in wild birds in their review. The first report was on European herring gulls from Lithuania (Ruzauskas & Vaskeviciute, 2016) and the second was on Kelp gulls (*Larus dominicanus*) from Argentina (Liakopoulos et al., 2016). In our 2016 article, we already reported, for the first time, on the plasmid-mediated colistin resistance extended-spectrum β-lactamase-producing *E. coli* strain PK-13 from a wild migratory bird (Eurasian coot, *Fulica atra*) in Asia (Mohsin et al., 2016). However, the authors have not described our findings in their review. Furthermore, it is important to note that the *E. coli* strain PK-13 carries the IncI2 plasmid, which is in agreement with the original Chinese study (Liu et al., 2016) and previous reports from wild birds (Ruzauskas & Vaskeviciute, 2016; Liakopoulos et al., 2016). Therefore, it is likely that plasmid IncI2 is involved in the spread of the *mcr-1* gene in *E. coli* isolates from wild birds. Every winter, Pakistan hosts more than a million wild migratory birds from Siberia and Central Asia (Mohsin et al., 2016). There is already a dearth of data on the presence of *mcr-1* in wild birds and omitting the only article from Asia is misleading and does not provide up-to-date information to the reader. We also recently reported on the high carriage of CTX-M-15-producing *Klebsiella pneumoniae* in wild migratory birds in Pakistan (Raza et al., 2017). Finally, we agree with the authors that long-range migration of birds could be involved in the global dissemination of AMR.

Mashkoor Mohsin*, Shahbaz Raza
Institute of Microbiology, University of Agriculture, Faisalabad, Pakistan
*Corresponding author, E-mail: mashkoormohsin@uaf.edu.pk

REFERENCES

Liakopoulos A, Mevius DJ, Olsen B, Bonnedahl J. 2016. The colistin resistance *mcr-1* gene is going wild. *Journal of Antimicrobial Chemotherapy,* **71**(8): 2335-2336.

Liu YY, Wang Y, Walsh TR, Yi LX, Zhang R, Spencer J, Doi Y, Tian GB, Dong BL, Huang XH, Yu LF, Gu DX, Ren HW, Chen XJ, Lv LC, He DD, Zhou HW, Liang ZS, Liu JH, Shen JZ. 2016. Emergence of plasmid-mediated colistin resistance mechanism MCR-1 in animals and human beings in China: a microbiological and molecular biological study. *The Lancet Infectious Diseases,* **16**(2): 161-168.

Mohsin M, Raza S, Roschanski N, Schaufler K, Guenther S. 2016. First description of plasmid-mediated colistin-resistant extended-spectrum β-lactamase-producing *Escherichia coli* in a wild migratory bird from Asia. *International Journal of Antimicrobial Agents,* **48**(4): 463-464.

Raza S, Mohsin M, Madni WA, Sarwar F, Saqib M, Aslam B. 2017. First report of $bla_{\text{CTX-M-15}}$-type ESBL-producing *Klebsiella pneumoniae* in wild migratory birds in Pakistan. *EcoHealth,* **14**(1):182-186.

Ruzauskas M, Vaskeviciute L. 2016. Detection of the *mcr-1* gene in *Escherichia coli* prevalent in the migratory bird species *Larus argentatus*. *Journal of Antimicrobial Chemotherapy,* **71**(8): 2333-2334.

Wang J, Ma ZB, Zeng ZL, Yang XW, Huang Y, Liu JH. 2017. The role of wildlife (wild birds) in the global transmission of antimicrobial resistance genes. *Zoological Research,* **38**(2): 55-80.

Received: 02 May 2017; Accepted: 26 June 2017
DOI: 10.24272/j.issn.2095-8137.2017.023

Response to Comment on "The role of wildlife (wild birds) in the global transmission of antimicrobial resistance genes"

DEAR EDITOR,

Since our first identification of plasmid-mediated colistin resistance gene *mcr-1* in 2015 (Liu et al., 2016), it has been described in human clinics, domestic animals, foods, and the environment worldwide (Schwarz & Johnson, 2016). Although it is still rare, the emergence of *mcr-1* in wild animals is of great concern. We summarized two previous reports on *mcr-1* in wild birds from Lithuania and Argentina to describe its emergence and characteristics in wildlife and highlight the potentially important role of wild animals, particularly birds, in its global transmission (Wang et al., 2017). The first detection of *mcr-1* in wildlife in Asia was identified in an extended-spectrum β-lactamase-producing *Escherichia coli* strain isolated from Eurasian coot (*Fulica atra*), which was located on a ~63 kb IncI2 plasmid, frequently associated with the global transmission of *mcr-1* (Mohsin et al., 2016). The description of *mcr-1* in wild birds in Asia is very important to better understand the role that wild birds may play in the global spread of *mcr-1*, and should have been summarized in our recent review. However, our review only summarized articles published up to December 2016, and as such the then unpublished report on CTX-M-15-producing *Klebsiella pneumoniae* in wild birds in Pakistan (Raza et al., 2017) was not included.

Jing Wang, Zhen-Bao Ma, Zhen-Ling Zeng, Xue-Wen Yang, Ying Huang, Jian-Hua Liu*
College of Veterinary Medicine, South China Agricultural University, Guangzhou Guangdong 510642, China
*Corresponding author, E-mail: jhliu@scau.edu.cn

REFERENCES

Liu YY, Wang Y, Walsh TR, Yi LX, Zhang R, Spencer J, Doi Y, Tian GB, Dong BL, Huang XH, Yu LF, Gu DX, Ren HW, Chen XJ, Lv LC, He DD, Zhou HW, Liang ZS, Liu JH, Shen JZ. 2016. Emergence of plasmid-mediated colistin resistance mechanism MCR-1 in animals and human beings in China: a microbiological and molecular biological study. *The Lancet Infectious Diseases,* **16**(2): 161-168.

Mohsin M, Raza S, Roschanski N, Schaufler K, Guenther S. 2016. First description of plasmid-mediated colistin-resistant extended-spectrum β-lactamase-producing *Escherichia coli* in a wild migratory bird from Asia. *International Journal of Antimicrobial Agents,* **48**(4): 463-464.

Raza S, Mohsin M, Madni WA, Sarwar F, Saqib M, Aslam B. 2017. First report of $bla_{CTX-M-15}$-type ESBL producing *Klebsiella pneumoniae* in wild migratory birds in Pakistan. *EcoHealth,* **14**(1): 182-186.

Schwarz S, Johnson AP. 2016. Transferable resistance to colistin: a new but old threat. *Journal of Antimicrobial Chemotherapy,* **71**(8): 2066-2070.

Wang J, Ma ZB, Zeng ZL, Yang XW, Huang Y, Liu JH. 2017. The role of wildlife (wild birds) in the global transmission of antimicrobial resistance genes. *Zoological Research,* **38**(2): 55-80.

Received: 18 May 2017; Accepted: 26 June 2017
Foundation items: This study was partially supported by grants from the National Key Basic Research Program of China (2013CB127200) and the National Natural Science Foundation of China (81661138002)
DOI: 10.24272/j.issn.2095-8137.2017.024

Zoological Research Editorial Board

ZOOLOGICAL RESEARCH
动物学研究
Bimonthly, Since 1980

Project for Enhancing International Impact of China STM Journals

中国精品科技期刊
中国科技核心期刊
中国百强报刊

Editor-in-Chief: Yong-Gang Yao

Executive Editor-in-Chief: Wai-Yee Chan

Editors: Su-Qing Liu Long Nie

Edited by Editorial Office of Zoological Research

(Kunming Institute of Zoology, Chinese Academy of Sciences, 32 Jiaochang Donglu, Kunming, Yunnan, Post Code: 650223 Tel: +86 871 65199026 E-mail: zoores@mail.kiz.ac.cn)

Sponsored by Kunming Institute of Zoology, Chinese Academy of Sciences; China Zoological Society©

Supervised by Chinese Academy of Sciences

Published by Science Press (16 Donghuangchenggen Beijie, Beijing 100717, China)

Printed by Kunming Xiaosong Plate Making & Printing Co, Ltd

Domestic distribution by Yunnan Post and all local post offices in China

International distribution by China International Book Trading Corporation (Guoji Shudian) P.O.BOX 399, Beijing 100044, China

Advertising Business License 广告经营许可证：滇工商广字66号

Domestic Postal Issue No.: 64-20

Price: 10.00 USD/60.00 CNY Post No.: BM358

ISSN 2095-8137